UNIVERSIDADE DE BRASÍLIA
Faculdade de Tecnologia

MASTER'S DISSERTATION

Macroscopic Quantities of Dilute Non-Brownian Magnetic Suspensions in a Shear Flow

Gesse A. Roure Neto

Dissertation submitted to the Department of Mechanical Engineering in partial fulfillment of the requirements for the degree of Master of Mechanical Sciences

EXAMINING COMMITEE

Professor Francisco Ricardo da Cunha, PhD
Advisor (ENM - UnB)

Professor Taygoara Felamingo de Oliveira, PhD
Internal Member (ENM - UnB)

Professor Jader Riso Barbosa Junior, PhD
External Member (UFSC)

UNIVERSIDADE DE BRASÍLIA
FACULDADE DE TECNOLOGIA
DEPARTAMENTO DE ENGENHARIA MECÂNICA

Macroscopic Quantities of Dilute Non-Brownian Magnetic Suspensions in a Shear Flow

Gesse A. Roure Neto

DISSERTAÇÃO DE MESTRADO SUBMETIDA AO DEPARTAMENTO DE ENGENHARIA MECÂNICA COMO PARTE DOS REQUISITOS NECESSÁRIOS PARA A OBTENÇÃO DO GRAU DE MESTRE EM CIÊNCIAS MECÂNICAS

APROVADA POR:

Professor Francisco Ricardo da Cunha, PhD
Orientador (ENM - UnB)

Professor Taygoara Felamingo de Oliveira, PhD
Examinador interno (ENM - UnB)

Professor Jader Riso Barbosa Junior, PhD
Examinador externo (UFSC)

BRASÍLIA, MAIO DE 2018

FICHA CATALOGRÁFICA

ROURE NETO, GESSE ARANTES

Macroscopic Quantities of Dilute Non-Brownian Magnetic

Suspensions in a Shear Flow [Distrito Federal] 2018.

xxii, 138p., 297 mm (ENM/FT/UnB, Mestre, Ciências Mecânicas, 2018)

Dissertação de Mestrado - Universidade de Brasília,

Faculdade de Tecnologia. Departamento de Engenharia Mecânica.

1. Suspensões magnéticas. 2. Interações hidrodinâmicas.
3. Difusão hidrodinâmica. 4. Agregação induzida por cisalhamento.
5. Magnetização.

I. ENM/FT/UnB II. Título (Série)

REFERÊNCIA BIBLIOGRÁFICA

ROURE NETO, G. A. (2018). Macroscopic Quantities of Dilute Non-Brownian Magnetic Suspensions in a Shear Flow. Dissertação de Mestrado, Publicação DM-280, Departamento de Engenharia Mecânica, Universidade de Brasília, Brasília, DF, 138p.

CESSÃO DE DIREITOS

NOME DO AUTOR: Gesse Arantes de Roure Neto.

TÍTULO DA DISSERTAÇÃO DE MESTRADO: Macroscopic Quantities of Dilute Non-Brownian Magnetic Suspensions in a Shear Flow.

GRAU / ANO: Mestre / 2018

Gesse A. Roure Neto
Condomínio Quintas Bela Vista Quadra E Casa 12
71.680-604, Jardim Botânico - DF - Brasil

Aos meus pais, irmão e avós dedico este trabalho.

AGRADECIMENTOS

Previamente, gostaria de agradecer ao meu orientador, amigo e professor Francisco Ricardo da Cunha por toda a paciência e confiança depositada ao longo destes três anos de trabalho em conjunto. Agradeço também por todas as discussões, ensinamentos e puxões de orelha que recebi durante este período, que certamente me tornaram não só um pesquisador melhor, como uma pessoa melhor. Gostaria também de agradecer aos professores Yuri Dumaresq e Gustavo Abade por todas as lições, orientação e pela caminhada conjunta nos estágios iniciais dos meus estudos.

Agradeço a todos os meus amigos do Vortex, em especial aos meus companheiros de sala: Filipe, Igor e Yuri Zeniti, por todas as refeições que compartilhamos, congressos, pizzas e risadas que demos. Obrigado a todos vocês por terem tornado suportável, e até mesmo agradável, todos estes períodos extensos de trabalho no grupo. Filipe, você que sempre compartilhou minha paixão pela física e ciências naturais, agradeço por todas as discussões que tivemos neste período. Igor, além de um exemplo de companheirismo e dedicação você é um experimentalista brilhante. Jamais deixe de valorizar sua capacidade. Yuri, eu nunca vou poder agradecer o suficiente por você ter aberto as portas da sua casa para mim durante aqueles dias na Itália. Você é um verdadeiro exemplo de companheirismo, hospitalidade, tranquilidade e competência para mim.

Gostaria também de agradecer aos colegas Álvaro, Adriano Possebon e Camila, que também foram parte importante nesta caminhada do mestrado. Álvaro, obrigado por todo o companheirismo, conversas, bolachas e travesseiros em formato de U. Adriano, obrigado por todas as discussões acadêmicas que tivemos neste tempo a respeito de nossas pesquisas. Camila, obrigado pela sua prestatividade neste período e por estar presente em algumas das ocasiões mais críticas.

Agradeço à toda minha família e aos meus amigos mais próximos por todo o suporte prestado ao longo deste período.

Agradeço também ao CNPq pelo apoio financeiro durante a realizaçao do mestrado.

ABSTRACT

In recent years, many applications of magnetic suspensions were found in engineering, medical sciences, and other areas. These applications are mainly due to the fact that the rheological properties of these suspensions change in the presence of an external magnetic field. In this dissertation, we investigate the dynamics of two identical spherical magnetic particles undergoing a simple shear flow in the presence of magnetic and hydrodynamic interactions in order to analyze macroscopic quantities of magnetic suspensions in a regime out of equilibrium. Some particularities of the dynamical problem are investigated, including the interplay between aggregative and dispersive collisional trajectories. In addition, we perform a numerical computation of the hydrodynamic self-diffusivity, down-gradient diffusivity and the rate of particle doublet formation resulting from aggregative closed trajectories. The numerical computation of the diffusivities and aggregation rates is performed via a Monte-Carlo integration for different values of the magnetic interaction parameter α, which represents the non-dimensional strength of the dipole-dipole magnetic interactions. We compare the results found for the diffusivities and doublet formation rates with theoretical predictions. Finally, we explore the problem of magnetization of magnetic suspensions undergoing a simple shear flow for large values of Péclet number in the presence of an external magnetic field. Starting with the problem of an isolated magnetic particle in suspension, we can obtain the first order of magnetization by analyzing the orientational dynamics of the particle. Further, we use the numerical simulation of two particles for obtaining numerical values for the second-order steady-state magnetization.

Keywords: Magnetic suspensions, dipole-dipole interaction, hydrodynamic interactions, shear-induced diffusion, shear-induced aggregation, magnetization

RESUMO

Recentemente, têm-se encontrado várias aplicações de suspensões magnéticas nas áreas de engenharia, ciências médicas, entre outras, devido ao fato destas suspensões sofrerem alterações em seu comportamento na presença de campos magnéticos externos. A presente dissertação tem como objetivo investigar a dinâmica de duas partículas magnéticas esféricas em um escoamento cisalhante na presença de interações hidrodinâmicas e magnéticas, a fim de analisar propriedades macroscópicas de suspensões magnéticas diluídas em um regime fora do equilíbrio. Algumas particularidades desta dinâmica são analisadas, incluindo as relações entre trajetórias colisionais agregativas e dispersivas. Utilizando-se da simulação computacional da dinâmica de partículas juntamente a uma integração de Monte-Carlo, é possível se obter valores numéricos para os coeficientes de difusão hidrodinâmica induzida por cisalhamento e para a taxa de formação de pares agregados em suspensões diluídas para diferentes valores do parâmetro α, que representa a intensidade adimensional das interações dipolares. Neste trabalho também é explorado o problema da magnetização de suspensões cisalhadas para altos números de Péclet na presença de um campo magnético externo. Partindo do problema de uma partícula isolada em suspensão, é possível obter a primeira ordem da magnetização em estado estacionário analisando a dinâmica orientacional da partícula. Utilizando-se da simulação de duas partículas, é possível também obter valores numéricos para a segunda ordem da magnetização em estado estacionário em um regime fora do equilíbrio.

Palavras-chave: Suspensões magnéricas, interação dipolo-dipolo, interações hidrodinâmicas, difusão induzida por cisalhamento, agregação induzida por cisalhamento, magnetização

CONTENTS

LIST OF FIGURES

LIST OF TABLES

LIST OF SYMBOLS

Latin Symbols

Symbol	*Description*
a	Size or radius of a particle
A	Area
$B_\delta(\boldsymbol{x})$	Open ball of radius δ centered at the point $\boldsymbol{x}$
$\boldsymbol{B}$	Magnetic field
d	Diameter of a spherical particle
$\boldsymbol{D}$	Hydrodynamic dipole moment
$\boldsymbol{D}_f$	Electric displacement field
$\boldsymbol{\mathcal{D}}$	Diffusivity tensor
$\boldsymbol{E}$	Strain rate tensor
$\boldsymbol{E}_f$	Electric field
$\boldsymbol{f}$	Nondimensional shear-induced diffusivity tensor
$\boldsymbol{F}$	Force

$\boldsymbol{F}^H$	Hydrodynamic force
$\boldsymbol{F}^M$	Magnetic force
$\widetilde{\boldsymbol{\mathfrak{F}}}$	Flux of particles
g	Gravity
$g(\boldsymbol{r})$	Pair correlation function
$\boldsymbol{G}$	Oseen tensor
h	Volumetric distribution of sources
$\hat{\boldsymbol{h}}$	Nondimensional external magnetic field
$\boldsymbol{H}$	Auxiliary magnetic field
$\mathbb{I}$	Indicator function
$\boldsymbol{j}$	Current density
J_{11}	Nondimensional doublet formation rate
K_B	Boltzmann constant
ℓ	Characteristic length
m	Mass
m_0	Magnetic dipole intensity
$\boldsymbol{m}$	Magnetic dipole moment
$\boldsymbol{M}$	Magnetization
n	Number density
N	Number of particles
$\hat{\boldsymbol{n}}$	Normal vector
p	Pressure
$\boldsymbol{P}$	Polarization field
P	Probability density

$\mathcal{P}$	Probability measure
$\mathcal{P}(A\|B)$	Conditional probability
$\hat{\boldsymbol{p}}$	Particle orientation
$\boldsymbol{Q}$	Hydrodynamic quadrupole
r	Relative distance
R	Radius of an agglomerate
$\boldsymbol{r}$	Distance vector
$\hat{\boldsymbol{r}}$	Normalized distance vector
$\boldsymbol{S}$	Stresslet
t	Time
$\boldsymbol{t}$	Traction vector
T	Temperature
$\boldsymbol{T}^H$	Hydrodynamic torque
$\boldsymbol{T}^M$	Magnetic torque
$\boldsymbol{u}(\boldsymbol{x})$	Velocity field
$\boldsymbol{U}$	Velocity of a particle
U	Characteristic velocity
V	Volume
$\boldsymbol{V}$	Phase space velocity
$\boldsymbol{W}$	Relative displacement
$\boldsymbol{x}$	Position vector (in $\mathbb{R}^3$)
$\boldsymbol{X}$	Position in phase space

Greek Symbols

α	Nondimensional dipole interaction intensity
β	Nondimensional magnetic field strength
$\dot{\gamma}$	Shear rate
$\boldsymbol{\Gamma}$	Velocity gradient tensor
$\delta(\boldsymbol{x})$	Dirac's delta distribution
η_r	Rotational viscosity
μ	Viscosity
μ_{eff}	Effective viscosity
μ_0	Vacuum permeability
$\boldsymbol{\xi}$	Vorticity
ρ	Density of mass
ρ_e	Density of electric charges
$\boldsymbol{\sigma}$	Stress tensor
τ	Relaxation time
ϕ	Particle volume fraction
χ	Magnetic susceptibility
$\boldsymbol{\Omega}$	Angular velocity of the flow
$\boldsymbol{\omega}$	Angular velocity of a particle

Mathematical Notation

$\sum$	Summation
$\int_A$	Integral over A
$\odot$	Tensor contraction product
$\wedge$	Vector product
$\frac{D}{Dt}$	Material derivative
∇	Gradient operator
$\frac{\partial}{\partial \boldsymbol{X}}$	Gradient operator in phase space
$\times$	Cartesian product
$\bigcup$	Union
∂	Boundary operator

Coordinate systems

x, y, z	Cartesian coordinates
r, θ, φ	Spherical coordinates

CHAPTER 1

INTRODUCTION

> " I wish I could shut up like a telescope! I think I could, if I only knew how to begin. "
>
> Lewis Carroll, *Alice in Wonderland*

1.1 Motivation

Lately, a lot of the soft materials used in the industry are not pure liquids, but suspensions. In our context, we define a suspension as being a mixed material consisting of particles (*e.g.* drops, polymer macromolecules, solids) mixed in a ambient fluid without chemical bonding. The presence of these particles can influence severely the macroscopic behavior of the bulk material, which ceases to behave like a purely viscous fluid and can show viscoelastic behavior [1, 2]. Particle suspensions have been known and studied for a long time. Several applications of these suspensions in engineering are due to the unique characteristics present in the macroscopic behavior of these suspensions.

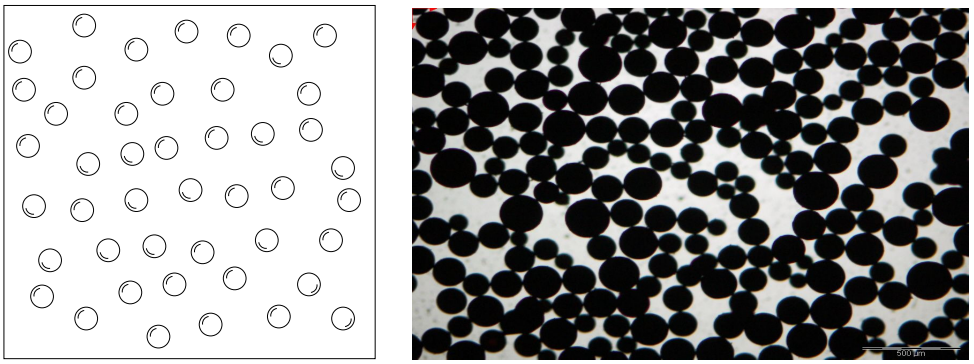

(a) (b)

Figure 1.1: (a): Representation of an ideal homogeneous monodisperse particle suspension in an ambient fluid. (b): Microscopy of real ferromagnetic particles utilized in the fabrication of a magnetorheological suspension. The diameter of the particles is at the order of 100 μm. (Courtesy of the microhydrodynamics and rheology laboratory at VORTEX-UnB)

Among many types of suspensions, one of particular interest, especially in the past few years, is the kind of magnetic suspensions. These are suspensions of ferromagnetic particles in an ambient fluid. The interest in those suspensions is mainly due to the fact that the rheological properties[1] of magnetic suspensions can be altered by the presence of an external magnetic field and also the fact that one can manipulate the fluid by using an external magnet. The most common examples of magnetic suspensions are the ones known as ferrofluids. Ferrofluids are colloidal suspensions of magnetic nanoparticles, typically with a size of 10 nm, dispersed in a Newtonian liquid (*e.g* ester, mineral oil, water). These particles are usually coated with a surfactant material, as shown in Figure 1.2. The presence of the surfactant forms a thin layer near the surface of the particle with a typical thickness of 2 nm.

In the past few years, several applications for ferrofluids and other types of magnetic suspensions in multiple areas were discovered. Another widely explored type of magnetic suspensions are the magnetorheological fluids. The main structural difference between magnetorheological fluids and ferrofluids is the size of the particles. Namely, the colloidal particles in ferrofluids are much smaller than

[1]Rheology is the field which investigates the response of a material to an applied stress [3]

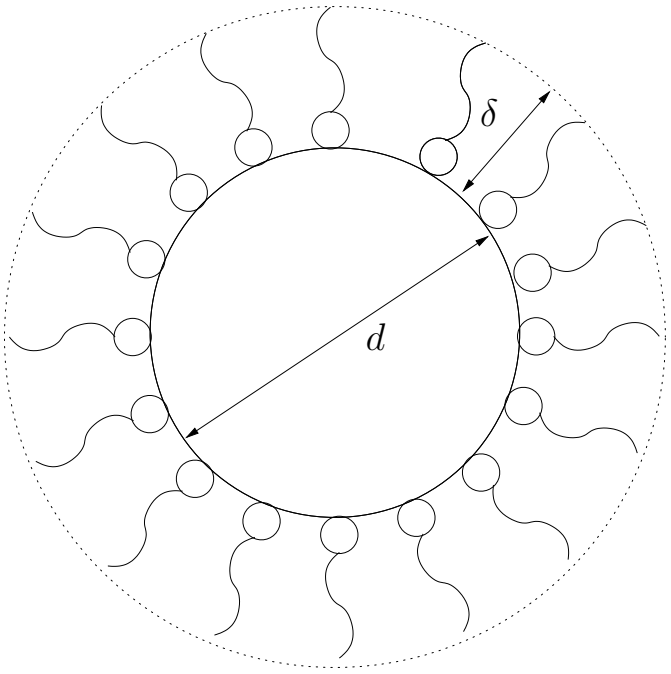

Figure 1.2: Anatomy of a ferrofluid nanoparticle with a cover of surfactant molecules. A typical value for the diameter of the particle is 10 nm with a typical surfactant layer of 2 nm. The hydrodynamic diameter is given by $d^H = d + 2\delta$.

the ones in magnetorheological suspensions. This contrast in size of the particles causes significant differences between the rheological and mechanical behavior of these two suspensions [4].

1.2 Magnetic suspensions

Magnetic suspensions are hydrodynamic suspensions of ferromagnetic particles dispersed in a Newtonian liquid. Depending on the size of the particles, the suspension is called a ferrofluid, in the case of colloidal particles, or a magnetorheological suspension, in the case of non-colloidal particles. These magnetic particles can be composed of different materials, such as magnetite (Fe_3O_4) and Mn-Zn ferrites, which have ferromagnetic properties. Table 1.1 shows the typical particle sizes for both ferrofluids and magnetorheological suspensions.

Table 1.1: Typical particle size for different magnetic suspensions

Suspension	**Typical size of particles**
Ferrofluids	~ 10 nm
Magneto-Rheological	~ 100 μm

The magnetic suspensions exhibit unusual characteristics, such as the dependence of their transport properties on the presence of an external magnetic field. At small volume fractions, magnetic suspensions of rigid spherical particles usually behave like Newtonian fluids in the absence of an external magnetic field. Actually, the suspension can be seen as a homogeneous Newtonian liquid with Einstein viscosity [5] $\mu_{eff} = \mu(1 + 2.5\phi)$, where ϕ is the particle volume fraction. Nevertheless, these suspensions can also exhibit a non-linear viscoelastic behavior at moderate particle volume fractions, as a direct consequence of the restoration effect produced by the magnetic dipole-dipole interactions between the particles and the formation of induced aggregate structures due to the magnetic field.

Another characteristic of the magnetic suspensions is the anisotropic behavior of the material. For instance, the shear resistance in the direction of the magnetic field has a different value from the shear resistance perpendicular to it. Due to the unique properties of these materials, they have a vast range of applications, ranging from hard drive disk seals to liquid body armor, cancer treatment via magnetic hyperthermia and magnetorheological dampers [6].

The study of ferrofluids and ferrohydrodynamics, in general, started around the middle of the 1960s, with names such as Rosensweig, which provided the first treatise on the subject in 1985 [7]. Other significant contributions were made in the field by names such as Felderhof [8, 9, 10], Shliomis [11, 12], Odenbach [13], Ivanov [14], and others. These contributions include models for the magnetization in and out of equilibrium and alterations of the original constitutive equation for the stress tensor proposed by Rosensweig.

Still, ferrohydrodynamics continues to be a current subject, with a lot of room for further contributions in the field. In this work, we investigate the influence of hydrodynamic and magnetic interaction between particles on hydrodynamic diffusion, aggregation rate and magnetization in monodisperse dilute non-colloidal magnetic suspensions of spherical rigid particles.

1.2.1 Hydrodynamic diffusion

The so-called hydrodynamic diffusion effect has appeared for the first time in the paper by Eckstein, Bailey and Shapiro [15]. In this paper, the authors have shown experimentally the existence of a shear-induced self-diffusion in a suspension of spherical rigid particles as a direct consequence of irreversible hydrodynamic interactions between the particles. These irreversible interactions are caused by the breaking of Stokes' symmetry and can be caused by different factors such as particle roughness [16], non-sphericity of the particles [17, 18], deformability [19], field interactions between particles [20, 21], and the presence of a third particle [22].

The symmetry breaking by irreversible particle interactions together with the randomness of collisions between particles produce a random walk along and across the streamlines. This random walk effect causes a hydrodynamic self-diffusion of the particles [23, 24]. Unlike molecular Brownian diffusion, the hydrodynamic diffusion depends on the interaction between particles and, consequently, on the particle volume fraction. More recently, shear-induced hydrodynamic diffusion has been a topic of interest due to a wide range of applications in numerous practical problems occurring in the microhydrodynamical scale of suspension flows instead of the molecular scale. For instance, this includes from aggregation-flocculation of suspended particles to mixing-diffusion and migration of cells in blood flows [25]. Several experimental and theoretical works have been carried out in order to compute the values of the shear-induced hydrodynamic diffusivities in the shear plane and vorticity plane [15, 26, 27, 16, 22, 28, 29, 30, 31].

In particular, Cunha & Hinch [16] calculated the hydrodynamic shear-induced

self and down-gradient diffusivities for dilute suspensions of rough spheres by examining the dynamics of two interacting particles. In addition, the authors proposed a theory which establishes a relationship between the hydrodynamic self-diffusivity induced by shear and the roughness of the particles for small values of roughness. This theory was later shown to be valid for other parameters which break the Stokes' symmetry of the relative motion of two particles, such as the viscosity ratio of drops [19]. In the work of Lopez et al. [18], the self-diffusivity is calculated by considering the case of anisotropic agglomerates of particles. The work of Cunha & Couto [20] computes the down-gradient diffusivity for a polydisperse suspension of sedimenting magnetic particles.

1.2.2 Aggregation rate

Even in the absence of Van der Waals attractive forces, as a result of the attractive dipolar forces between particles, magnetic particles in a suspension tend to form aggregates (dimers, trimers, so on). Particle aggregation and aggregation kinetics are topics widely studied in order to control the stability of colloidal and non-colloidal suspensions [32, 33, 34]. The present work deals with the aggregation of pairs of interacting non-colloidal particles. When two particles are brought close together by the flow, the magnetic dipole-dipole interactions being attractive may result in the formation of a doublet. The rate of doublet formation was studied before by Davis [35] for the case of non-Brownian sedimenting particles with aggregation due to short-range van der Waals interactions in the absence of any magnetic effect.

More recently, the phenomenon of aggregation in non-Brownian magnetic suspensions was investigated by Cunha & Couto [36] in the case of a polydisperse suspension of sedimenting particles interacting hydrodynamically and magnetically. However, as well as in the authors' paper on diffusion [20], the authors have not considered the rotation of the particles in order to compute the rate of doublet formation. In this work, we propose a more robust formulation by considering the full motion of the particles (*i.e.* translation and rotation) in the presence of

hydrodynamic and dipole-dipole particle interaction.

1.3 Magnetization

Magnetism in materials manifests itself in numerous forms, with a wide range of classifications such as ferromagnetism, antiferromagnetism, paramagnetism, diamagnetism, superparamagnetism, mictomagnetism and others [37]. In the context of the present dissertation, it is important to clarify the definitions of ferromagnetism, paramagnetism, and superparamagnetism.

Ferromagnetism is a cooperative type of magnetic behavior (*i.e.* where the interactions between the magnetic moments of the constituent atoms are intrinsically important) which presents a long-range correlation in which the magnetic moments tend to align in the same direction, even in the absence of an external magnetic field, forming permanent magnets. Figure 1.3 shows a typical configuration of ferromagnetic spin alignment in a body-centered cubic lattice found in simple metals.

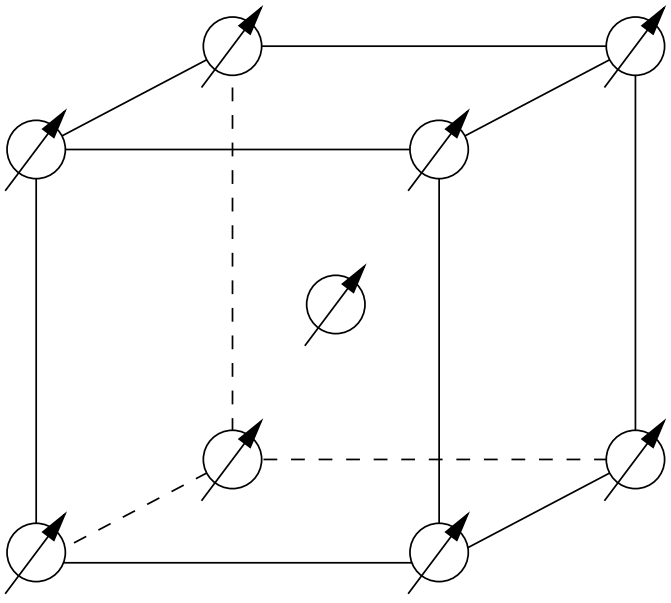

Figure 1.3: Ferromagnetic spin alignment in a body-centered cubic lattice

In contrast to ferromagnetism, *paramagnetism* is a non-cooperative type of magnetic behavior (*i.e.* where the magnetic moments of the constituent atoms or molecules are weakly correlated) in which the orientation of each magnetic moment is randomized by its thermal energy $K_B T$ while trying to align with an external applied magnetic field. This randomization results in a zero magnetization in the absence of an external magnetic field. On the other hand, paramagnetic materials exhibit a non-zero magnetization in the presence of an applied magnetic field.

Several materials exhibit paramagnetic behavior. For instance, ferromagnetic materials can transition into paramagnetic when heated above what is called the Curie temperature. In general, the dependence of the magnetization M on the applied field H can be non-linear [38, 39]. However, the magnetization of paramagnetic materials is often described in the limit of small H, which yields the linear relation

$$M = \chi(T) H. \tag{1.1}$$

The constant χ is called the magnetic susceptibility[2] defined by the relation

$$\chi = \lim_{H \to 0} \frac{M}{H} = \left(\frac{\partial M}{\partial H} \right)_{H=0}. \tag{1.2}$$

In the case of ideal paramagnetic materials (in the total absence of interparticle correlation), the property $\chi(T)$ increases linearly with the inverse of the temperature. Namely, $\chi = C/T$. This dependence is called the Curie law. The constant C is called the Curie constant. Curie's law is a special case of the more general Curie-Weiss law, where $\chi = C/(T - \theta)$ and θ is a parameter related to the interparticle coupling. This parameter arises naturally in Weiss' *mean-field theory* [40].

Without considering the limit $H \to 0$, one can express the relationship between the magnetization of the paramagnetic material and the applied field in terms of a generalized susceptibility $\chi(H, T)$ defined such as $M = \chi(H, T) H$. In

[2] In general, for anisotropic materials, where the magnetization $\boldsymbol{M}$ does not have the same direction of the field $\boldsymbol{H}$, the susceptibility is a tensor with components χ_{ij}.

this case, the generalized susceptibility $\chi(H,T)$ yields the susceptibility $\chi(T)$ the limit $H \to 0$. However, such nomenclature is not used often in the context of paramagnetic materials and it is more commonly used for the so-called *superparamagnetic materials*.

Superparamagnetism is a phenomenon similar to paramagnetism, but with its origins in small ferromagnetic single domains in contrast with atomic spins. A superparamagnetic material contains several ferromagnetic single domains. In the case where the size of single-domain ferromagnetic particles is very small, the particles can experience relaxation processes (*e.g.* Néel relaxation [41] and Brownian relaxation), which tends to randomize the direction of the magnetization of the domain in the absence of an external magnetic field. These relaxation phenomena result in a global behavior a similar to the one of a paramagnetic material. Thus, a superparamagnetic material only exhibits magnetization when subjected to an externally applied field.

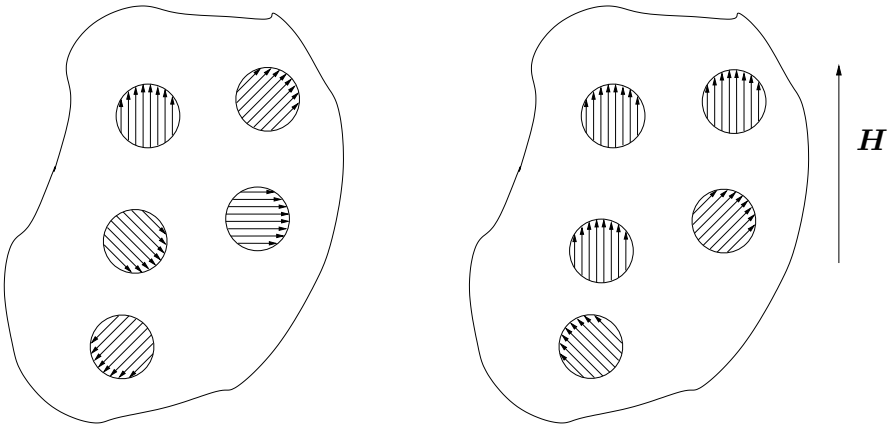

Figure 1.4: Illustration of the behavior of a superparamagnetic material in the presence of an external magnetic field.

The susceptibility of a superparamagnetic material is much larger than the one of a paramagnetic material. This contrast happens because the fluctuating moments in superparamagnetic materials are the magnetic moments of an entire ferromagnetic domain. These domains contain several microscopically ordered atoms in their composition. A ferrofluid is a typical example of a material that exhibits superparamagnetic behavior. In this context, the ferromagnetic domains

are the nanoparticles on suspension.

The investigation of magnetic properties of materials is a very recurrent topic in physics and engineering [40]. Equilibrium statistical mechanical models for magnetic materials date from the early 20^{th} century. Among these models, a well-known one is the Ising model [42] for ferromagnetism, which can be thought a simplification of the Heisenberg model [39]. This model is one of the simplest models to exhibit a phase transition at finite temperatures. In fact, for dimensions greater or equal two the model shows a transition from paramagnetic to ferromagnetic[3]. Variations of the Ising model are widely used for modeling several kinds of systems.

In the context of paramagnetism, one of the first attempts to describe the phenomenon was performed by Langevin in 1905 [44]. Langevin's model considers non-interacting $3-$dimensional classical magnetic dipoles interacting with an external applied magnetic field. Later, with the discovery of the Bohr-van Leeuwen theorem [45], which implies that paramagnetic phenomena cannot be described correctly by classical mechanics, the Langevin model was overthrown in favor of quantum mechanical models [40]. However, Langevin's model was later shown to be suitable for modeling superparamagnetic materials, due to the fact that their ferromagnetic single domains are macroscopic objects. In particular, this model can be applied for extracting the magnetic properties of very dilute ferrofluids in equilibrium, as ferrofluids exhibit superparamagnetic behavior. A second-order correction for the equilibrium magnetization was calculated analytically by Ivanov & Kuznetsova [14].

The study of a magnetic suspension out of equilibrium, in the presence of a flow, requires the investigation of magnetization dynamics. To this end, Shliomis [11, 12] has proposed a kinetic equation which describes the evolution of the magnetization of a dilute ferrofluid. His model takes into consideration the fluid flow and the magnetic relaxation. Felderhof [10] proposed a similar, but slightly different, kinetic model for describing the magnetization in the case of concentrated

[3]The first analytical solution for the two-dimensional Ising model was found by Lars Onsager in 1944 [43]

suspensions. Relaxation phenomena in dipolar suspensions have been also investigated by other works [9, 46].

Although magnetization in ferrofluids is an extensively explored subject, very little is known on the magnetization properties of non-colloidal magnetic suspensions, as the orientational relaxation effects are very weak. In addition, the effect of the hydrodynamic interaction between particles on the magnetization has not been explored yet.

In this dissertation we perform a computation of the magnetization $\mathcal{O}(\phi^2)$ at high Péclet numbers (non-equilibrium steady-state produced by a simple shear flow). Therefore, we consider both effects of hydrodynamic particle interactions and dipole-dipole magnetic interactions.

1.4 Dimensional analysis of the problem

In order to justify our treatment for investigating the properties of magnetorheological suspensions, such as the creeping flow hypothesis and the absence of Brownian motion, we need to analyze the dimensional scales of the physical quantities of the problem.

In the case of magneto-rheological suspensions, we consider the diameters of the particles to be $a \approx 10^{-4}$ m. We consider the ambient fluid to be a kind of mineral oil, with viscosity given approximately by $\mu \approx 1$ Pa $\cdot$ s. The density of the fluid is of the order $\rho \approx 900$ kg/m^3. We also consider a range of typical values for the shear rate $\dot{\gamma}$ of the order 50 s^{-1} up to 10^3 s^{-1}.

With these considerations in mind, a typical particle Reynolds number is given by $Re = \frac{\rho \dot{\gamma} a^2}{\mu}$ and ranges from 4.5×10^{-4}, for smaller values of $\dot{\gamma}$, to 10^{-2}, in the case of $\dot{\gamma} = 10^3 \text{s}^{-1}$. These small values for the Reynolds number enables us to consider the creeping flow hypothesis.

The Péclet number of the particle is given by $Pe = \frac{\dot{\gamma} 6\pi\mu a^3}{K_B T}$, where T is the temperature, which we consider to be 298 K, and K_B is the Boltzmann constant, which

is given by approximately $1.38 \times 10^{-23}\ J/K$. Hence, by considering $\dot{\gamma} = 50\ s^{-1}$, we have $Pe \approx 1.14 \times 10^{13}$. This high value for the Péclet number suggests that Brownian effects are almost negligible in the case of magneto-rheological suspensions.

In the context of the present dissertation, in which we investigate effects due to particle interactions, a parameter of interest is the dipolar strength $\alpha = \mu_0 m_0/(8\pi^2\mu a^6\dot{\gamma})$. This parameter is a ratio between dipolar magnetic forces and viscous forces due to the flow. Considering the particles to be of the same density as the fluid and using tabulated values for the saturation magnetization of magnetite ($M_s \approx 8.1 \times 10^4 A/m$), we can estimate the parameter α. By our estimations, we have α ranging from 0.1 to 1.8.

Table 1.2: Typical values of the main nondimensional parameters of the problem

Nondimensional parameter	**Physical Meaning**	**Magnitude**
Reynolds Number $Re = \frac{\rho\dot{\gamma}a^2}{\mu}$	Ratio between the vorticity diffusion time and the characteristic flow time	$\approx 4.5 \times 10^{-4} - 10^{-2}$ (M.R.) $\approx 10^{-11} - 10^{-7}$ (F.F.)
Péclet Number $Pe = \frac{\dot{\gamma}6\pi\mu a^3}{K_B T}$	Ratio between the Brownian relaxation time and the characteristic flow time	$\approx 1.14 \times 10^{13}$ (M.R.) ≈ 0.5 (F.F.)
Dipolar intensity $\alpha = \frac{\mu_0 m_0^2}{8\pi^2\mu a^6\dot{\gamma}}$	Intensity of dipolar interaction between particles	$\approx 0.1 - 1.8$ (Independent of particle size)

1.5 Objectives

The primary focus of the present dissertation is to calculate transport properties such as hydrodynamic diffusivity and aggregation rate of a non-Brownian magnetic suspension from a numerical simulation of the dynamics of two particles undergoing a simple shear flow in the presence of dipolar and hydrodynamic interactions. We also investigate the effects of these hydrodynamic and magnetic interactions between particles on the magnetization of magnetic suspensions very far from equilibrium (*i.e.* $Pe \gg 1$).

The more specific goals of this work are listed below:

1. To carry out numerical simulations concerning the dynamics of two particles in a dilute suspension undergoing a simple shear flow and an external magnetic field with hydrodynamic and magnetic particle interactions.

2. To implement far-field and near-field expressions for hydrodynamic mobilities under creeping flow. In addition, to test the behavior of the asymptotic expressions of the mobility functions for intermediate values of the relative distance between the particles.

3. To implement dipole-dipole magnetic force and torque interactions between particles.

4. To verify the numerical code comparing it with the asymptotic solution proposed by Cunha and Hinch [16] in the absence of magnetic interactions.

5. To investigate the interplay between aggregative and dispersive trajectories during particle encounters resulting in irreversible trajectories.

6. To derive a more general representation of Cunha and Hinch's theory in a tensorial form for the down-gradient diffusivity.

7. To perform a numerical simulation for computing the hydrodynamic self-diffusivities as a function of the magnetic interaction physical parameter using a Monte-Carlo integration algorithm developed in this dissertation. Based on the numerical simulation results, to propose a theoretical correlation between the hydrodynamic self-diffusivities as a function of the magnetic parameter and the dependence on the irreversibility parameter given in the work of Cunha and Hinch. [16]

8. To perform a numerical simulation for computing the down-gradient diffusivities, associated with a flux term contribution.

9. To propose a theoretical prediction by a simple scaling argument of the doublet formation rate as a function of the dipole interaction parameter.

10. To perform a numerical simulation for computing the doublet formation rate by using the Monte-Carlo integration algorithm developed in this work.

11. To develop a dynamical analysis of a single magnetic particle response including a stability analysis for the particle dipole orientation and the determination of an analytical expression for the orientational orbits.

12. To develop and validate a theoretical model in order to compute the order ϕ^2 of the non-equilibrium magnetization by using the two-particle problem. Therefore, the effect of particle magnetic and hydrodynamic interactions on the magnetization is also examined.

1.6 Scope of the work

Figure 1.5 shows a schematic representation of the distribution of the seven chapters in this dissertation.

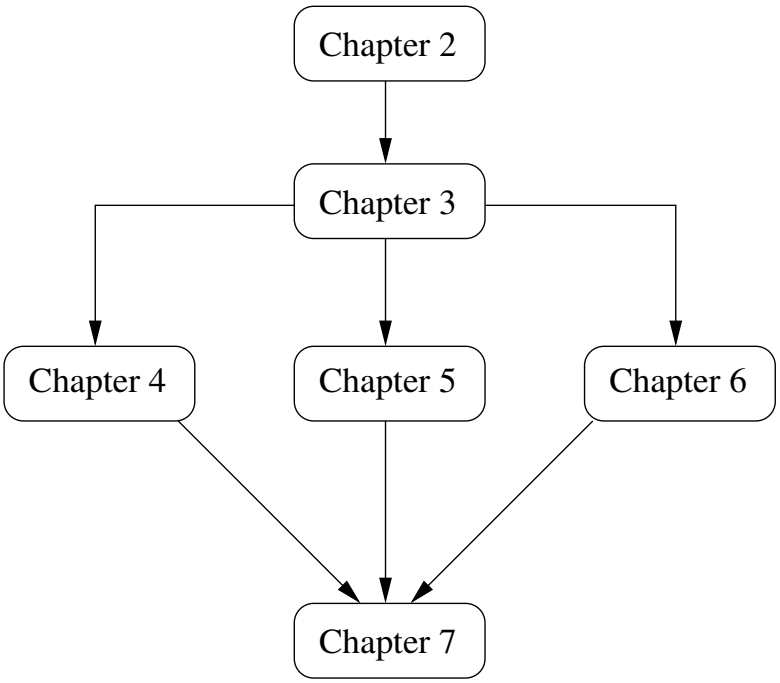

Figure 1.5: Schematic representation of the structure of the work

Chapter 2 presents the basic theoretical fundamentals of suspension mechanics. The main equations and principles used throughout this work are discussed in this chapter. Chapter 3 is concerned with the theory and numerical computation of the dynamical problem of two magnetic spherical particles undergoing a simple shear flow in the presence of hydrodynamic and dipolar interactions. These simulations are used in order to compute the diffusivity and aggregation rate. Chapter 4 describes the theory and numerical procedure for computing the shear-induced hydrodynamic diffusivities of a dilute non-Brownian magnetic suspension of spherical polarized particles. This chapter also includes a more general representation of the Cunha & Hinch theory for computing the full down-gradient diffusivity tensor, taking into account the influence of particle orientation. Chapter 5 presents

the theory and numerical procedure for the computation of the doublet formation rate as a function of the magnetic (dipolar) interaction parameter. Later in the same chapter, we compute numerical values for the doublet formation rate, showing that the numerical results are described very well by a power law predicted by scaling argument. Chapter 6 starts by examining the rotational dynamics of a single magnetic particle in creeping flow in the presence of an external magnetic field under the condition of high Péclet number. With this analysis, we are able to obtain a steady-state magnetization out of equilibrium for high values of the magnetic field parameter. Later in the chapter, we apply the two-particle problem to investigate the effects of particle interaction on the steady-state magnetization far from equilibrium. Chapter 7 presents a summary of the general discussions and results of the work, including suggestions for future works.

CHAPTER 2

THEORETICAL FUNDAMENTALS

The purpose of this chapter is to provide an overview of the essential theoretical fundamentals in which this work is grounded. The chapter begins by stating the basic principles of continuum mechanics and hydrodynamics at low Reynolds' numbers, such as the governing equations, Green's functions for Stokes' flows and Faxèn's laws. Then we introduce Maxwell's equations of classical electrodynamics, which we use in order to derive expressions for the forces and torques in the context of magnetic dipolar interactions, which are used extensively throughout the present work. Most of the derivations contained in this chapter can be found in textbooks such as [47, 48, 49, 50].

2.1 The continuum hypothesis

The continuum hypothesis in the physical context[1] states that it is possible to describe the physical properties of a material as continuous functions of points in a continuum, overlooking the molecular nature of matter. This hypothesis is grounded in the concept of a material point.

A material point is a point $\boldsymbol{x}$ in the continuum (*e.g.* $\boldsymbol{x} \in V \subseteq \mathbb{R}^3$) associated with a very small neighborhood $\delta V_{\boldsymbol{x}}$ containing a sufficiently large number of molecules in order to obtain a reliable volume average of a given local property (density). Thus, we can define the local properties of the continuum by using volume averages of microscopic densities. For instance, we can define the local density of a continuous material as being[2]:

$$\rho(\boldsymbol{x}) = \lim_{\delta V_{\boldsymbol{x}} \to \delta V_{\boldsymbol{x}}^*} \frac{1}{V(\delta V_{\boldsymbol{x}})} \int_{\delta V_{\boldsymbol{x}}} \sum_k m_k \delta(\boldsymbol{y} - \boldsymbol{x}_k) d\boldsymbol{y}, \tag{2.1}$$

where $\delta V_{\boldsymbol{x}}^*$ is the smallest neighborhood of $\boldsymbol{x}$ which contains a sufficiently large number of molecules to obtain a reliable volume average. This continuum hypothesis is the fundamental assumption behind the classical theories concerning the dynamics of fluids and solids.

2.2 Balance equations

In this section, we present some of the physical laws concerning the mechanics of continuous media. These laws yield the governing equations that are used directly or indirectly on this work.

[1] This physical continuum hypothesis is also known as the local thermodynamic equilibrium (LTE) hypothesis, usually with a slightly different statement.

[2] When convenient, we adopt the notation $d\boldsymbol{x}$ to indicate volume integration, following the notation used in many statistical mechanics textbooks and papers.

2.2.1 Localization theorem

The localization theorem is essential when formulating the differential equations for continuous media. The theorem states the following: Let $G : \Omega \to \mathbb{R}$ be a continuous measurable function, with Ω being a measurable metric space. If $\int_B G(\boldsymbol{x})d\boldsymbol{x} = 0 \ \ \forall B \subseteq \Omega$, then $G(\boldsymbol{x}) = 0$ for all $\boldsymbol{x} \in \Omega$. This theorem allows the crossing between an integral (global) formulation and a differential (local) formulation of the equations of motion for a continuum in the case where the function $G(\boldsymbol{x})$ is continuous.

The theorem is a direct consequence of Chebychev's inequality, which is shown and derived in Appendix I, and the continuity of G. In fact, let G be a measurable function, then:

$$\int_\Omega G(\boldsymbol{x})d\boldsymbol{x} = \int_{\Omega^0} G(\boldsymbol{x})d\boldsymbol{x} + \int_{\Omega^+} G(\boldsymbol{x})d\boldsymbol{x} + \int_{\Omega^-} G(\boldsymbol{x})d\boldsymbol{x} = 0, \tag{2.2}$$

where $\Omega^0 = \{\boldsymbol{x} \in \Omega \ ; \ G(\boldsymbol{x}) = 0\}$, $\Omega^+ = \{\boldsymbol{x} \in \Omega \ ; \ G(\boldsymbol{x}) > 0\}$ and $\Omega^- = \{\boldsymbol{x} \in \Omega \ ; \ G(\boldsymbol{x}) < 0\}$. As $\Omega^+, \Omega^- \subseteq \Omega$, then $\int_{\Omega^+} G(\boldsymbol{x})d\boldsymbol{x}$ and $\int_{\Omega^-} G(\boldsymbol{x})d\boldsymbol{x}$ vanish. Thus, as a Corollary of Chebyshev's inequality, $\mu(\Omega^+ \cup \Omega^-) = 0$. As the space Ω is Hausdorff and G is a continuous function, the set $\Omega^+ \cup \Omega^- = \{x \in \Omega | G(x) \neq 0\}$ is open. Now, supposing by contradiction that the set $\Omega^+ \cup \Omega^-$ is not empty, then for $\boldsymbol{x} \in \Omega^+ \cup \Omega^-$ there exists an open ball $B_\delta(\boldsymbol{x})$ in $\Omega^+ \cup \Omega^-$ which contains $\boldsymbol{x}$. Then, we have $0 < \mu(B_\delta(\boldsymbol{x})) \leq 0$, which leads to a contradiction. Therefore, $\Omega^+ \cup \Omega^-$ is the empty set. So $G(\boldsymbol{x}) = 0$ for all $\boldsymbol{x} \in \Omega$ and the theorem is proven.

2.2.2 Reynolds' transport theorem

We now introduce the Reynolds' transport theorem. This theorem is used in order to differentiate under the sign of integration in the case in which the domain depends on the differentiation parameter.

The Reynolds' transport theorem states that if an arbitrary field $G(\boldsymbol{x}, t)$ is continuous and differentiable with respect to $\boldsymbol{x}$ and t, as well as the material

volume $V(t)$ moving with the flow given by the velocity field $\boldsymbol{u}(x,t)$, we have:

$$\frac{d}{dt}\int_{V(t)} G(\boldsymbol{x},t)\ dV = \int_{V(t)} \left[\frac{\partial G}{\partial t} + \nabla\cdot(G\boldsymbol{u})\right] dV. \tag{2.3}$$

In order to prove the theorem, we use the fact that the derivative of the integral of $G(\boldsymbol{x},t)$ is given by definition as:

$$\frac{d}{dt}\int_{V(t)} G(\boldsymbol{x},t)\ dV = \lim_{\varepsilon\to 0}\frac{1}{\varepsilon}\left[\int_{V(t+\varepsilon)} G(\boldsymbol{x}',t+\varepsilon)dV' - \int_{V(t)} G(\boldsymbol{x},t)dV\right] \tag{2.4}$$

As $\boldsymbol{x}(t)$ is continuous at every time, we can expand it in a Taylor series as

$$\boldsymbol{x}' = \boldsymbol{x} + \varepsilon\boldsymbol{u} + \mathcal{O}(\varepsilon^2), \tag{2.5}$$

where $\boldsymbol{u}(\boldsymbol{x},t)$ is the velocity field. Hence, the Jacobian of the transformation $\boldsymbol{x}\to\boldsymbol{x}'$ is given by:

$$J = 1 + \varepsilon\nabla\cdot\boldsymbol{u} + \mathcal{O}(\varepsilon^2). \tag{2.6}$$

Similarly, we can expand $G(\boldsymbol{x},t)$ in a Taylor series, resulting in:

$$G(\boldsymbol{x}',t+\varepsilon) = G(\boldsymbol{x},t) + \varepsilon\boldsymbol{u}\cdot\nabla G + \varepsilon\frac{\partial G}{\partial t} + \mathcal{O}(\varepsilon^2). \tag{2.7}$$

Substituting in equation (2.4), we have:

$$\frac{d}{dt}\int_{V(t)} G(\boldsymbol{x},t)\ dV = \int_{V(t)} \left[\frac{\partial G}{\partial t} + \boldsymbol{u}\cdot\nabla G + G\nabla\cdot\boldsymbol{u}\right]\ dV. \tag{2.8}$$

By using the product rule at the result, we find:

$$\frac{d}{dt}\int_{V(t)} G(\boldsymbol{x},t)\ dV = \int_{V(t)} \left[\frac{\partial G}{\partial t} + \nabla\cdot(G\boldsymbol{u})\right] dV. \tag{2.9}$$

This result is the well known Reynolds' transport theorem. This theorem is necessary to derive the balance equations. It also links the Lagrangian and Eulerian

descriptions of continuum mechanics, as $\int_{V(t)} G(\boldsymbol{x}, t) d\boldsymbol{x}$ can be thought as a property of a moving body. This theorem, coupled with the localization theorem, allows us to obtain differential equations for the fields (in Eulerian description) by using the conservation laws postulated in a Lagrangian description.

2.2.3 Conservation of mass

Let us consider a moving material volume. If the continuum hypothesis holds, there is no creation nor destruction of mass in the volume. Therefore, the mass $m(t)$ of the material volume is conserved thoughout its motion. Mathematically, this means that

$$\frac{dm}{dt} = 0. \tag{2.10}$$

By the definition of mass density, the mass of the material volume is given by:

$$m = \int_{V(t)} \rho(\boldsymbol{x}, t) dV. \tag{2.11}$$

Therefore, by applying the Reynolds' transport theorem and the localization theorem, we obtain the differential concerning mass conservation, or the continuity equation, in a Eulerian description as being

$$\frac{\partial \rho}{\partial t} + \nabla \cdot (\rho \boldsymbol{u}) = 0, \tag{2.12}$$

or, alternatively,

$$\frac{D\rho}{Dt} + \rho \nabla \cdot \boldsymbol{u} = 0. \tag{2.13}$$

The operator $\frac{D}{Dt} = \frac{\partial}{\partial t} + \boldsymbol{u} \cdot \nabla$ is called the *material or total derivative*[3]. Physically, the material derivative is a time derivative seen through the perspective of a referential frame of a material particle travelling with the velocity of the flow.

[3]In the context of continuum mechanics, the material derivative is defined as being $\left(\frac{\partial}{\partial t}\right)_{\boldsymbol{X}}$, with $\boldsymbol{X}$ being the initial position of a material particle in the Lagrangian description.

In the case of incompressible media, whereas $D\rho/Dt = 0$, the continuity equation takes the form of:

$$\nabla \cdot \boldsymbol{u} = 0, \tag{2.14}$$

which is the form used throughout this work.

2.2.4 Balance of linear momentum

The balance of linear momentum is governed by Newton's second law, namely:

$$\frac{d\boldsymbol{L}}{dt} = \sum \boldsymbol{F}, \tag{2.15}$$

where $\boldsymbol{L}$ is the total linear momentum of the material volume, given by:

$$\boldsymbol{L} = \int_{V(t)} \rho(\boldsymbol{x}, t)\boldsymbol{u}(\boldsymbol{x}, t)\ dV. \tag{2.16}$$

The resulting force $\sum \boldsymbol{F}$ can be written as the sum of volume field forces $\boldsymbol{F}_V$ togheter with the forces $\boldsymbol{F}_S$ acting on the surface of the material volume, therefore

$$\sum \boldsymbol{F} = \boldsymbol{F}_S + \boldsymbol{F}_V, \tag{2.17}$$

Now, the field force term can be written in terms of a force density in the following form:

$$\boldsymbol{F}_V = \int_{V(t)} \boldsymbol{f}(\boldsymbol{x}, t)\ dV. \tag{2.18}$$

On the other hand, the surface force term can be represented by the integral of the traction distributed over the body surface. As the traction vector is given by $\boldsymbol{t} = \hat{\boldsymbol{n}} \cdot \boldsymbol{\sigma}$, where $\boldsymbol{\sigma}$ is the Cauchy stress tensor, we have:

$$\boldsymbol{F}_S = \int_{\partial V(t)} \hat{\boldsymbol{n}} \cdot \boldsymbol{\sigma}(\boldsymbol{x}, t) dS = \int_{V(t)} \nabla \cdot \boldsymbol{\sigma}\ dV \tag{2.19}$$

Applying the Reynolds transport theorem togheter with the localization theorem, we find that the general differential equation governing the motion of continuum media is given by

$$\rho \frac{D\boldsymbol{u}}{Dt} = \boldsymbol{f} + \nabla \cdot \boldsymbol{\sigma}. \tag{2.20}$$

This equation is the so-called Cauchy momentum equation and describes the dynamics of any continuum, such as fluids and solids. In order to close the set of equations governing the motion of a continuum medium, a constitutive equation for $\boldsymbol{\sigma}$ is required. In general, for fluids, $\boldsymbol{\sigma}$ can be a functional of the velocity gradient, with dependence on the memory of the fluid for times $\tau \leq t$, considering the full history of deformation. Namely,

$$\boldsymbol{\sigma}(\boldsymbol{x}, t) = \mathscr{F}\{\nabla \boldsymbol{u}\}_{\tau \leq t}. \tag{2.21}$$

In the case of an incompressible Newtonian fluid with instantaneous relaxation, the stress tensor is given by:

$$\boldsymbol{\sigma} = \mathscr{F}\{\boldsymbol{E}\}_t = -p\mathbf{1} + 2\mu \boldsymbol{E}, \tag{2.22}$$

where $\boldsymbol{E}$ is the symmetric part of the velocity gradient, namely:

$$\boldsymbol{E} = \frac{1}{2}\left[\nabla \boldsymbol{u} + (\nabla \boldsymbol{u})^T\right]. \tag{2.23}$$

Thus, the equation of motion for a Newtonian incompressible fluid is given by:

$$\rho\left(\frac{\partial \boldsymbol{u}}{\partial t} + \boldsymbol{u} \cdot \nabla \boldsymbol{u}\right) = \boldsymbol{f} - \nabla p + \mu \nabla^2 \boldsymbol{u}. \tag{2.24}$$

This equation togheter with the equation of continuity form the set of equations known as Navier-Stokes equations for an incompressible fluid.

2.3 Stokes equation

When studying the motion of microscopic particles dispersed in a Newtonian viscous fluid, we are mainly interested in a specific regime of Navier-Stokes equation known as *creeping flow*. Creeping flows are solutions of an asymptotic regime of the Navier-Stokes equations in the case where the Reynolds number is very small.

Let us start with the incompressible Navier-Stokes equation in the absence of body forces. Thus,

$$\rho\left(\frac{\partial \boldsymbol{u}}{\partial t} + \boldsymbol{u}\cdot\nabla\boldsymbol{u}\right) = -\nabla p + \mu\nabla^2\boldsymbol{u}. \tag{2.25}$$

Now, we choose appropriate scales for velocity and spatial dimensions as follows:

$$\boldsymbol{u} \sim U \tag{2.26}$$

$$\boldsymbol{x} \sim L \tag{2.27}$$

The chosen scale for time is based on a characteristic frequency ω, so that $t \sim \omega^{-1}$. Instead of choosing the appropriate scale for the pressure as ρU^2, as the viscous effects are more important than inertial effects, the scale for pressure in the creeping flow regime is determined directly by a simple balance between the terms ∇p and $\mu\nabla^2\boldsymbol{u}$, which yields:

$$p \sim \frac{\mu\, U}{L}. \tag{2.28}$$

Hence, the Navier-Stokes equation can be written in terms of nondimensional quantities as:

$$Re\left(Sh\frac{\partial \boldsymbol{u}'}{\partial t'} + \boldsymbol{u}'\cdot\nabla'\boldsymbol{u}'\right) = -\nabla' p' + \nabla'^2\boldsymbol{u}', \tag{2.29}$$

where $Re = \rho UL/\mu$ is the Reynolds number, which can be regarded as a ratio between inertial and viscous forces, and $Sh = \omega L/U$ is the Strouhal number, which

is the ratio between convective time and the characteristic time ω^{-1}. Considering the asymptotic regime as $Re \ll 1$ and $Re\ Sh \ll 1$, we have the homogeneous Stokes equation, given by:

$$\mu \nabla^2 \boldsymbol{u} = \nabla p, \tag{2.30}$$

which together with the continuity equation for incompressible fluids, given by $\nabla \cdot \boldsymbol{u} = 0$, governs the hydrodynamics of small Reynolds number flows. This equation can also be written as:

$$\nabla \cdot \boldsymbol{\sigma} = 0, \tag{2.31}$$

with $\boldsymbol{\sigma} = -p\mathbf{1} + 2\mu \boldsymbol{E}$ being the stress tensor for an incompressible Newtonian fluid.

2.4 Reciprocal identity

We consider the non-homogeneous Stokes equation, given by:

$$\nabla \cdot \boldsymbol{\sigma} = \boldsymbol{f}(\boldsymbol{x}). \tag{2.32}$$

Let the pairs $[\boldsymbol{\sigma}_1, \boldsymbol{u}_1]$ and $[\boldsymbol{\sigma}_2, \boldsymbol{u}_2]$ be two different solutions of (2.32) with non-homogeneities $\boldsymbol{f}_1$ and $\boldsymbol{f}_2$, respectively. Thus, we have the following vector identities:

$$\nabla \cdot (\boldsymbol{\sigma}_1 \cdot \boldsymbol{u}_2) = (\nabla \cdot \boldsymbol{\sigma}_1) \cdot \boldsymbol{u}_2 + 2\mu \boldsymbol{E}_1 : \boldsymbol{E}_2 \tag{2.33}$$

and

$$\nabla \cdot (\boldsymbol{\sigma}_2 \cdot \boldsymbol{u}_1) = (\nabla \cdot \boldsymbol{\sigma}_2) \cdot \boldsymbol{u}_1 + 2\mu \boldsymbol{E}_1 : \boldsymbol{E}_2. \tag{2.34}$$

Subtracting (2.34) from (2.33), we find the reciprocal identity, given by:

$$\nabla \cdot (\boldsymbol{\sigma}_1 \cdot \boldsymbol{u}_2) - \nabla \cdot (\boldsymbol{\sigma}_2 \cdot \boldsymbol{u}_1) = \boldsymbol{f}_1 \cdot \boldsymbol{u}_2 - \boldsymbol{f}_2 \cdot \boldsymbol{u}_1 \tag{2.35}$$

Equation (2.35) has a large number of applications when dealing with creeping flows. Among these applications, the reciprocal identity can be used to prove of the uniqueness of solutions of creeping flows [51]. The reciprocal identity also yields the boundary integral representation of the flow, which is used extensively throughout this work.

2.5 Formal solution of Stokes equation in terms of generalized functions

In this section we discuss the formal solution for Stokes equation and the boundary integral representation for the velocity field of the flow due to the movement of a rigid particle. This will enable us to find the multipole expansion for the velocity field, which will be used in later chapters. In the case of a non-homogeneous Stokes equation in a free $\mathbb{R}^3$ space with vanishing boundary conditions at infinity, we have:

$$\mu \nabla^4 \boldsymbol{u} = \left(\mathbf{1}\nabla^2 - \nabla\nabla\right) \cdot \boldsymbol{f}(\boldsymbol{x}). \tag{2.36}$$

Using the fact that $\boldsymbol{f}(\boldsymbol{x}) = \int \boldsymbol{f}(\boldsymbol{x}')\delta(\boldsymbol{x} - \boldsymbol{x}')d\boldsymbol{x}'$ and using the uniqueness of the solution for the Laplace operator, we have:

$$\boldsymbol{u}(\boldsymbol{x}) = \frac{1}{\mu} \int_{\mathbb{R}^3} \left[(\mathbf{1}\nabla^2 - \nabla\nabla)H(\boldsymbol{x} - \boldsymbol{x}')\right] \cdot \boldsymbol{f}(\boldsymbol{x}')d\boldsymbol{x}' \tag{2.37}$$

with the integration ranging througout the whole space $\mathbb{R}^3$ and H being the solution for equation:

$$\nabla^4 H = \delta(\boldsymbol{x} - \boldsymbol{x}'). \tag{2.38}$$

This bi-harmonic equation has solution $H = -r/8\pi$, satisfying the condition that both $\nabla^2 H$ and $\nabla\nabla H$ vanish at infinity. Thus, the formal solution of Stokes equation in $\mathbb{R}^3$ without external flow or internal boundaries is given by:

$$\boldsymbol{u}(\boldsymbol{x}) = -\frac{1}{8\pi\mu}\int_{\mathbb{R}^3} \boldsymbol{G}(\boldsymbol{x}-\boldsymbol{x}')\cdot\boldsymbol{f}(\boldsymbol{x}')d\boldsymbol{x}', \tag{2.39}$$

where

$$\boldsymbol{G}(\boldsymbol{r}) = \frac{\mathbf{1}}{r} + \frac{\boldsymbol{r}\boldsymbol{r}}{r^3} \tag{2.40}$$

is the Green's function for the Stokes equation also known as the Oseen tensor.

2.5.1 Fundamental solution for Stokes equation

One special application of interest for the formal solution of Stokes equation is to study the disturbance in the flow caused by a single point-force. This kind of disturbance is often called in literature by the name of stokeslet [52]. Considering the force distribution $\boldsymbol{f}(\boldsymbol{x})$ as the force exerted by the fluid on the single point particle located at $\boldsymbol{x_0}$, we have $\boldsymbol{f}(\boldsymbol{x}) = \boldsymbol{F}\ \delta(\boldsymbol{x}-\boldsymbol{x}_0)$. Hence, by substituting $\boldsymbol{f}(\boldsymbol{x})$ in equation (2.39), we find that the disturbance in the velocity field due to a single stokeslet is given by:

$$\boldsymbol{u}^*(\boldsymbol{x}-\boldsymbol{x}_0) = -\frac{1}{8\pi\mu}\boldsymbol{G}(\boldsymbol{x}-\boldsymbol{x}_0)\cdot\boldsymbol{F} \tag{2.41}$$

The pressure and stress fields of this flow can also be easily evaluated, resulting in [53]

$$p^*(\boldsymbol{x}-\boldsymbol{x}_0) = \frac{1}{8\pi}\boldsymbol{P}(\boldsymbol{x}-\boldsymbol{x}_0)\cdot\boldsymbol{F} \tag{2.42}$$

$$\boldsymbol{\sigma}^*(\boldsymbol{x}-\boldsymbol{x}_0) = \frac{1}{8\pi}\boldsymbol{T}(\boldsymbol{x}-\boldsymbol{x}_0)\cdot\boldsymbol{F}, \tag{2.43}$$

where

$$\boldsymbol{P}(\boldsymbol{r}) = 2\frac{\boldsymbol{r}}{r^3} \tag{2.44}$$

$$\boldsymbol{T}(\boldsymbol{r}) = 6\frac{\boldsymbol{rrr}}{r^5} \tag{2.45}$$

are the Green's functions for the pressure and stress fields, respectively. The solution for a single stokeslet is also called the fundamental solution for the Stokes equation.

2.5.2 Boundary integral representation for the flow in the presence of rigid particles

Considering now the solution for the creeping flow governed by the homogeneous Stokes equation with the possible presence of particles. The domain Ω of the fluid in the presence of a single particle is illustrated by Figure 2.1.

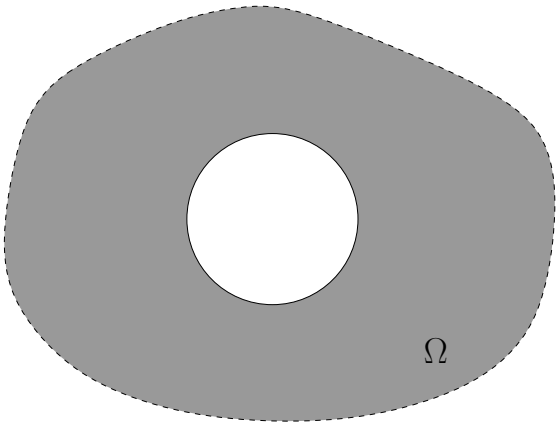

Figure 2.1: Domain of fluid in the presence of a particle. The dashed line indicates that the flow extends to infinity.

Now, we consider two different creeping flows on Ω. The pair $[\boldsymbol{u}, \boldsymbol{\sigma}]$ is the solution for the problem of the flow due to the presence of rigid particles. The pair $[\boldsymbol{u}^*(\boldsymbol{x} - \boldsymbol{x}'), \boldsymbol{\sigma}^*(\boldsymbol{x} - \boldsymbol{x}')]$ is the fundamental solution for the Stokes equation for a source at $\boldsymbol{x}'$.

If both flows satisfy Stokes equation, the reciprocal relation holds. Thus, integrating equation (2.35), one finds the velocity field to be given by

$$\boldsymbol{u}(\boldsymbol{x}) = \frac{1}{8\pi\mu}\int_{\partial\Omega} \boldsymbol{G}(\boldsymbol{x}-\boldsymbol{x}')\cdot\boldsymbol{t}(\boldsymbol{x}')dS' + \frac{1}{8\pi}\int_{\partial\Omega} \boldsymbol{u}(\boldsymbol{x}')\cdot\boldsymbol{T}(\boldsymbol{x}-\boldsymbol{x}')\cdot\ \hat{\boldsymbol{n}}\ dS', \quad (2.46)$$

where $\partial\Omega$ is the boundary of the fluid domain Ω and $\boldsymbol{t} = \hat{\boldsymbol{n}}\cdot\boldsymbol{\sigma}$ is the traction on a surface. We can decompose the fluid domain for the unbounded fluid as $\Omega = \mathbb{R}^3 - \bigcup_k V_k$, where V_k is the volume of a particle labeled k. Considering a boundary condition at infinity in which the flow is given by $\boldsymbol{u}^\infty(\boldsymbol{x})$, and the particles to be rigid, we have:

$$\boldsymbol{u}(\boldsymbol{x}) = \boldsymbol{u}^\infty(\boldsymbol{x}) - \sum_k \frac{1}{8\pi\mu}\int_{\partial V_k} \boldsymbol{G}(\boldsymbol{x}-\boldsymbol{x}')\cdot\boldsymbol{t}(\boldsymbol{x}')\ dS'. \quad (2.47)$$

This is the boundary integral representation of the flow. The minus sign is due to the orientation of the normal vector. In the case of a single particle, the boundary integral representation reduces to:

$$\boldsymbol{u}(\boldsymbol{x}) = \boldsymbol{u}^\infty(\boldsymbol{x}) - \frac{1}{8\pi\mu}\int_{\partial V} \boldsymbol{G}(\boldsymbol{x}-\boldsymbol{x}')\cdot\boldsymbol{t}(\boldsymbol{x}')\ dS'. \quad (2.48)$$

This equation expresses the contribution on the velocity field due to the presence of a single particle as a convolution integral involving the traction vector and the Green's function $\boldsymbol{G}(\boldsymbol{x})$.

2.5.3 Multipole expansion

Now we consider the case of the disturbance of a single particle on a steady flow at low Reynolds number. By the integral representation (2.48), we find the flow external to the particle to be given by

$$\boldsymbol{u}(\boldsymbol{x}) = -\frac{1}{8\pi\mu}\int_{\partial V} \boldsymbol{G}(\boldsymbol{x}-\boldsymbol{x}')\cdot\boldsymbol{t}(\boldsymbol{x}')\ dS'. \quad (2.49)$$

Expanding $\boldsymbol{G}(\boldsymbol{x}-\boldsymbol{x}')$ in a Taylor series over a point $\boldsymbol{x}_0 \in V$, we have:

$$\boldsymbol{G}(\boldsymbol{x}-\boldsymbol{x}') = \boldsymbol{G}(\boldsymbol{r}) - \boldsymbol{r}'\cdot\nabla\boldsymbol{G}(\boldsymbol{r}) + \frac{1}{2!}\boldsymbol{r}'\boldsymbol{r}' : \nabla\nabla\boldsymbol{G}(\boldsymbol{r}) + \dots \tag{2.50}$$

where

$$\boldsymbol{r} = \boldsymbol{x} - \boldsymbol{x}_0 \tag{2.51}$$

$$\boldsymbol{r}' = \boldsymbol{x}' - \boldsymbol{x}_0. \tag{2.52}$$

Therefore, the velocity field can be written as:

$$\boldsymbol{u}(\boldsymbol{x}) = -\frac{1}{8\pi\mu}\left[\boldsymbol{F}\cdot\boldsymbol{G}(\boldsymbol{r}) - \boldsymbol{D} : \nabla\boldsymbol{G}(\boldsymbol{r}) + \boldsymbol{Q}\odot\nabla\nabla\boldsymbol{G}(\boldsymbol{r}) + \dots\right], \tag{2.53}$$

where $\odot$ indicates contraction over the larger number of indices as possible. The terms $\boldsymbol{F}$, $\boldsymbol{D}$, $\boldsymbol{Q}$ and so on are called *multipole moments*. The expressions for the monopole $\boldsymbol{F}$, dipole $\boldsymbol{D}$, quadrupole $\boldsymbol{Q}$ and the other multipole moments are given by:

$$\boldsymbol{F} = \int_{\partial V} \boldsymbol{t}\, dS \tag{2.54}$$

$$\boldsymbol{D} = \int_{\partial V} \boldsymbol{r}\boldsymbol{t}\, dS \tag{2.55}$$

$$\boldsymbol{Q} = \frac{1}{2!}\int_{\partial V} \boldsymbol{r}\boldsymbol{r}\boldsymbol{t}\, dS \tag{2.56}$$

and so on. The monopole $\boldsymbol{F}$ is clearly the force exerted on the particle by the fluid. The dipole $\boldsymbol{D}$ can be decomposed in symmetric and skew-symmetric parts, respectivelly called $\boldsymbol{S}$ and $\boldsymbol{\mathcal{T}}$. The tensor $\boldsymbol{\mathcal{T}}$ is called the torque tensor and is related to the torque exerted on a particle by the flow, while the $\boldsymbol{S}$, called the stresslet tensor, is related to the stress contribution by the particle on the flow.

Using the multipole expansion, we can write the flow due to a particle as the solution of a non-homogeneous Stokes equation on the whole $\mathbb{R}^3$ as:

$$\nabla \cdot \boldsymbol{\sigma} = \boldsymbol{F}\delta(\boldsymbol{x} - \boldsymbol{x_0}) + \boldsymbol{D} \cdot \nabla\delta(\boldsymbol{x} - \boldsymbol{x_0}) + \dots \tag{2.57}$$

2.6 Faxén's laws

Faxén's laws provide a way to calculate the multipole moments of an isolated rigid spherical particle without prior knowledge on the solution of the flow. In this section, we derive Faxén's laws for monopole and dipole moments.

2.6.1 Faxén's first law

Starting from the boundary integral representation of the flow due to a moving rigid spherical particle:

$$\boldsymbol{u}(\boldsymbol{x}) = \boldsymbol{u}^{\infty}(\boldsymbol{x}) - \frac{1}{8\pi\mu}\int_S \boldsymbol{t} \cdot \boldsymbol{G}(\boldsymbol{x} - \boldsymbol{\xi}) dS(\boldsymbol{\xi}). \tag{2.58}$$

Integration of equation (2.58) along the surface of the particle results in:

$$\int_S \left[\boldsymbol{u}^{\infty}(\boldsymbol{x}) - \boldsymbol{u}(\boldsymbol{x})\right] dS(\boldsymbol{x}) = \frac{1}{8\pi\mu}\int_{S'} \boldsymbol{t} \cdot \left[\int_S \boldsymbol{G}(\boldsymbol{x} - \boldsymbol{\xi})\ dS(\boldsymbol{x})\right] dS(\boldsymbol{\xi}). \tag{2.59}$$

Performing a Taylor series expansion of $\boldsymbol{G}$ centered in $\boldsymbol{x}_0$, we find:

$$\boldsymbol{G}(\boldsymbol{x} - \boldsymbol{\xi}) = \boldsymbol{G}(\boldsymbol{x}_0 - \boldsymbol{\xi}) + (\boldsymbol{x} - \boldsymbol{x}_0) \cdot \nabla\boldsymbol{G}|_{\boldsymbol{x}_0 - \boldsymbol{\xi}} + \dots. \tag{2.60}$$

Using the fact that $\boldsymbol{G}$ is a bi-harmonic function with divergent zero, by direct integration we have:

$$\int_S \boldsymbol{G}(\boldsymbol{x}-\boldsymbol{\zeta})\, dS(\boldsymbol{x}) = 4\pi a^2 \left[\boldsymbol{G} + \frac{a^2}{6}\nabla^2\boldsymbol{G}\right]_{\boldsymbol{x}_0-\boldsymbol{\xi}} \tag{2.61}$$

$$= 4\pi a^2 \left[\frac{\mathbf{1}}{r} + \frac{\boldsymbol{r}\boldsymbol{r}}{r^3} + \frac{a^2}{6}\left(2\,\frac{\mathbf{1}}{r^3} - 6\,\frac{\boldsymbol{r}\boldsymbol{r}}{r^5}\right)\right], \tag{2.62}$$

where $\boldsymbol{r} = \boldsymbol{x}_0 = \boldsymbol{\xi}$ and a is the radius of the rigid sphere. At the surface of the sphere, $r = a$ and therefore:

$$\int_S \boldsymbol{G}(\boldsymbol{x}-\boldsymbol{\zeta})\, dS(\boldsymbol{x}) = \frac{16\pi a}{3}\mathbf{1}. \tag{2.63}$$

Hence:

$$\boldsymbol{F} = \frac{3\mu}{2a}\int_S [\boldsymbol{u}^\infty(\boldsymbol{x}) - \boldsymbol{u}(\boldsymbol{x})]\, dS(\boldsymbol{x}). \tag{2.64}$$

As the particle is rigid, the boundary condition imposes that $\boldsymbol{u}(\boldsymbol{x}) = \boldsymbol{U} + \boldsymbol{\Omega} \times (\boldsymbol{x} - \boldsymbol{x}_0)$ on the surface of the particle. Moreover, $\boldsymbol{u}^\infty(\boldsymbol{x})$ can be written as a Taylor series around the particle center $\boldsymbol{x}_0$

$$\boldsymbol{u}^\infty(\boldsymbol{x}) = \boldsymbol{u}^\infty(\boldsymbol{x}_0) + (\boldsymbol{x}-\boldsymbol{x}_0)\cdot\nabla\boldsymbol{u}^\infty(\boldsymbol{x}_0) + \frac{1}{2}(\boldsymbol{x}-\boldsymbol{x}_0)(\boldsymbol{x}-\boldsymbol{x}_0) : \nabla\nabla\boldsymbol{u}^\infty(\boldsymbol{x}_0) + \ldots. \tag{2.65}$$

Thus, the integral in equation (2.64) results in:

$$\boldsymbol{F} = 6\pi\mu a\left[\boldsymbol{u}^\infty(\boldsymbol{x}_0) + \frac{a^2}{6}\nabla^2\boldsymbol{u}^\infty(\boldsymbol{x}_0) - \boldsymbol{U}\right]. \tag{2.66}$$

This means that for a rigid spherical particle, one can determine the force exerted by the fluid on the particle only by knowing the external flow at infinity $\boldsymbol{u}^\infty(\boldsymbol{x})$, the position and the velocity of the particle. Note that for a force-free neutrally buoyant particle in a linear field $\boldsymbol{u}^\infty(\boldsymbol{x}) = \boldsymbol{\Gamma}\cdot\boldsymbol{x}$, in the absence of any magnetic effect, the particle translates with velocity $\boldsymbol{U} = \boldsymbol{u}^\infty(\boldsymbol{x}_0) = \boldsymbol{\Gamma}\cdot\boldsymbol{x}_0$.

2.6.2 Faxén's second and third laws

In this subsection, we shall use a procedure similar to the one explored in 2.6.1 in order to derive the expressions for the second and third Faxén's laws. Faxén's second and third laws can be used to find the dipole moments of a single spherical particle as a function of the externally applied flow. By the integral representation, we have:

$$\boldsymbol{u}(\boldsymbol{x})\boldsymbol{x} = \boldsymbol{u}^{\infty}(\boldsymbol{x})\boldsymbol{x} - \frac{1}{8\pi\mu}\int_S \boldsymbol{G}(\boldsymbol{\xi}-\boldsymbol{x})\cdot\boldsymbol{t}\boldsymbol{x}dS(\boldsymbol{\xi}). \tag{2.67}$$

Integration on $\boldsymbol{x}$ over the surface gives the terms:

$$\int_S G_{ik}(\boldsymbol{\xi}-\boldsymbol{x})x_j dS(\boldsymbol{x}) = -\frac{4}{3}\pi a^4\left[G_{ik,j} + \frac{a^2}{10}\nabla^2 G_{ik,j}\right]_{\boldsymbol{x}=\boldsymbol{x}_0} \tag{2.68}$$

and

$$\int_S u_i^{\infty} x_j dS = \frac{4}{3}\pi a^4\left[\Gamma_{ij} + \frac{a^2}{10}\nabla^2\Gamma_{ij}\right]_{\boldsymbol{x}=\boldsymbol{x}_0}. \tag{2.69}$$

Thus, we have:

$$\left[\Gamma_{ij} + \frac{a^2}{10}\nabla^2\Gamma_{ij}\right]_{\boldsymbol{x}=\boldsymbol{x}_0} = -\frac{1}{8\pi\mu}\int_S\left(G_{ik,j} + \frac{a^2}{10}\nabla^2 G_{ik,j}\right)f_k dS. \tag{2.70}$$

At the surface of the sphere with radius a:

$$G_{ik,j} + \frac{a^2}{10}\nabla^2 G_{ik,j} = \frac{2}{5a^3}\left[\delta_{kj}x_i + \delta_{ij}x_k - 4\delta_{ik}x_j\right] \tag{2.71}$$

Therefore, by collecting the symmetrical and anti-symmetrical parts of the dipole (2.55), we find the expression for the torque and stresslet for an isolated rigid spherical particle of radius a subject to an external flow. Namely, the expression for the torque is given by:

$$\boldsymbol{T} = 8\pi\mu a^3\left[\boldsymbol{\Omega}^{\infty}|_{\boldsymbol{x}_0} - \boldsymbol{\omega}\right], \tag{2.72}$$

which is Faxén's second law. Again, as an isolated particle free of inertia is undergoing a simple-shear motion without an applied magnetic field (*i.e.* the particle is torque-free), it rotates with angular velocity $\boldsymbol{\omega} = \frac{1}{2}\nabla \times \boldsymbol{u}^{\infty}|_{\boldsymbol{x_0}}$. So, the particle rotates with the local angular velocity of the external flow evaluated in its center. On the other hand, in the presence of a magnetic torque $\boldsymbol{T}^M$ acting on the particle[4],

$$\boldsymbol{\omega} = \boldsymbol{\Omega}^{\infty}\big|_{\boldsymbol{x}_0} + \frac{\boldsymbol{T}^M}{8\pi\mu a^3}. \tag{2.73}$$

This result already indicates that in the case of a magnetic particle, the particle is not necessarily free to rotate with the vorticity of the flow. There is an apparent competition between the vorticity and the effect of the magnetic torque. Analogously, the expression for the stresslet is given by:

$$\boldsymbol{S} = \frac{20}{3}\pi\mu a^3 \left[1 + \frac{a^2}{10}\nabla^2\right] \boldsymbol{E}^{\infty}|_{\boldsymbol{x}_0}. \tag{2.74}$$

which is Faxén's third law.

2.7 Maxwell's equations

The Maxwell's equations are a Lorentz-invariant set of equations which governs the dynamics of the electromagnetic field. Since the focus of this work is to study the movement of slow-moving particles in creeping flow, we can ignore any relativity discussion here. Considering the electric field $\boldsymbol{E}_f(\boldsymbol{x}, t)$ and the magnetic field $\boldsymbol{B}(\boldsymbol{x}, t)$, the macroscopic Maxwell equations can be written in standard vector differential notation as[5]:

[4]The change of sign in the expression happens because the torque calculated by Faxén's law is the hydrodynamical torque.

[5]In order to avoid any confusion with previous notation for the shear rate tensor and the hydrodynamic dipole we use the nomenclature $\boldsymbol{E}_f$ and $\boldsymbol{D}_f$ for the electric and electric displacement fields.

$$\nabla \cdot \boldsymbol{E}_f = \frac{\rho_e}{\varepsilon_0}, \tag{2.75}$$

$$\nabla \cdot \boldsymbol{B} = 0, \tag{2.76}$$

$$\nabla \times \boldsymbol{E} = -\frac{\partial \boldsymbol{B}}{\partial t} \tag{2.77}$$

$$and \quad \nabla \times \boldsymbol{B} = \mu_0 \boldsymbol{j} + \mu_0 \varepsilon_0 \frac{\partial \boldsymbol{E}}{\partial t}, \tag{2.78}$$

where ρ_e is the electric charge density, which can be broken into a monopole contribution ρ_e^m and a dipole contribution ρ_e^d, ε_0 is the vacuum dielectric constant, μ_0 is the vacuum magnetic permeability and $\boldsymbol{j}$ is the current density.

The electric field $\boldsymbol{E}_f$ can be decomposed in the form of:

$$\boldsymbol{E}_f = \frac{1}{\varepsilon_0} \left(\boldsymbol{D}_f - \boldsymbol{P} \right), \tag{2.79}$$

where $\boldsymbol{D}_f$ is the so-called *electric displacement field*. The field $\boldsymbol{P}$, which represents the electric dipole density, is called the *polarization field*. In a similar way, the magnetic field $\boldsymbol{B}$ can be decomposed in two parts, as

$$\boldsymbol{B} = \mu_0 \left(\boldsymbol{H} + \boldsymbol{M} \right), \tag{2.80}$$

where $\boldsymbol{H}$ is called the auxiliary magnetic field and $\boldsymbol{M}$ is the magnetization, which is the density of magnetic dipoles. Considering that the magnetic field can be generated by an electric current or by magnetic dipoles, we can also write the current density term as:

$$\boldsymbol{j} = \boldsymbol{j}_F + \boldsymbol{j}_M, \tag{2.81}$$

where $\boldsymbol{j}_F$ is the electrical current density due to the motion of free charges and the term $\boldsymbol{j}_M$ is related to the presence of magnetic dipoles and the motion of polarized charges, such that:

$$\boldsymbol{j}_M = \nabla \times \boldsymbol{M} + \frac{\partial \boldsymbol{P}}{\partial t} \tag{2.82}$$

These assumptions result in the form of Maxwell's equations suitable for material media. Namely:

$$\nabla \cdot \boldsymbol{D}_f = \rho_e^m, \tag{2.83}$$

$$\nabla \cdot \boldsymbol{B} = 0, \tag{2.84}$$

$$\nabla \times \boldsymbol{E}_f = -\frac{\partial \boldsymbol{B}}{\partial t} \tag{2.85}$$

$$and \quad \nabla \times \boldsymbol{H} = \boldsymbol{j}_F + \frac{\partial \boldsymbol{D}_f}{\partial t}. \tag{2.86}$$

In the present dissertation, all of our considerations focus on the magnetostatic regime. At this regime, there is no free electric charge distribution nor electric current densities. We also consider variations in the magnetic field $\boldsymbol{B}$ to be very slow. Thus, the governing equations take the form of:

$$\nabla \cdot \boldsymbol{B} = 0 \tag{2.87}$$

$$\nabla \times \boldsymbol{H} = 0. \tag{2.88}$$

As the curl of the vector field $\boldsymbol{H}$ is null, we can write $\boldsymbol{H}$ in terms of a potential ϕ as $\boldsymbol{H} = -\nabla\phi$. Hence, the potential ϕ is governed by the Poisson equation:

$$\nabla^2\phi = \nabla \cdot \boldsymbol{M}, \tag{2.89}$$

where the field $\boldsymbol{M}$ is given.

2.8 Magnetic interaction between two dipoles

In this section, we examine the force and torque interactions between two point dipoles. The expressions found in this section will be very relevant in subsequent chapters for the dynamical simulation of two magnetic particles interacting magnetically and hydrodynamically in a simple shear flow.

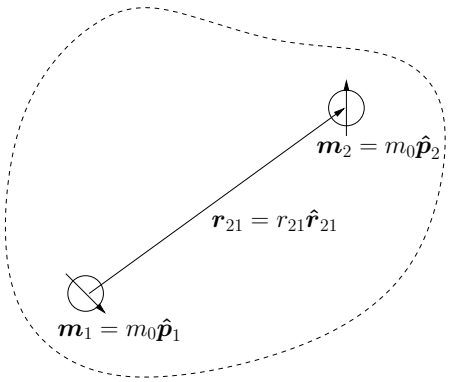

Figure 2.2: Sketch of two magnetic dipoles interacting magnetically.

Since the magnetization of a single dipole located at $\boldsymbol{x}_1$ is given by $\boldsymbol{M}(\boldsymbol{x}) = \boldsymbol{m}\delta(\boldsymbol{x} - \boldsymbol{x}_1)$, considering that the magnetic field produced by the dipole can be written as $\boldsymbol{H}_D = -\nabla\phi_D$, the equation for $\boldsymbol{\phi}_D$ is given by:

$$\nabla^2\phi_D = \nabla \cdot \boldsymbol{M} = \boldsymbol{m}_1 \cdot \nabla\delta(\boldsymbol{x} - \boldsymbol{x}_1) \tag{2.90}$$

Solving the equation in free space, we find ϕ_D to be given by

$$\phi_D = -\frac{1}{4\pi}\boldsymbol{m}_1 \cdot \nabla\left(\frac{1}{|\boldsymbol{x} - \boldsymbol{x}_1|}\right). \tag{2.91}$$

Hence, the magnetic field due to a single dipole can be written as:

$$\boldsymbol{H}_D(\boldsymbol{x}) = -\frac{1}{4\pi}\boldsymbol{m}_1 \cdot \boldsymbol{J}(\boldsymbol{x} - \boldsymbol{x}_1), \tag{2.92}$$

where $\boldsymbol{J}$ is the Green's function for the magnetic field $\boldsymbol{H}$, given by:

$$\boldsymbol{J}(\boldsymbol{r}) = \frac{1}{r^3}\left(\mathbf{1} - 3\ \hat{\boldsymbol{r}}\hat{\boldsymbol{r}}\right). \tag{2.93}$$

Here, $r = |\boldsymbol{r}|$ and $\hat{\boldsymbol{r}} = \boldsymbol{r}/r$. The magnetic force exerted on the dipole located at the point $\boldsymbol{x}_2$ due to the magnetic field generated by the dipole at $\boldsymbol{x}_1$ is given by:

$$\boldsymbol{F}_2 = \mu_0\ \boldsymbol{m}_2 \cdot \nabla\boldsymbol{H}_D(\boldsymbol{x}_2). \tag{2.94}$$

Using the expression for $\boldsymbol{H}_D(\boldsymbol{x})$, we find:

$$\boldsymbol{F}_2 = -\frac{\mu_0}{4\pi}\nabla\left(\boldsymbol{m}_1\boldsymbol{m}_2 : \boldsymbol{J}(\boldsymbol{x}-\boldsymbol{x}_1)\right)_{\boldsymbol{x}_2}, \tag{2.95}$$

or more explicitly:

$$\boldsymbol{F}_2 = \frac{3\mu_0 m_0^2}{4\pi r_{21}^4}\left[(\hat{\boldsymbol{p}}_1\cdot\hat{\boldsymbol{p}}_2)\,\hat{\boldsymbol{r}}_{21} + (\hat{\boldsymbol{p}}_1\cdot\hat{\boldsymbol{r}}_{21})\,\hat{\boldsymbol{p}}_2 + \right.$$
$$\left. + (\hat{\boldsymbol{p}}_2\cdot\hat{\boldsymbol{r}}_{21})\,\hat{\boldsymbol{p}}_1 - 5\,(\hat{\boldsymbol{p}}_1\cdot\hat{\boldsymbol{r}}_{21})\,(\hat{\boldsymbol{p}}_2\cdot\hat{\boldsymbol{r}}_{21})\,\hat{\boldsymbol{r}}_{21}\right]. \tag{2.96}$$

The expression for the magnetic torque on the dipole located at $\boldsymbol{x}_2$ is given by:

$$\boldsymbol{T}_2 = \mu_0\ \boldsymbol{m}_2 \wedge \boldsymbol{H}_D(\boldsymbol{x}_2). \tag{2.97}$$

Now, substituting the expression (2.92) for $\boldsymbol{H}_D(\boldsymbol{x})$ into (2.97), we find the torque exerted on the dipole at $\boldsymbol{x}_2$ by the dipole at $\boldsymbol{x}_1$ to be given by:

$$\boldsymbol{T}_2 = \frac{3\mu_0 m_0^2}{4\pi r_{21}^3}\left[-\frac{1}{3}\hat{\boldsymbol{p}}_2\wedge\hat{\boldsymbol{p}}_1 + (\hat{\boldsymbol{p}}_2\wedge\hat{\boldsymbol{r}}_{21})\,(\hat{\boldsymbol{p}}_1\cdot\hat{\boldsymbol{r}}_{21})\right]. \tag{2.98}$$

These expressions for the force and torque interactions between two dipoles, given respectivelly by equations (2.96) and (2.98), will be used later in the following chapters concerning the investigation of the dynamics of two particles interacting hydrodynamically and magnetically in creeping flow.

2.9 Conservation of probability

Now, we use the generalized Reynolds' transport theorem in order to derive a differential equation concerning the probability density for a general phase space. In the context of the present dissertation, the probability densities used in order to compute the transport coefficients involve variables such as orientations of the dipolar moment of the magnetic particles. Considering the dynamics of a system as a measure-invariant transformation, the probability measure $\mathcal{P}$ of a set Ω_t has the same values for all times, so that:

$$\frac{d\mathcal{P}(\Omega_t)}{dt} = 0 \tag{2.99}$$

In terms of the probability density $P(\boldsymbol{X})$, with $\boldsymbol{X} \in \Omega_t$ being a possible state, we have

$$\frac{d}{dt}\int_{\Omega_t} P(\boldsymbol{X}) d\boldsymbol{X} = 0. \tag{2.100}$$

Direct application of Reynolds' Transport Theorem leads to

$$\int_{\Omega_t} \left[\frac{\partial P}{\partial t} + \frac{\partial}{\partial \boldsymbol{X}} \cdot (\boldsymbol{V} P)\right] d\boldsymbol{X} = 0, \tag{2.101}$$

where $\boldsymbol{V}$ is the generalized velocity of an element of the phase space, which is given by the dynamics of the system. Therefore, by using the localization theorem, we have the equation for conservation of probability, namely:

$$\frac{\partial P}{\partial t} + \frac{\partial}{\partial \boldsymbol{X}} \cdot (\boldsymbol{V} P) = 0. \tag{2.102}$$

For conservative classical systems, Liouville's theorem states that $\frac{\partial \boldsymbol{V}}{\partial X} = 0$, which means that the flow on phase space is incompressible. In this case, the conservation of probability takes the form of

$$\frac{\partial P}{\partial t} + \boldsymbol{V} \cdot \frac{\partial P}{\partial \boldsymbol{X}} = 0. \tag{2.103}$$

This is known as Liouville's equation and it is the main equation in classical statistical mechanics [50].

CHAPTER 3

TWO-PARTICLE DYNAMICS IN CREEPING FLOW

In this chapter, we investigate the dynamics of two magnetic non-Brownian particles free of inertia moving in a viscous fluid. This dynamical problem is the base for most of the results presented in this dissertation. Here, we perform numerical simulations taking into account hydrodynamic and magnetic interactions between the particles. The first sections of this chapter present the general formulation of the particle motion and the mobility formulation of hydrodynamic interactions between the particles, introduce the magnetic forces and torques used in this work and also present the most relevant nondimensional physical parameters. Then, we examine some the results from the numerical simulations concerning the dynamics of the particles and the interplay between diffusive and aggregative mechanisms.

3.1 Formulation of the mobility problem

In this section, we formulate the general governing equations for the motion of two rigid spherical particles moving in a Stokes flow free of inertia in the presence of an external flow.

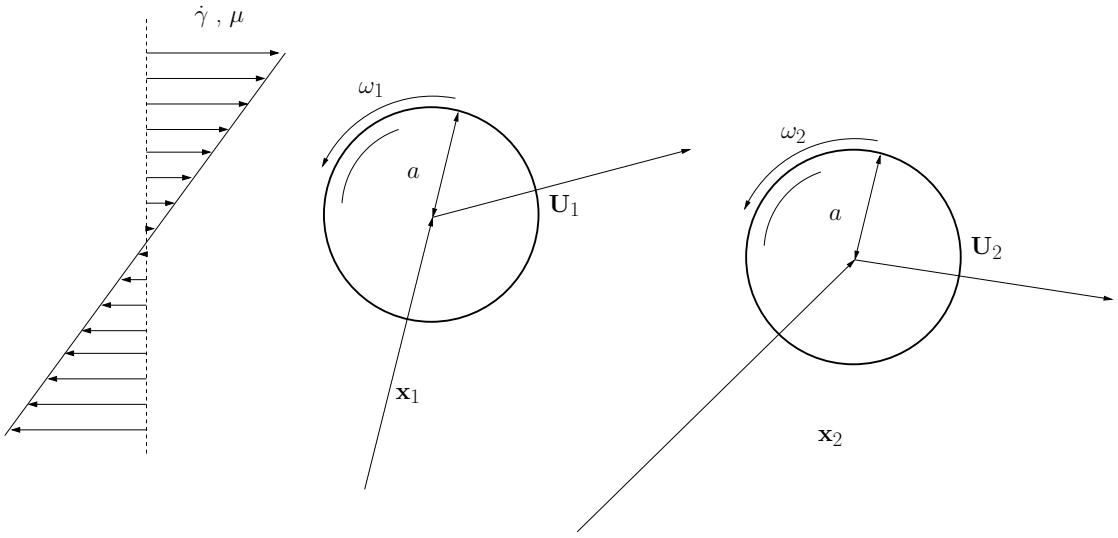

Figure 3.1: Sketch of the problem of two interacting rigid spheres of radius a moving in a fluid with viscosity μ in the presence of an external simple shear flow with shear rate $\dot{\gamma}$. The particles have translational velocity $\boldsymbol{U}$ and angular velocity $\boldsymbol{\omega}$.

Considering the problem of a spherical rigid particle moving in a fluid, the governing equation for the translational motion of the particle is given by Newton's second law, reading:

$$m\frac{d\boldsymbol{U}}{dt} = \boldsymbol{F}_H + \boldsymbol{F}_{NH}, \tag{3.1}$$

where $\boldsymbol{F}_H$ accounts for the hydrodynamic forces and $\boldsymbol{F}_{NH}$ accounts for the non-hydrodynamic forces, such as external fields or field interactions between particles. We introduce the following characteristic scales of the flow problem:

$$\boldsymbol{x} \sim a, \tag{3.2}$$

$$\boldsymbol{U} \sim \dot{\gamma}\ a, \tag{3.3}$$

$$\boldsymbol{F} \sim 6\pi\mu a^2\dot{\gamma}, \tag{3.4}$$

$$t \sim \frac{1}{\dot{\gamma}}, \tag{3.5}$$

where a is the radius of the particle, ρ_s is the density of the particle and $\dot{\gamma}$ is the shear rate. Writing equation (3.1) in nondimensional form, we have:

$$St\frac{d\boldsymbol{U}'}{dt'} = \boldsymbol{F}'_H + \boldsymbol{F}'_{NH}, \tag{3.6}$$

where St is the Stokes' number, defined as

$$St = \frac{2}{9}\frac{\rho_s\dot{\gamma}a^2}{\mu}. \tag{3.7}$$

In addition, the particle Reynolds number is given by $Re = \frac{\rho\dot{\gamma}a^2}{\mu}$. In the case of creeping flow regime, $Re \ll 1$. Since

$$St \sim Re\ \frac{\rho_s}{\rho} \tag{3.8}$$

and $\rho_s/\rho \sim 1$ (*i.e.* Neutrally buoyant condition), we have $St \sim Re \ll 1$. When the Stokes' number is small, we can neglect the inertia term on the *l.h.s.* of equation (3.1)[1], resulting in:

$$0 = \boldsymbol{F}_H + \boldsymbol{F}_{NH}, \tag{3.9}$$

This result gives us an apparent contradiction if we look at the principles of classical mechanics. Originally, we had a second-order differential equation for $\boldsymbol{x}(t)$, which needs two initial conditions in order to have a unique solution: position and

[1]The same procedure can be used to show the negligibility of the rotational inertia by the analysis of a rotational Stokes number

velocity. When we neglect particle inertia, the governing equation for the position $\boldsymbol{x}(t)$ of the particles reduces to a first order differential equation, given by:

$$\frac{d\boldsymbol{x}}{dt} = \boldsymbol{U}, \tag{3.10}$$

which is uniquely satisfied given the initial condition. Actually, there is no contradiction in this problem. In this case, we have a quasi-stationary motion. This phenomenon occurs due to the strong effect of vorticity diffusion on Stokes flow. In fact, the vorticity diffusion time $\tau_\mu = \frac{\rho a^2}{\mu}$ is much smaller than the flow time $\dot{\gamma}^{-1}$, which results in an almost instantaneous relaxation of the flow. Thus, we consider the velocity of the particle to be defined in every time step by just giving the position of the particle, its forces, torques, and external flow by equation (3.9) together with the solution of the flow.

Now, we consider the motion of two particles free of inertia in a quasi-stationary condition. The governing equations for the relative position $\boldsymbol{x} = \boldsymbol{x}_2 - \boldsymbol{x}_1$ and orientation $\hat{\boldsymbol{p}}$ of the particles are given by the first-order evolution equations:

$$\frac{d\boldsymbol{x}}{dt} = \boldsymbol{U} = \boldsymbol{U}_2 - \boldsymbol{U}_1 \tag{3.11}$$

$$\text{and} \quad \frac{d\hat{\boldsymbol{p}}_i}{dt} = \boldsymbol{\omega}_i \wedge \hat{\boldsymbol{p}}_i. \tag{3.12}$$

By the linearity of the Stokes equation, the velocities and angular velocities of the particles are linear functions of the forces, torques and external flow. The most general form of this linear relation is given by [48, 54]:

$$\begin{bmatrix} \boldsymbol{u}^\infty(\boldsymbol{x}_1) - \boldsymbol{U}_1 \\ \boldsymbol{u}^\infty(\boldsymbol{x}_2) - \boldsymbol{U}_2 \\ \boldsymbol{\Omega}^\infty(\boldsymbol{x}_1) - \boldsymbol{\omega}_1 \\ \boldsymbol{\Omega}^\infty(\boldsymbol{x}_1) - \boldsymbol{\omega}_2 \\ \boldsymbol{S}_1/\mu \\ \boldsymbol{S}_2/\mu \end{bmatrix} = \begin{bmatrix} \boldsymbol{a}_{11} & \boldsymbol{a}_{12} & \tilde{\boldsymbol{b}}_{11} & \tilde{\boldsymbol{b}}_{12} & \tilde{\boldsymbol{g}}_1 \\ \boldsymbol{a}_{21} & \boldsymbol{a}_{22} & \tilde{\boldsymbol{b}}_{21} & \tilde{\boldsymbol{b}}_{22} & \tilde{\boldsymbol{g}}_2 \\ \boldsymbol{b}_{11} & \boldsymbol{b}_{12} & \boldsymbol{c}_{11} & \boldsymbol{c}_{12} & \tilde{\boldsymbol{h}}_1 \\ \boldsymbol{b}_{21} & \boldsymbol{b}_{22} & \boldsymbol{c}_{21} & \boldsymbol{c}_{22} & \tilde{\boldsymbol{h}}_2 \\ \boldsymbol{g}_{11} & \boldsymbol{g}_{12} & \boldsymbol{h}_{11} & \boldsymbol{h}_{12} & \boldsymbol{m}_1 \\ \boldsymbol{g}_{21} & \boldsymbol{g}_{22} & \boldsymbol{h}_{21} & \boldsymbol{h}_{22} & \boldsymbol{m}_2 \end{bmatrix} \odot \begin{bmatrix} \boldsymbol{F}_1/\mu \\ \boldsymbol{F}_2/\mu \\ \boldsymbol{T}_1/\mu \\ \boldsymbol{T}_2/\mu \\ \boldsymbol{E}^\infty/\mu \end{bmatrix}, \tag{3.13}$$

where the external strain rate $\boldsymbol{E}^{\infty}$ is a parameter of the problem and $\boldsymbol{a}$, $\boldsymbol{b}$, $\tilde{\boldsymbol{b}}$ and $\boldsymbol{c}$ are second-order tensors; $\boldsymbol{g}$, $\boldsymbol{h}$, $\tilde{\boldsymbol{g}}$ and $\tilde{\boldsymbol{h}}$ are third-order tensors and the quantities labeled by $\boldsymbol{m}$ are fourth-order tensors. These are called mobility tensors. The symbol $\odot$ indicates contraction over the larger number of indices as possible.

For the closure of the problem, one must determine the expressions for the mobility tensors. The mobility tensors are given by the solution of the hydrodynamic problem. Although Stokes' equations are linear, the geometry of the problem can turn the process of finding an analytic solution very hard or almost impossible.

3.2 Exact solution for the problem of two spherical particles in creeping flow

The problem of two rigid spherical particles moving in creeping flow has an exact solution given in terms of bi-spherical harmonics. An outline for this solution can be found in the classical paper of Lin et al. [55]. The authors were able to calculate the exact expressions for the mobilities of two interacting force and torque-free particles.

Although exact solutions are always wanted, there are a few disadvantages of using these expressions for numerical computation, as they are given in terms of infinite series involving Legendre polynomials. As shown by Batchelor & Green [56], these solutions have some convergence problems as the particles are brought close together. In fact, for the regimes when particles are nearby or far apart from each other, it is more advantageous to use asymptotic solutions of the problem. In the next few sections, we describe, concisely, two distinct procedures for obtaining asymptotic expressions for the examined flow problem at the two distinct asymptotic regimes.

3.3 Far-field asymptotics

For the study of particles interacting far away from each other, in far-field

regime ($r \gg 2a$), we apply an asymptotic method known as the method of reflections. This method was first introduced by Smoluchowski [57] and has been used since then in microhydrodynamic simulations. In this section we explain the basic principles the method, which is used in our simulations.

3.3.1 Resistance problem

Consider two particles moving in an infinite fluid which is initially steady. The movement of a single particle with label A produces a disturbance in the fluid flow, with a velocity field $\boldsymbol{u}_1^A(\boldsymbol{x})$ satisfying the following boundary conditions:

$$\begin{cases} \boldsymbol{U}_A & \text{at } \partial D_A \\ \boldsymbol{U}^\infty(\boldsymbol{x}) & \text{for } r \to \infty \end{cases} \tag{3.14}$$

with the same applying for the second particle, labeled B. However, considering the two particles problem, the mere sum of the velocity fields $\boldsymbol{u}_1^A(\boldsymbol{x})$ and $\boldsymbol{u}_1^B(\boldsymbol{x})$ does not satisfy the boundary conditions for any of the two particles.

In order to fix this problem, we introduce the following perturbation scheme in the region next to the particle A:

$$\boldsymbol{u}(\boldsymbol{x}) = \boldsymbol{u}_1^A(\boldsymbol{x}) + \boldsymbol{u}_2^A(\boldsymbol{x}) + \dots . \tag{3.15}$$

In a similar way, in the region next to particle B we have:

$$\boldsymbol{u}(\boldsymbol{x}) = \boldsymbol{u}_1^B(\boldsymbol{x}) + \boldsymbol{u}_2^B(\boldsymbol{x}) + \dots , \tag{3.16}$$

where $\boldsymbol{u}_n^A$ for $n \neq 1$ are velocity fields satisfying the following boundary conditions:

$$\begin{cases} 0 & \text{at } \partial D_A \\ \boldsymbol{u}_{n-1}^B & \text{for } r \to \infty \end{cases} \tag{3.17}$$

Thus, the boundary condition for particle A is satisfied. The force, torque, stresslet and higher order multipoles are given by:

$$\begin{cases} \boldsymbol{F}_H^A = \boldsymbol{F}_1^A + \boldsymbol{F}_2^A + \dots \\ \boldsymbol{T}_H^A = \boldsymbol{T}_1^A + \boldsymbol{T}_2^A + \dots \\ \boldsymbol{S}^A = \boldsymbol{S}_1^A + \boldsymbol{S}_2^A + \dots \\ \dots \end{cases} \tag{3.18}$$

These poles can be calculated by using Faxén's laws. The recursive nature of this method can be noticed by the boundary conditions. The velocity field $\boldsymbol{u}_1^A$ generates a boundary condition at the infinity for the velocity field $\boldsymbol{u}_2^B$. On the other hand, $\boldsymbol{u}_2^B$ gives the boundary condition for the velocity field $\boldsymbol{u}_3^A$ and so on.

Thus, the odd pertubations of the force of particle A are the ones which depend on the velocity of the particle itself. The even perturbations are the ones due to the velocity of particle B. The steps to obtain the perturbation terms of the forces are the following:

- Calculate $\boldsymbol{u}_1^A(\boldsymbol{x})$
- Calculate $(\boldsymbol{F}_2^B, \boldsymbol{T}_2^B, \boldsymbol{S}_2^B, \dots)$ using Faxén's laws
- Calculate $\boldsymbol{u}_2^B(\boldsymbol{x})$ by the multipole expansion
- Repeat the procedure

3.3.2 Mobility problem

In contrast with the resistance problem, the boundary conditions for the velocity of the particles in the mobility problem are unknown. This is due to the fact that the governing equation for the particle position is a first order differential equation and has only the position as initial condition. In the case of the mobility problem, we have:

$$\boldsymbol{F}_H = -\boldsymbol{F}_{NH} \tag{3.19}$$

$$\boldsymbol{T}_H = -\boldsymbol{T}_{NH} \tag{3.20}$$

Now, we introduce a perturbation in the force of the particle A, where:

$$\boldsymbol{F}_H^A = \boldsymbol{F}_1^A + \boldsymbol{F}_2^A + \ldots, \tag{3.21}$$

so that:

$$\begin{cases} \boldsymbol{F}_1^A = -\boldsymbol{F}_{NH} \\ \boldsymbol{F}_2^A = \boldsymbol{F}_3^A = \cdots = 0 \end{cases} \tag{3.22}$$

The same is done for the torques and its valid for particles A and B. Here the recursive method to obtain the velocities of the particles is slightly different. We introduce a perturbation scheme in the velocity, given in the case of particle A by:

$$\boldsymbol{U}^A = \boldsymbol{U}_1^A + \boldsymbol{U}_2^A + \ldots \tag{3.23}$$

In this case, $\boldsymbol{U}_1^A$ and the field $\boldsymbol{u}_1^A$ are determined by the single particle problem with the constraints of the force, torque and uniform velocity at the surface of the particle. The subsequent terms $\boldsymbol{U}_k^A$ and $\boldsymbol{u}_k^A$ are determined by a single particle problem with force and torque free conditions and the flow at infinity given by $\boldsymbol{u}_{k-1}^B$.

3.4 Near-field asymptotics

For the investigation of the hydrodynamic interaction between two spherical particles when they are close to each other, the lubrication theory provides the leading order and the further corrections for the mobility functions due to the interaction between them. The whole method of solution, including the calculations, is explained step by step in [48].

The approach to find the near-field mobilities is to consider the general movement of two close particles as a superposition of three types of motion: Shear, squeezing and rotating. Every other configuration can be written as a superposition of these. Each of these problems can be solved asymptotically in the region

with small values of separation, considering the value $\xi = (r - a - b)/a$ of the minimal gap between the spheres to be very small. The main idea of the method is to expand the velocities and pressure fields in an asymptotic series on ξ, simplifying the problem.

Details of the solution can be found in the book by Kim & Karrila's book [48]. The compilation of all the expressions for the different types of mobilities in the case of two spheres of the same size can be found on the Appendix II of this work. These were extracted from the tables found in the book by Kim & Karrila [48], with results originally due to Jeffrey and Onishi [54], and were modified in order to fit this work.

3.5 Nondimensionalization of the equations of motion

When dealing with the simulation of physical problems, it is often more apropriate to use nondimensional quantities. For the nondimensionalization of the set of equations representing the two-particle model here, we use the following appropriated scales:

$$|\boldsymbol{x}| \sim a \tag{3.24}$$

$$t \sim \dot{\gamma}^{-1} \tag{3.25}$$

$$|\boldsymbol{F}| \sim 6\pi\mu\dot{\gamma}a^2 \tag{3.26}$$

$$|\boldsymbol{T}| \sim 8\pi\mu\dot{\gamma}a^3 \tag{3.27}$$

For the investigation of the magnetic interaction between two particles, we consider the approximation of dipole-dipole interaction. In this case, the forces and torques between two-particles are given by the expressions presented in section 2.8. Substituting the dimensional variables by the nondimensional ones, the expressions for the magnetic forces and torques written in terms of non-dimensional quantities result, respectively, in

$$\boldsymbol{F}_2^M = \frac{\alpha}{r^4}\left[(\hat{\boldsymbol{p}}_1\cdot\hat{\boldsymbol{p}}_2)\,\hat{\boldsymbol{r}} + (\hat{\boldsymbol{p}}_1\cdot\hat{\boldsymbol{r}})\,\hat{\boldsymbol{p}}_2 + (\hat{\boldsymbol{p}}_2\cdot\hat{\boldsymbol{r}})\,\hat{\boldsymbol{p}}_1 - 5\,(\hat{\boldsymbol{p}}_1\cdot\hat{\boldsymbol{r}})\,(\hat{\boldsymbol{p}}_2\cdot\hat{\boldsymbol{r}})\,\hat{\boldsymbol{r}}\right] \tag{3.28}$$

$$\boldsymbol{T}_2^M = \frac{3\alpha}{4r^3}\left[-\frac{1}{3}\hat{\boldsymbol{p}}_2\wedge\hat{\boldsymbol{p}}_1 + (\hat{\boldsymbol{p}}_2\wedge\hat{\boldsymbol{r}})\,(\hat{\boldsymbol{p}}_1\cdot\hat{\boldsymbol{r}})\right], \tag{3.29}$$

where

$$\alpha = \frac{\mu_0 m_0^2}{8\pi^2\mu a^6\dot{\gamma}}. \tag{3.30}$$

The nondimensional parameter α represents the intensity of the dipolar interaction between particles in the homogeneous suspension. Therefore, by substituting equations (3.28) and (3.29) in equation (3.13), we obtain the equations of motion governing the dynamics of the two-particle problem.

3.6 Numerical simulation

For the numerical simulation of the motion of the two particles, we have used a 4th order Runge-Kutta method with an adaptive time step. The algorithm of the FORTRAN code used for performing the dynamical simulation of two spheres undergoing a simple shear flow in the presence of hydrodynamic and magnetic interactions is presented in Figure 3.2.

The implementation of an adaptative time step is made necessary when the particles get very close to each other during the motion. In order to implement that feature we first chose a value greater than unity for the variable **AMP** and a value for a reference time step **H0** so the time step **H** is equal to **MIN(GAP/AMP,H0)**, where **GAP** is the gap between the two particles. This method by itself has a clear disadvantage, due to the fact that some trajectories require greater values for **AMP** than others. Thus, the simulation of many different trajectories using the single value of **AMP** required for the simulation of the closest trajectories would demand a large computational time.

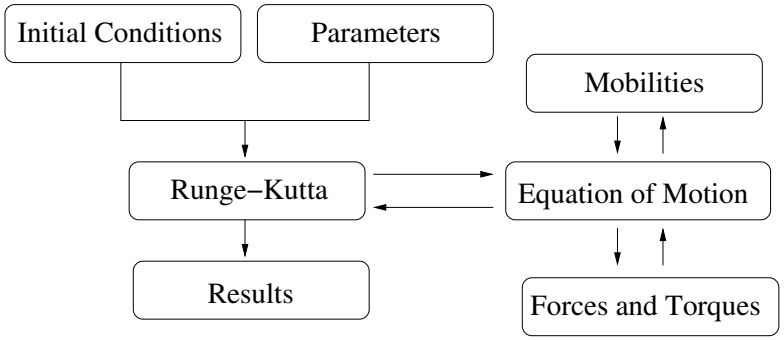

Figure 3.2: Sketch of the algotithm used for the numerical simulation of two particles interacting magnetically and hydrodynamically in creeping flow.

In order to reduce the computational time, we set an inicial value for **AMP** before the Runge-Kutta loop. Before the calculation of the $(i+1)^{\text{th}}$ step, we verify the possibility of overlap during the process of the next time step. If an overlap is detected, the value of **AMP** is doubled and the procedure for the current time step is redone.

For the simulation, we have broke the problem into three different regions, in which we use different expressions for mobilities. These regions are the far-field, near field and matching regions as shown in figure 3.3.

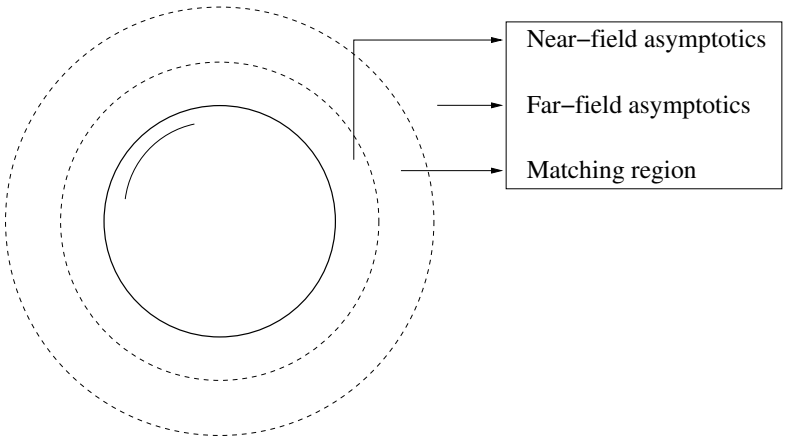

Figure 3.3: Different mobility regimes

For the far-field and near-field regions we used the mobility expressions in Kim & Karrila [48]. These expressions can be found on Appendix II. For the matching

region we used a polynomial fit of the analytical solution by Lin [55].

3.7 Validation of the code

One of the consequences of the linearity of Stokes equations is the kinematic reversibility in the movement of an isolated rigid particle. This kinematic reversibility holds for the relative trajectory in the interaction of two spherical particles without field interactions between them. Figure 3.4 shows the simulation for two perfect spheres, illustrating this symmetry.

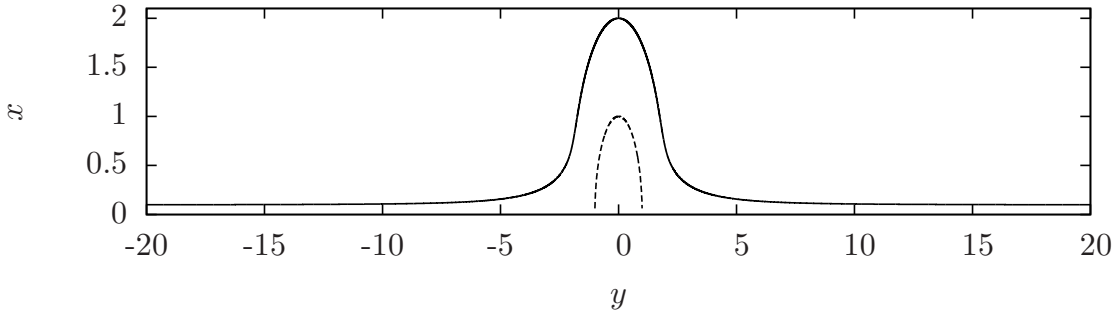

Figure 3.4: Symmetry in the relative motion of a spherical rigid particle undergoing a simple shear flow in the absence of magnetic interactions. The dashed line indicates the position and size of the reference particle. The initial relative position of the test particle is $\boldsymbol{x}^{-\infty} = (-20, 0.1, 0)$.

One of the ways to test the validation of the numerical simulation of the motion of two non-magnetic spheres undergoing a simple shear flow is to verify if the code maintains this trajectory symmetry after a large number of collisions. For this test, we imposed a periodic boundary condition at $x = \pm 20$. The result is shown in Figure 3.5. The same results were obtained by Cunha and Hinch [16].

We have also validated the code for the case of force-free and torque-free particles by using the asymptotic solution developed in the paper by Cunha and Hinch [16]. Here, we describe some details of this asymptotic solution.

The governing equation of the motion of a test particle relative to a reference particle in a simple shear flow is given in coordinates by [56]:

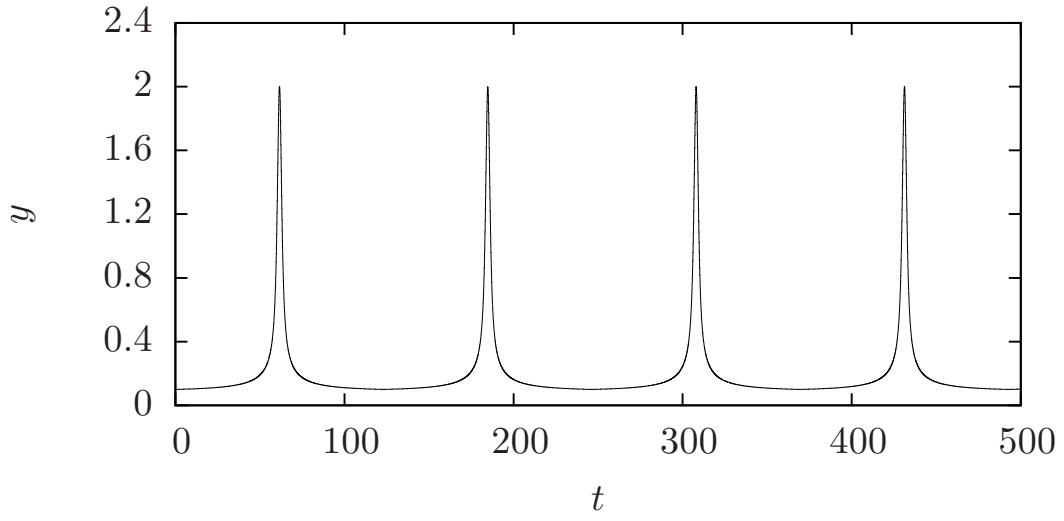

Figure 3.5: Test of the kinematical reversibility in periodic trajectories for a large number of colisions. The initial relative position of the test particle is $\boldsymbol{x}^{-\infty} = (-20, 0.1, 0)$.

$$\begin{aligned}
\dot{x} &= y + ex - \frac{1}{2}By, \\
\dot{y} &= ey - \frac{1}{2}Bx, \\
\dot{z} &= ez,
\end{aligned}$$

where $e = xy(B - A)/r^2$ and A and B are the shear mobilities. For the regime when $x \gg 1$, where the particles are far apart from each other, we can obtain an asymptotic expression for the trajectories. At leading order we have $x \sim x_0 + y_0 t$, $y \sim y_0$ and $z \sim z_0$. By recursion, collecting the next order terms and using the fact that $A \sim \frac{5}{r^3}$ and $B \sim \frac{16}{3r^5}$, we obtain for the next order:

$$\dot{y} \sim -\frac{(x_0 + y_0 t)(5y_0^2 + \frac{8}{3})}{[(x_0 + y_0 t)^2 + y_0^2 + z_0^2]^{5/2}} \tag{3.31}$$

$$\dot{z} \sim -\frac{5y_0 z_0 (x_0 + y_0 t)}{[(x_0 + y_0 t)^2 + y_0^2 + z_0^2]^{5/2}}. \tag{3.32}$$

By performing a simple integration in t, we find the following expressions for

the extrapolation of positions:

$$y^{\infty} \sim y + \frac{r^2 \dot{y}}{3x\dot{x}} \tag{3.33}$$

$$z^{\infty} \sim z + \frac{r^2 \dot{z}}{3x\dot{x}} \tag{3.34}$$

These approximations are valid for $x \gg 1$, $y \sim \mathcal{O}(1)$ and $z \sim \mathcal{O}(1)$. We can also derive an asymptotic expression for positions for the case where $y \ll 1$. In this case, the velocities take the form of:

$$\dot{y} \sim -\frac{8}{3} x \left(x^2 + z^2\right)^{-5/2}, \tag{3.35}$$

$$\dot{z} \sim 0. \tag{3.36}$$

Hence, by simple integration, we find the following expressions for y^{∞} and z^{∞}:

$$y^2 \sim (y^{\infty})^2 + \frac{16}{9} \left(x^2 + z^2\right)^{-3/2} \tag{3.37}$$

$$z \sim z^{\infty} \tag{3.38}$$

We can use these asymptotic expressions for extrapolate the trajectories in order to obtain the end positions of the particles. They, however, cannot be used even for magnetic interacting particles, due to the fact that the velocity term due to the magnetic dipole interaction is of order $\mathcal{O}(r^{-4})$, which is of the same order or bigger than the shear terms.

Figure 3.6 shows a comparison between the numerical simulation of a particle starting at $x = -500$ with the asymptotic expression for small y, at an interval $[-500, -100]$ and a time step of $h = 0.01$, the deviation between the two trajectories is of order $\mathcal{O}(10^{-5})$. The very good agreement between numerical and asymptotic solutions reinforces the validity of the numerical simulation for the case of force and torque free particles.

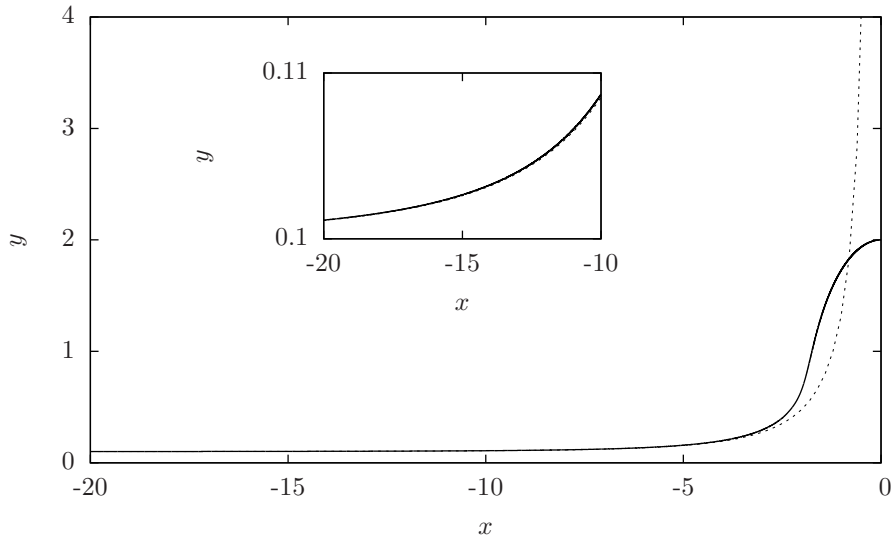

Figure 3.6: Comparison of the numerical simulation results (solid line) with the asymptotic prediction (dashed line) for a particle coming from $x = -500$, $y = 0.1$ and $z = 0$. The insert in the plot shows details of the region where the asymptotic solution works.

3.8 Symmetry breaking and scatter sections

The kinematic revesibility in the creeping flow motion of two sperical interacting particles can be broken by the introduction of some extra effect during particle collision such as particle roughness [16], the presence of a third particle [28], deformability of the particles [19], non-sphericity of the particles [17] or a field interaction between the particles [20, 21]. In this dissertation, we investigate the symmetry breaking in the case of two magnetic particles interacting hydrodynamically and magnetically in the presence of a simple shear flow.

In the case of symmetry breaking, the particle undergoes a displacement from its original trajectory. In order to visualize the displacement from the original trajectories due to the dipolar interaction between particles, we plot a *scatter section*, which shows the deviation from the reversible trajectories for multiple particles with the same initial orientations and different initial positions. The main idea of this scatter sections is illustrated by Fig 3.7.

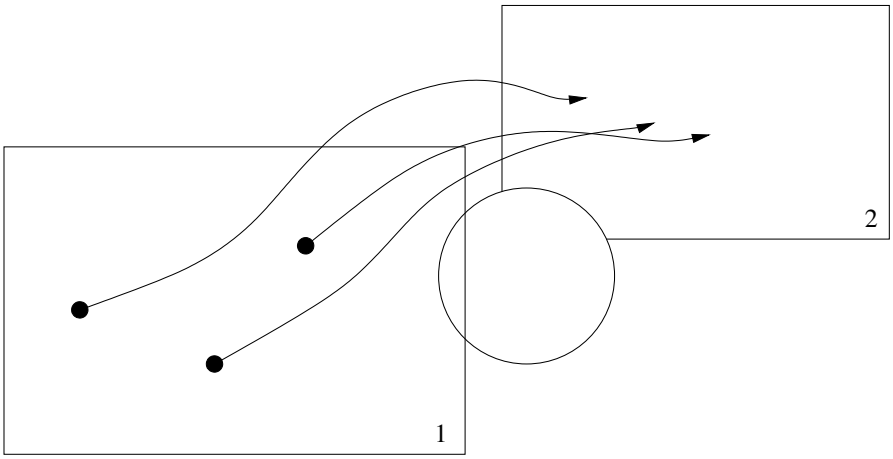

Figure 3.7: Concept of a scatter section: Given an initial pair of orientations, we consider the flux of all possible relative particle trajectories which start in the plane 1 at $x = x^{-\infty}$. The scatter section displays the transverse endpoints of the trajectories as they cross the plane 2 at $x = x^{\infty}$ after the collision with the reference particle at the origin. As we consider the domain to be periodic on x, the plot may also display the transverse endpoints of trajectories which cross the plane 1 after the collision with the reference particle.

These scatter sections provide a qualitative view for dispersive open trajectories. Scatter sections have already appeared in the works of Cunha & Hinch [16], Loewenberg & Hinch [19], Cunha & Couto [20, 36], and Cunha, Gontijo & Sobral [21].

In the present context of magnetic particles, the dynamics depend strongly on the orientation of the particles. Thus, in a simple shear flow, as the flow tries to rotate the particles at every time, the scatter sections are quite different from the ones found previously by Cunha & Couto [20, 36] and Cunha & Gontijo & Sobral [21] in the context of sedimenting magnetic particles.

Figure 3.8 shows the scatter section obtained by numerical simulation for $\alpha = 0.5$, $\hat{\boldsymbol{p}}_1 = (1, 0, 0)$ and $\hat{\boldsymbol{p}}_2 = (1/\sqrt{2}, 1/\sqrt{2}, 0)$ for particles starting at the first and second quadrants. By examining the results displayed on Figure 3.8, one can observe three different kinds of behavior for the open trajectories. Namely, there are particles with both positive and negative y and $z-$displacements. In particular, some of the particles have their end trajectories on the third or fourth quadrants.

For values of y greater than 2.5, there is almost no observable displacement of the particles.

Furthermore, Figure 3.9 depicts another scatter section for $\alpha = 0.5$, $\hat{\boldsymbol{p}}_1 = (1, 0, 0)$ and $\hat{\boldsymbol{p}}_2 = (1/\sqrt{3}, 1/\sqrt{3}, 1/\sqrt{3})$. The result displayed in Figure 3.9 shows the symmetry breaking between quadrants 1 and 2 due to the asymmetry of the initial orientations.

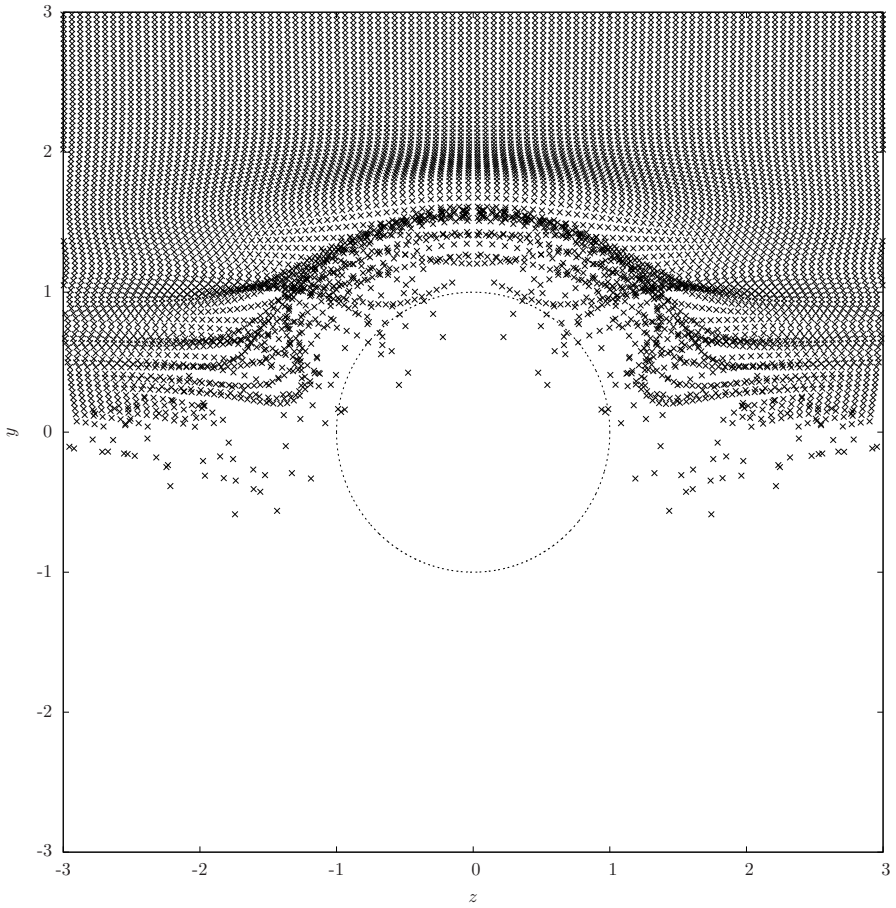

Figure 3.8: Scatter diagram for $\alpha = 0.5$ with initial relative position $x^{-\infty} = -20$ and symmetrical initial orientations $\hat{\boldsymbol{p}}_1 = (1, 0, 0)$ and $\hat{\boldsymbol{p}}_2 = (1/\sqrt{2}, 1/\sqrt{2}, 0)$.

Both scatter sections displayed in Figures 3.8 and 3.9, obtained by the simulation of a pair of magnetic particles undergoing a simple shear flow, show multiple trajectories ending at the third and fourth quadrants of the zy plane. At a first glimpse this does not seem to make much sense, since the negative y quadrants

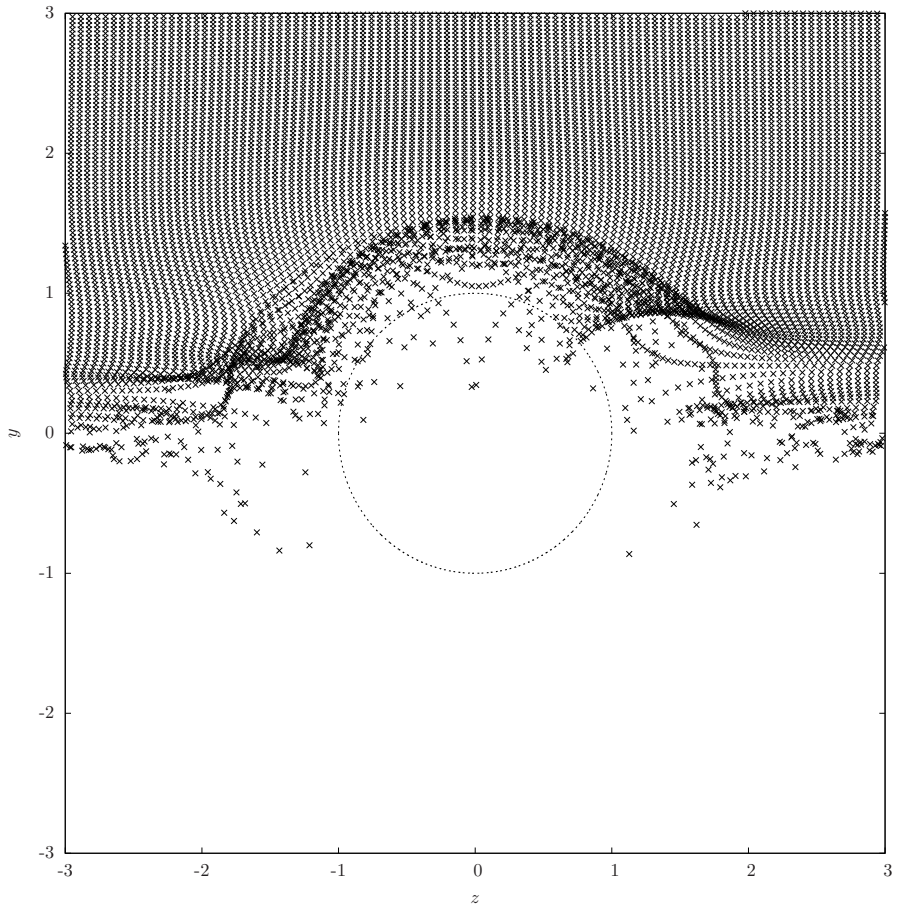

Figure 3.9: Scatter diagram for $\alpha = 0.5$ with initial relative position $x^{-\infty} = -20$ and symmetrical initial orientations $\hat{\boldsymbol{p}}_1 = (1, 0, 0)$ and $\hat{\boldsymbol{p}}_2 = (1/\sqrt{3}, 1/\sqrt{3}, 1/\sqrt{3})$. It can be noticed that the image is not symmetric due to asymmetric initial conditions.

constitute the region where the shear velocity is negative. However, by further inspection, we observe that those negative end positions appear in the form of orbital trajectories on the relative motion due to the magnetic interaction between the particles. These interactions may cause the test particle to cross the plane 1 at $x^{-\infty}$ instead of the plane 2. Figure 3.10 shows some examples of trajectories with end positions at the third or fourth quadrants (*i.e.* negative y).

Trajectories such as these are very common in the context of non-linear dynamical systems. Although the relative trajectories in the context of smooth spherical

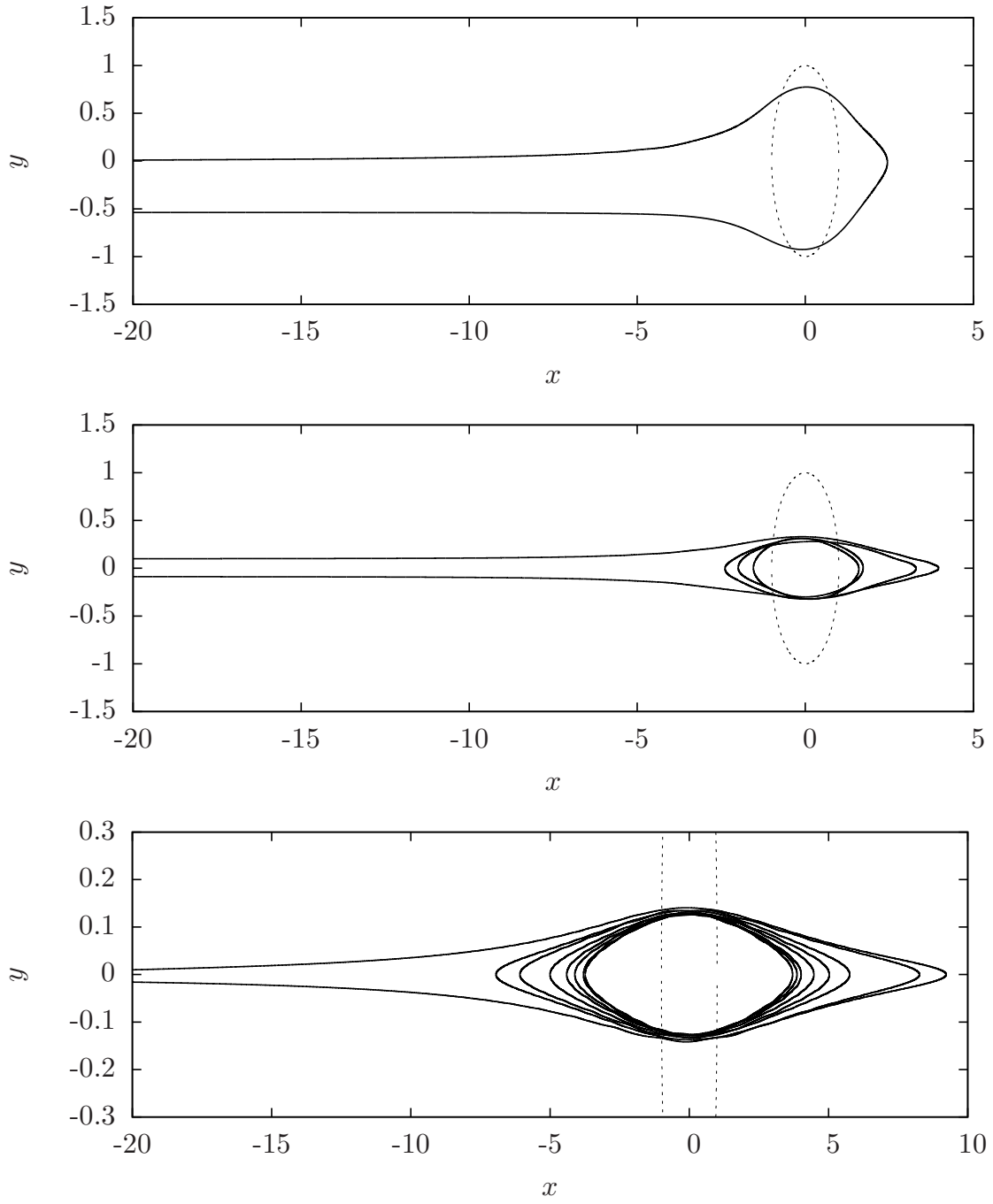

Figure 3.10: Examples of irreversible open trajectories with negative end positions in the y direction (*i.e.* third and fourth quadrants).

rigid particles undergoing a simple shear flow are symmetric [56], the particle collision in our context is perturbed by the presence of the magnetic interaction between the particles. Consequently, it originates these orbital and sometimes seemingly chaotic[2] trajectories.

Another test performed in order to characterize these trajectories was tracking the evolution of particle displacement after several collisions. This concept is very similar to the one of a Poincaré section in the context of dynamical systems [58]. With this end, we incorporate a periodic condition on the x axis. By using this condition, we have ploted the end points of successive collisions in the yz plane.

Figures 3.11 and 3.12 show these plots for the cases of $y = 1.01, z = 1.0$ and $y = 2.01, z = 1.0$ respectively with the initial orientations $\hat{\boldsymbol{p}}_1 = (1, 0, 0)$ and $\hat{\boldsymbol{p}}_2 = (1/\sqrt{2}, 1/\sqrt{2}, 0)$ for the first 10^5 collisions and given values of α. For $\alpha = 0$, the graph displays only a single point, as expected from periodic trajectories due to the Stokes' reversibility.

Although the two figures show results for different initial conditions and magnetic interaction intensity α, there are similarities in the patterns found by the simulations. In the results shown on Figures 3.11(a), 3.11(b) and 3.12(a), no aggregation occurred before 10^6 collisions. An exception was the case illustrated on Figure 3.12(b), where the particles aggregated after 5703 collisions.

3.9 Aggregative trajectories

Due to the magnetic dipole interaction between the spheres, some initial conditions may result in particle aggregation, forming a doublet. In this work, we also compute the rate at which these doublets are formed. In chapter 5, we show that this rate depends on an integral over all closed irreversible aggregative trajectories.

In order to visualize qualitatively the region containing all the aggregative trajectories for different initial conditions on phase space, we present the plot of

[2]In this work, we have not performed any type of test to measure the chaotic behavior of the system, such as the computation of Lyapunov exponents or a value for the system's entropy.

a typical *aggregative section* of the examined system. This concept is very similar to the one of a basin of attraction, which appears very frequently in the context of dynamical systems and it is usually defined as the region on the phase space which will be attracted to some attractor [58]. In fact, the particle centered at the origin can be thought of as an attractor. In this case, where the phase space is 7-dimensional, only two-dimensional sections of the basin of attraction can be plotted. Therefore, the aggregative section is a two-dimensional section of the basin of attraction for a fixed pair of orientations and an initial $x-$position.

In these plots, the area in black represents the starting positions in the plane in which particles aggregate and the white area of the plane represents the starting positions in the plane in which the particles do not aggregate. We denote the area in black by the name of *aggregative region*, or the region of closed trajectories, and the area in white as the *dispersive region*, or the region of open trajectories. Figure 3.13 shows multiple sections of the basin of attraction at $x^{-\infty} = -20$ for different pairs of initial orientations.

It is interesting to note that the aggregative collisional area is not simply connected, like in the relative trajectories of a two-particle system in sedimentation [36]. This remarkable difference is a direct consequence of the vorticity of the external shear flow acting on the particles together with the high sensibility of the system on particle orientation. In particular, the observed aggregative regions are very irregular, appearing to present some fractal structure at the interface with the dispersive region, as seen in Figure 3.15. This non-linear response characterized by the observed non-regular geometry is related to the strong sensibility of the problem on its initial conditions. This kind of behavior is quite typical in the context of non-linear dynamical systems.

A mirror symmetry on the $y-$axis can be observed on the patterns shown in Fig 3.13 due to symmetric initial orientations with respect to the $y-$axis. This picture is a bitmap in which every pixel corresponds to a different trajectory. The dark-colored points represent a region containing starting positions resulting in aggregative trajectories, whereas, the white points represent a region which contains the starting positions which lead to dispersive trajectories. In the same

way that the symmetry of the scatter section is broken by asymmetric initial conditions, the same is valid for these sections of the basin of attraction. Actually, by giving asymmetric initial orientations with respect to the $y-$axis, the reflection symmetry no longer holds. Figure 3.14 shows the asymmetric patterns that arise from non-symmetrical initial conditions for orientation.

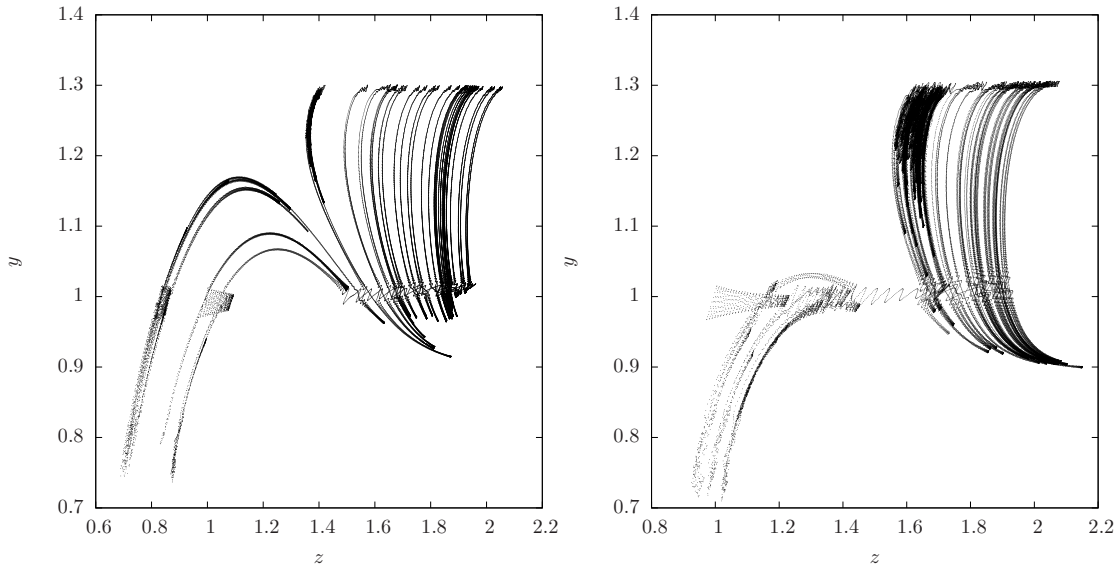

(a) $\alpha = 0.005$ (b) $\alpha = 0.010$

Figure 3.11: Transverse positions at the end of each cycle of the trajectory of particle 2 starting at $y = 1.01$ and $z = 1.0$ with the pair of initial orientations $\hat{\boldsymbol{p}}_1 = (1, 0, 0)$ and $\hat{\boldsymbol{p}}_2 = (1/\sqrt{2}, 1/\sqrt{2}, 0)$ after 10^5 collisions. Figure (a) is the case where $\alpha = 0.005$. In Figure (b), $\alpha = 0.010$.

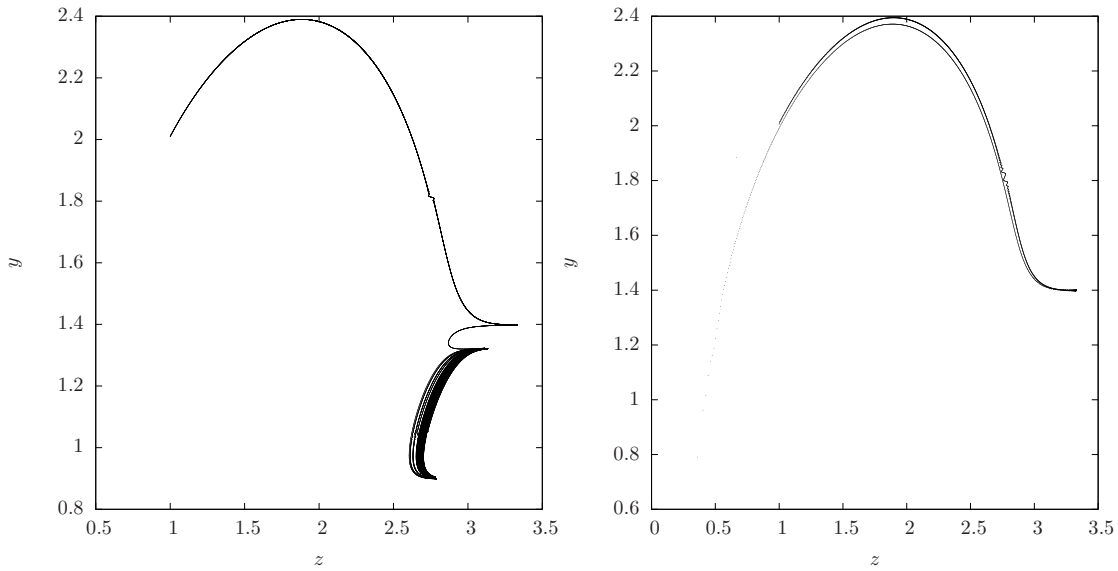

(a) $\alpha = 0.010$ (b) $\alpha = 0.050$

Figure 3.12: Transverse positions at the end of each cycle of the trajectory of particle 2 starting at $y = 2.01$ and $z = 1.0$ with the pair of initial orientations $\hat{\boldsymbol{p}}_1 = (1, 0, 0)$ and $\hat{\boldsymbol{p}}_2 = (1/\sqrt{2}, 1/\sqrt{2}, 0)$ after 10^5 collisions. Figure (a) is the case where $\alpha = 0.010$. In Figure (b), $\alpha = 0.050$.

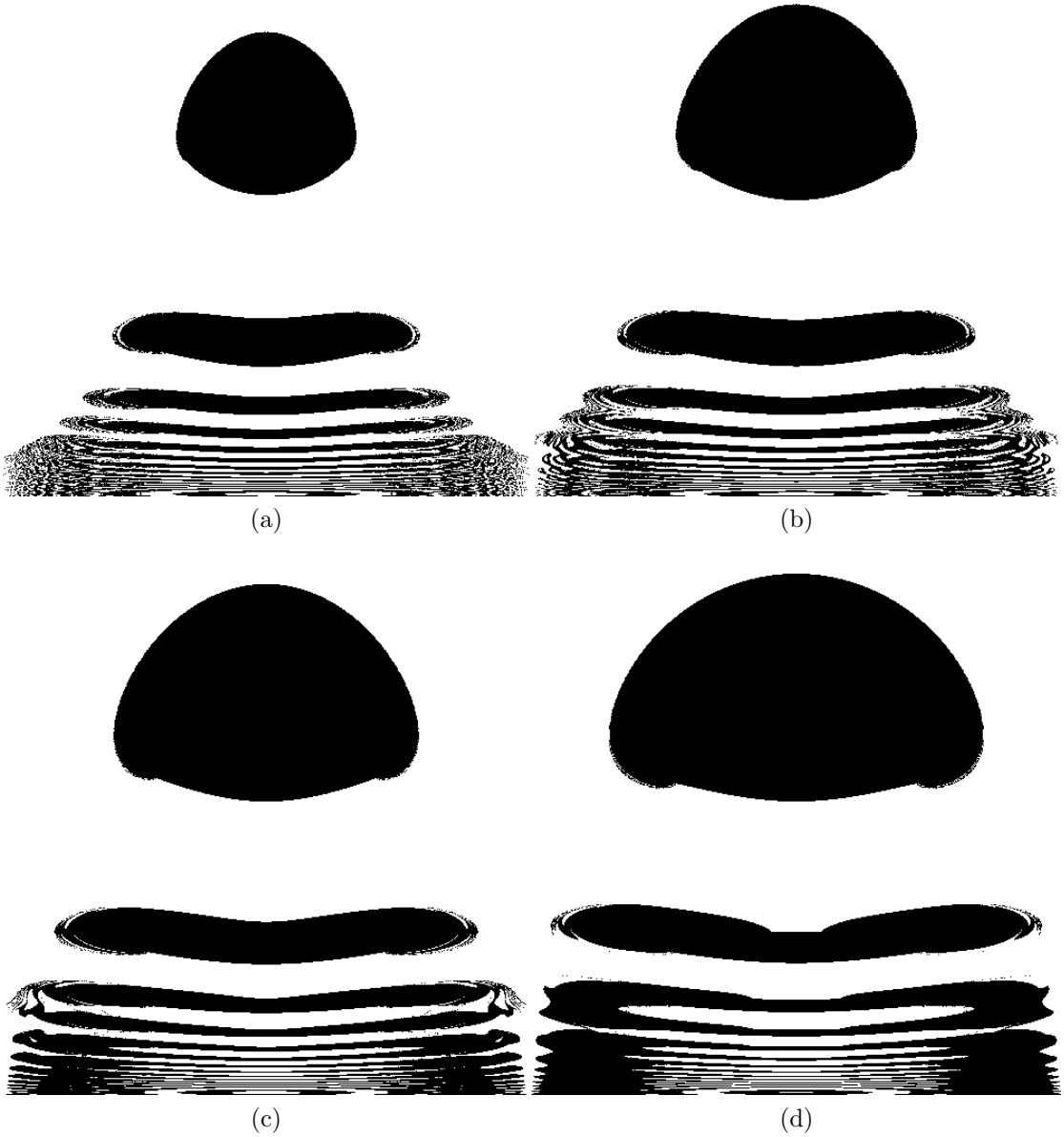

Figure 3.13: Sections from the basin of attraction showing different paterns for aggregation area. All figures consider initial orientations $\hat{\boldsymbol{p}}_1 = (1, 0, 0)$ and $\hat{\boldsymbol{p}}_2 = (1/\sqrt{2}, 1/\sqrt{2}, 0)$ for different magnetic interaction parameters. (a) $\alpha = 0.25$, (b) $\alpha = 0.5$, (c) $\alpha = 1.0$, (d) $\alpha = 2.0$.

(a) (b)

Figure 3.14: Symmetry breaking of aggregative sections due to asymmetric initial conditions. All figures consider initial orientations $\hat{\boldsymbol{p}}_1 = (1, 0, 0)$ and $\hat{\boldsymbol{p}}_2 = (1/\sqrt{3}, 1/\sqrt{3}, 1/\sqrt{3})$ for different magnetic interaction parameters. (a) $\alpha = 0.5$ and (b) $\alpha = 1.0$, .

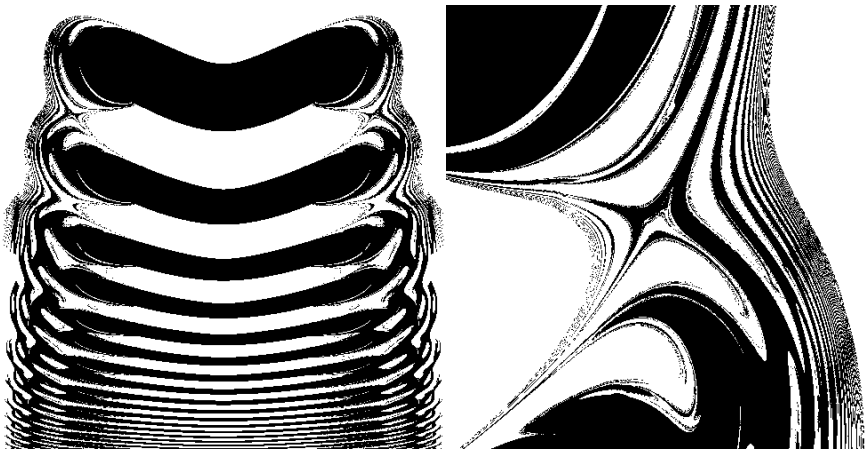

(a) (b)

Figure 3.15: Detail of the aggregative section for $\alpha = 0.5$. The black region represents the aggregative area on the collisional plane for a given pair of initial orientations. Figure (a) shows the region in which $z \in [-2.6, 2.6]$ and $y \in [10^{-3}, 0.3]$. (b) shows the detailed zoom of the region in which $z \in [1.2, 2.4]$ and $y \in [0.2, 0.25]$

CHAPTER 4

HYDRODYNAMIC DIFFUSION

In this chapter we discuss the main points concerning diffusive phenomena. We introduce the phenomenon of shear-induced hydrodynamic diffusion, deriving the expressions for calculating the shear-induced self-diffusivity and down-gradient diffusivity in the context of a dilute non-Brownian monodisperse suspension. The expressions are given in terms of integrals over all dispersive (i.e. open) trajectories. In addition, we use our numerical simulation of two particles in order to obtain numerical values for the shear-induced hydrodynamic self-diffusivities and down-gradient diffusivities for a dilute non-Brownian suspension of spherical rigid particles undergoing a simple shear flow in the presence of dipole-dipole magnetic interactions between the particles.

4.1 General diffusive phenomena

Diffusion is a macroscopic phenomenon that comes from statistical averages of random phenomena at smaller scales, causing the dispersion of some property. Examples of diffusive processes are the conduction of heat and molecular diffusion, where particles tends to spontaneously spread out through the space.

Unlike "ordinary" diffusive phenomena, which have their origins on the molecular level, hydrodynamic diffusion arises in the same scale of the particles as a consequence of the symmetry breaking on particle-particle interactions. The displacement across the streamlines due to irreversible particle collisions creates a random walk across the streamlines, due to the randomness of particle collisions. This random walk yields a self-diffusion of the particle [23].

In this section, we discuss the formulation of diffusive phenomena in a general context. Later, in subsequent sections, we apply the ideas developed here in order to investigate hydrodynamic diffusive phenomena in the context of a dilute magnetic suspension of non-Brownian spherical particles.

We start by the the equation of balance of a component ϕ in a material volume $V(t)$. The equation reads:

$$\frac{d}{dt}\int_{V(t)} \phi(\boldsymbol{x},t)dV = -\int_{S(t)} \hat{\boldsymbol{n}}\cdot\mathfrak{F}dS + \int_{V(t)} h\ dV, \tag{4.1}$$

where $\mathfrak{F}$ is the flux of particles going inside the volume $V(t)$ and h is the source volumetric distribution. The source or sink term can represent, for example, the formation of aggregates or chemical reactions. For the case where the diffusive phenomenon is generated by a random process which does not depend on particle volume fraction, considering the linear dependence between the flux and $\nabla\phi$, the net flux of particles going inside $V(t)$ can be formally written as:

$$\mathfrak{F} = -\int_0^t dt' \int d\boldsymbol{x}'\mathscr{D}(\boldsymbol{x}-\boldsymbol{x}',t-t')\cdot\nabla\phi(\boldsymbol{x}',t') \tag{4.2}$$

In the case where the flux is determined only by the instantaneous concentra-

tion gradient at the point, we have the integration kernel tensor $\mathscr{D}(\boldsymbol{x}-\boldsymbol{x}', t-t')$ given by:

$$\mathscr{D}(\boldsymbol{x}-\boldsymbol{x}', t-t') = \delta(t-t')\delta(\boldsymbol{x}-\boldsymbol{x}')\boldsymbol{\mathcal{D}}(\boldsymbol{x}', t'). \tag{4.3}$$

Thus, the net flux of particles is given by:

$$\mathfrak{F} = -\boldsymbol{\mathcal{D}}(\boldsymbol{x}, t)\cdot\nabla\phi, \tag{4.4}$$

where the tensor $\boldsymbol{\mathcal{D}}$ is called the *gradient diffusivity tensor*. This linear dependence between the flux and the volume concentration gradient is the general form of Fick's law. The material is not necessarily homogeneous nor isotropic, since $\boldsymbol{\mathcal{D}}$ is a second-order tensor which can have explicit dependence on the space. This law is a specific case of more general linear relations between thermodynamic forces and fluxes. Hence, by applying the Reynolds' transport theorem and the localization theorem, the governing differential equation for ϕ is given by:

$$\frac{\partial\phi}{\partial t} + \nabla\cdot(\phi\boldsymbol{u}) = \nabla\cdot(\boldsymbol{\mathcal{D}}(\boldsymbol{x}, t)\cdot\nabla\phi) + h(\boldsymbol{x}, t). \tag{4.5}$$

As we shall see, the terms $\boldsymbol{\mathcal{D}}$ and h can be generalized in order to consider dependences on the concentration ϕ.

4.1.1 Diffusive phenomena with spatial and temporal homogeneity

We start this section by performing a simple derivation of the well-known Fokker-Planck equation for the probability density $P(\boldsymbol{X}, t)$ considering temporal and spatial homogeneity[1]. By the definition of conditional probability density, we have

[1] A more general alternative derivation using a stochastic differential equation for the evolution of the stochastic process $\boldsymbol{X}_t$ and the equation of conservation of probability (2.102) can be found in Zwanzig's book [50].

$$P(\boldsymbol{X}, t+h) = \int d\boldsymbol{Y} P(\boldsymbol{X}, t+h|\boldsymbol{Y}, t) P(\boldsymbol{Y}, t), \tag{4.6}$$

where the integral is performed over all the phase space. By the time homogeneity of the process, we have:

$$P(\boldsymbol{X}, t+h|\boldsymbol{Y}, t) = P(\boldsymbol{X}, h|\boldsymbol{Y}). \tag{4.7}$$

Considering also space homogeneity, we have:

$$P(\boldsymbol{X}, h|\boldsymbol{Y}, 0) = P(\boldsymbol{W}, h), \tag{4.8}$$

where $\boldsymbol{W} = \boldsymbol{X} - \boldsymbol{Y}$. Thus, by substituting equations (4.7) and (4.8) at equation (4.6), we obtain:

$$P(\boldsymbol{X}, t+h) = \int d\boldsymbol{W}\ P(\boldsymbol{W}, h) P(\boldsymbol{X} - \boldsymbol{W}, t). \tag{4.9}$$

By performing a Taylor expansion at the neighborhood of $\boldsymbol{X}$, $P(\boldsymbol{X} - \boldsymbol{W}, t)$ can be expressed as:

$$P(\boldsymbol{X} - \boldsymbol{W}, t) = P(\boldsymbol{X}, t) - \boldsymbol{W} \cdot \nabla P + \frac{1}{2} \boldsymbol{W}\boldsymbol{W} : \nabla\nabla P + \ldots \tag{4.10}$$

Therefore, by ignoring terms greater than second order, substituting equation (4.10) on (4.9), dividing the equation by h, taking the limit as $h \to 0$ and using the definition of a time derivative, we have

$$\frac{\partial P}{\partial t} + \boldsymbol{\mathcal{V}} \cdot \nabla P = \boldsymbol{\mathcal{D}} : \nabla\nabla P. \tag{4.11}$$

where the terms $\boldsymbol{\mathcal{V}}$ and $\boldsymbol{\mathcal{D}}$ are given respectively by:

$$\boldsymbol{\mathcal{V}} \equiv \frac{\partial}{\partial t} \langle \boldsymbol{W} \rangle \tag{4.12}$$

and

$$\boldsymbol{\mathcal{D}} \equiv \frac{1}{2}\frac{\partial}{\partial t}\langle \boldsymbol{W}\boldsymbol{W}\rangle. \tag{4.13}$$

The terms in equations (4.12) and (4.13) are respectivelly the drift velocity and the diffusivity tensor. This expression for the diffusivity tensor is known as the self-diffusivity, which is the diffusion coeficient for a single particle. In the cases in which the diffusion mechanism does not depend on the particle interaction, the self-diffusivity is equal to the gradient diffusivity, which is the $\boldsymbol{\mathcal{D}}$ tensor on Fick's law.

4.2 Hydrodynamic diffusion

As seen in chapter 3, the reversibility of Stokes flow results in a kinematic reversibility for the relative motion of two rigid spheres free of inertia. Some factors can break this symmetry, thus causing the particles to depart from their original trajectories. Figure 4.1 shows this displacement of a particle from its original (reversible) trajectory.

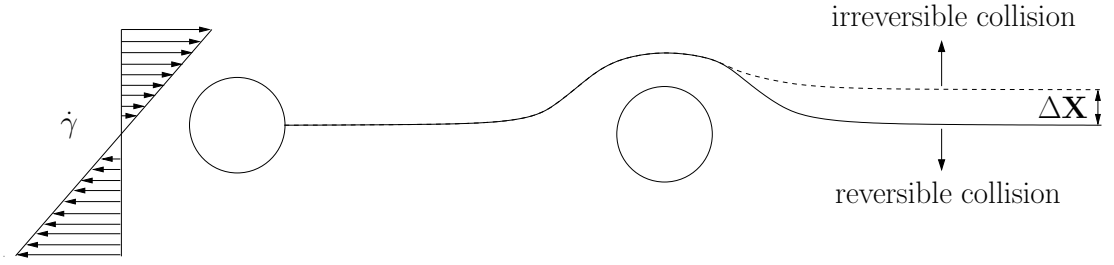

Figure 4.1: Net displacement of a particle from its original trajectory.

Let us consider a test particle in a suspension of particles. This symmetry breaking togheter with the randomness of the collisions between particles causes the particle to random walk across the streamlines, as shown in Figure 4.2, producing a self-diffusive phenomenon on the test particle.

In the case of hydrodynamic diffusion, the gradient diffusivity is different from the self-diffusivity. This is due to the fact that the hydrodynamic self-diffusion of a particle is not independent from the other particles. Figure 4.3 shows the

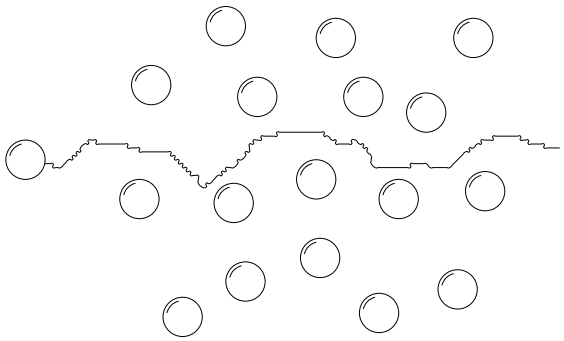

Figure 4.2: Series of displacements of a particle due to random interactions with other particles.

gradient diffusion effect, in which particles tend to migrate from a region with a high concentration to another region with low concentration.

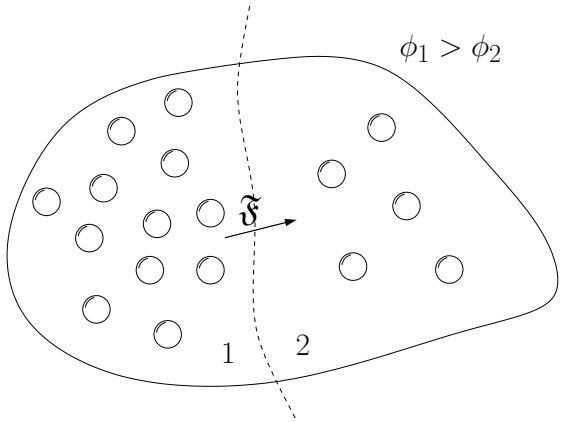

Figure 4.3: Flux of particles from a region with larger concentration to a region with smaller concentration.

Cunha & Hinch [16] have made a very important finding in the field of shear-induced hydrodynamic diffusion from their theoretical calculations for a monodisperse dilute suspension of non-Brownian rigid rough particles under shear flow. The authors discovered the exact relationship between self-diffusivity and down-gradient diffusivity to be given by

$$\mathcal{D}_k^G = 2\mathcal{D}_k^S + \mathcal{D}_k^F, \tag{4.14}$$

where $\mathcal{D}_k^F$ is a flux contribution and k represents one of the principal directions of

diffusion. Equation (4.14) means that the total gradient diffusivity has a contribution of the self-diffusivity on each side of a test sphere like Figure 4.3 and a flux contribution due to the small gradient of concentration. Cunha and Hinch show that $\mathcal{D}^G \sim 10\mathcal{D}^S$, in agreement with several experimental results in the context of shearing and sedimenting suspensions [23].

Due to the presence of the flow (non-equilibrium) and particle fluctuations governed by particle irreversible interactions, the hydrodynamic diffusivity is also anisotropic and always dependent on particle concentration and their orientation, so that $\boldsymbol{\mathcal{D}}^{hydro} = \mathcal{D}^0\mathbf{1} + \boldsymbol{\mathcal{D}}^G(\phi, \mathscr{C})$, where $\mathcal{D}_0$ is the ordinary molecular diffusivity. It is instructive to mention that in a paper of Leighton and Acrivos [26] the authors had already proposed a relation between $\mathcal{D}^G$ and $\mathcal{D}^S$ in the context of hydrodynamic diffusion but without the correct factor of 2, found theoretically by Cunha and Hinch [16]. In subsection 4.2.3, we derive a more general tensorial form of the expression for down-gradient diffusivity given by Cunha & Hinch [16].

4.2.1 Dimensional analysis

In this section, we perform a dimensional analysis in order to determine the general form of an expression for the shear-induced hydrodynamic diffusivity.

Considering that the diffusivity can be written as a function of the shear rate $\dot{\gamma}$, the size of the particles a, the fluid viscosity μ, the volume fraction of particles ϕ, and the parameters which break the symmetry of the particle motion, we have the diffusivity tensor given by the following fundamental relation:

$$\boldsymbol{\mathcal{D}}(\phi) = \boldsymbol{F}(\dot{\gamma}, a, \mu, \phi, \dots). \tag{4.15}$$

Thus, by applying Buckingham Pi theorem and performing a regular asymptotic expansion on ϕ , we can write the diffusivity as:

$$\boldsymbol{\mathcal{D}}(\phi) = \dot{\gamma}a^2\boldsymbol{f}(\phi, \dots) = \dot{\gamma}a^2\left[\phi\boldsymbol{f}_1(\dots) + \mathcal{O}(\phi^2)\right]. \tag{4.16}$$

In the case of a dilute suspension, we can neglect terms of order $\mathcal{O}(\phi^2)$. Therefore, we have an expression for the diffusivity tensor given by:

$$\boldsymbol{\mathcal{D}}(\phi) = \dot{\gamma} a^2 \boldsymbol{f}(\phi, \dots) = \dot{\gamma} a^2 \phi f[\boldsymbol{s}], \tag{4.17}$$

where $f[\boldsymbol{s}]$ is a functional of the relative trajectory between the particles, and a function of the nondimensional parameters related to the symmetry breaking of the problem. These parameters can be a roughness parameter, a capilary number Ca, a viscosity ratio or, as in our case, a magnetic interaction parameter.

4.2.2 Self-diffusion

In this section, we derive an expression for the self-diffusivity in the case of hydrodynamic shear-induced diffusion. Starting from the definition of self-diffusivity, we have:

$$\boldsymbol{\mathcal{D}}^S = \frac{1}{2} \frac{\partial}{\partial t} \langle \boldsymbol{W} \boldsymbol{W} \rangle , \tag{4.18}$$

where $\boldsymbol{W}$ is the total displacement of a test particle, as shown in Figure 4.2, due to collisions with other particles. This $\boldsymbol{W}$ can be written as the sum of the contributions of displacement due to each particle, namely:

$$\boldsymbol{W} = \sum_{k=1}^{N} \boldsymbol{W}_k. \tag{4.19}$$

In this context, we consider the particles to be identical and the collisions between the particles, as well as the displacements $\boldsymbol{W}_k$, to be independent. Thus, we have:

$$\langle \boldsymbol{W}\boldsymbol{W} \rangle = N \langle \boldsymbol{W}_1 \boldsymbol{W}_1 \rangle$$

$$= N \sum_{\Omega} \Delta\boldsymbol{X}\Delta\boldsymbol{X} \; \mathcal{P}_{col}(\boldsymbol{X}; t|\boldsymbol{X}_1). \tag{4.20}$$

The term $\mathcal{P}_{col}(\boldsymbol{X}; t|\boldsymbol{X}_1)$ is the conditional probability of the collision between the test particle at $\boldsymbol{X}$ given that the particle 1 is at $\boldsymbol{X}_1$. An expression for this probability distribution is given by:

$$\mathcal{P}_{col}(\boldsymbol{X}; t|\boldsymbol{X}_1) = P(\boldsymbol{X}) dV_{col}$$

$$= P(\boldsymbol{X}) \dot{\gamma} |y^{-\infty}| \; t \; d\Omega, \tag{4.21}$$

where $d\Omega$ in this case is equal to the "*infinitesimal area*" $dA^{-\infty}$ of the collisional plane[2]. Therefore, we find the expression for the self-diffusivity to be given by:

$$\boldsymbol{\mathcal{D}}^S = \frac{n(\boldsymbol{X})\dot{\gamma}}{2} \int_{\Omega} \Delta\boldsymbol{X}\Delta\boldsymbol{X} |y^{-\infty}| d\Omega \tag{4.22}$$

Alternativelly, expressing the integral in terms of nondimensional quantities:

$$\boldsymbol{\mathcal{D}}^S = \dot{\gamma} a^2 \phi \left(\frac{3}{8\pi} \int_{\Omega} \Delta\boldsymbol{X}' \Delta\boldsymbol{X}' |y'^{-\infty}| d\Omega' \right), \tag{4.23}$$

which agrees with the scaling argument presented in equation (4.17). The expression (4.23) was proposed before by Cunha and Hinch [16].

Although this derivation was made by considering that no other parameter of the particles, such as orientation, interferes with the total displacement, this can be made more general with the arguments presented in the following subsection.

[2]In this derivation, we use an argument similar to the one in kinetic theory. Namely, dV_{col} is the infinitesimal collisional volume, given by $dV_{col} = t|\boldsymbol{V}_2 - \boldsymbol{V}_1| dA^{-\infty}$, where $|\boldsymbol{V}_2 - \boldsymbol{V}_1|$ is the relative velocity between the particles.

4.2.3 Gradient diffusion

In this section, we perform a simple derivation of an invariant tensor form of Cunha & Hinch's theoretical expression for the shear-induced down-gradient diffusivity. This derivation takes into consideration "extra variables" of the particles, such as dipole orientation.

Considering now the collision of a particle starting in $\boldsymbol{X}$ with another particle with starting position $\boldsymbol{Y} = \boldsymbol{X} - \boldsymbol{x}$. The state space of each particle is given by the product between the position space and a space Ω_i with elements ω_i (where i is the label of the particle), which is related to other possible properties of the particle, such as particle orientation. For future convenience and agreement with the previous notation for the self-diffusivity, we define the set $\Omega \equiv \mathbb{R}^2 \times \Omega_1 \times \Omega_2$. Considering a volume V_0, invariant under flow transformations, with all possible initial conditions for $\boldsymbol{X}$. For a given $(\boldsymbol{x}, \omega_1, \omega_2) \in \Omega$, the initial volume is translated by a displacement of $\Delta\boldsymbol{X}$, as shown in Figure 4.4.

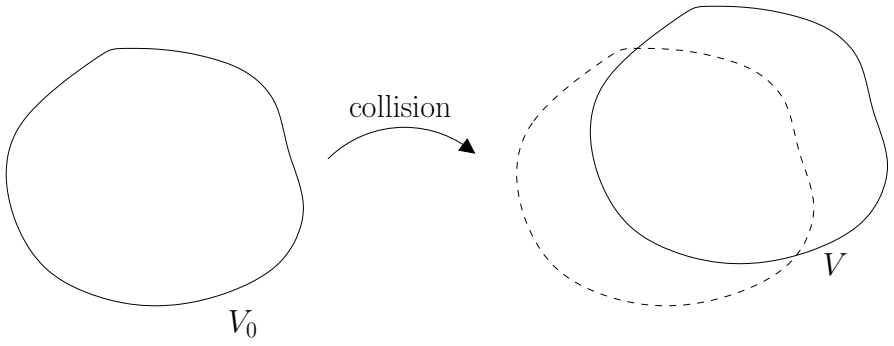

Figure 4.4: Displacement of the volume V_0 after undergoing a displacement of $\Delta\boldsymbol{X}$ for each point on the volume.

Thus, the net number of particles going inside the volume V is given by the difference between the particles entering the volume and the particles leaving the volume. This can be expressed explicitly by:

$$\frac{\Delta N_{in}}{N(N-1)} = \int_\Omega \left(\int_{\boldsymbol{X}\in V_0} - \int_{\boldsymbol{X}\in V} \right) d\mathcal{P}_{col}(\boldsymbol{\mathcal{X}}, \boldsymbol{\mathcal{Y}}; t) \tag{4.24}$$

$$\equiv \int_\Omega \int_R d\mathcal{P}_{col}(\boldsymbol{\mathcal{Y}}; t|\boldsymbol{\mathcal{X}}) d\mathcal{P}(\boldsymbol{\mathcal{X}}), \tag{4.25}$$

where $\boldsymbol{\mathcal{P}}_{col}(\boldsymbol{\mathcal{X}}, \boldsymbol{\mathcal{Y}}; t)$ is the probability of two particles initially at $\boldsymbol{\mathcal{X}} = (\boldsymbol{X}, \omega_1)$ and $\boldsymbol{\mathcal{Y}} = (\boldsymbol{Y}, \omega_2)$ collide after a given time t. The integral over R is just a notation for:

$$\int_R \equiv \int_{\boldsymbol{X}\in V_0} - \int_{\boldsymbol{X}\in V}. \tag{4.26}$$

For large separations between the particles, we consider the position and the variable ω_i of each particle to be statistically independent from one another. Thus, considering a large number of particles, the rate of change of the number of particles in the volume V is given by:

$$\frac{dN}{dt} = \dot{\gamma} \int_\Omega \int_R n(\boldsymbol{X}) n(\boldsymbol{Y}) |y^{-\infty}| d\boldsymbol{X} d\Omega. \tag{4.27}$$

where n is the number density and $d\Omega$ is an abuse of notation for $dA^{-\infty} d\mathcal{P}_{\omega_1} d\mathcal{P}_{\omega_2}$. Defining

$$f(\boldsymbol{X}) \equiv n(\boldsymbol{X}) n(\boldsymbol{X} - \boldsymbol{x}) \tag{4.28}$$

and using the fact that

$$\int_{V_0} f(\boldsymbol{X}) d\boldsymbol{X} = \int_V f(\boldsymbol{X} - \Delta\boldsymbol{X}) d\boldsymbol{X}, \tag{4.29}$$

we have:

$$\int_R n(\boldsymbol{X}) n(\boldsymbol{X} - \boldsymbol{x}) d\boldsymbol{X} = \int_V \left[f(\boldsymbol{X} - \Delta\boldsymbol{X}) - f(\boldsymbol{X}) \right] d\boldsymbol{X}. \tag{4.30}$$

Expanding $f(\boldsymbol{X} - \Delta\boldsymbol{X})$ in a Taylor series at the neighborhood of $\boldsymbol{X}$, we have:

$$f(\boldsymbol{X} - \Delta\boldsymbol{X}) - f(\boldsymbol{X}) \approx -\nabla \cdot (\Delta\boldsymbol{X} f) + \frac{1}{2} \nabla \cdot (\Delta\boldsymbol{X} \Delta\boldsymbol{X} \cdot \nabla f) + \ldots \tag{4.31}$$

Performing another Taylor series expansion, we find that $f(\boldsymbol{X})$ can be written as:

$$f(\boldsymbol{X}) \approx n(\boldsymbol{X})^2 - n(\boldsymbol{X})\boldsymbol{x} \cdot \nabla n + \ldots \tag{4.32}$$

Hence, by applying the divergence theorem, we find the integral in equation (4.30) to be:

$$\int_R n(\boldsymbol{X})n(\boldsymbol{Y})d\boldsymbol{X} = \int_{\partial V} \hat{\boldsymbol{n}} \cdot \big(-n^2\Delta\boldsymbol{X} + n\Delta\boldsymbol{X}\ \boldsymbol{x} \cdot \nabla n + \\ + n\Delta\boldsymbol{X}\Delta\boldsymbol{X} \cdot \nabla n + \mathcal{O}((\nabla n)^2, \nabla\nabla n)\big)\, dS \tag{4.33}$$

Assuming small gradients of n, we can neglect terms of order $\mathcal{O}(\nabla n^2)$ and $\mathcal{O}\left(\nabla\nabla n\right)$. Thus, we find that the down-gradient diffusivity is given by:

$$\boldsymbol{\mathcal{D}}^G = 2\boldsymbol{\mathcal{D}}^S + n\dot{\gamma}\int_\Omega \Delta\boldsymbol{X}\ \boldsymbol{x}|y^{-\infty}|d\Omega. \tag{4.34}$$

This result is the exact tensorial representation of the theoretical expression proposed by Cunha & Hinch [16] for the shear-induced hydrodynamic down-gradient diffusivity.

4.3 Numerical computation of the hydrodynamic diffusivity

For the numerical integration used to compute the self-diffusivity and down-gradient diffusivity, a Monte-Carlo integration scheme has been used. In particular, this method is used due to the fact that performing the numerical integration in six dimensions using a trapezoidal rule would require a large number of points, resulting in impracticable computational times. The Monte-Carlo integration, although requiring a large number of points for convergence in a small number of dimensions, is much more suitable for integration in a greater number of dimensions [59].

The method consists in a statistical interpretation of the integral as an average of a random variable. Let us suppose one has to evaluate the following integral:

$$\int_{\Omega} f(x) d\Omega, \tag{4.35}$$

where $x \in \Omega$. If the measure $\mu(\Omega) \equiv \int_{\Omega} d\Omega$ is equal to 1, this integral can be interpreted as the average of the random variable f with an uniform distribution for the random variable x. If the measure is not equal to 1, we can normalize the integral by the factor of $\mu(\Omega)$ and therefore keeping the definition of a statistical average. Hence:

$$\int_{\Omega} f(x) d\Omega = \mu(\Omega) \langle f \rangle . \tag{4.36}$$

Now, by the law of large numbers (see details in Appendix I), the average $\langle f \rangle$ for an uniform distribution of the variable x can be approximated by the sum of a large number N of randomly generated values of f divided by N. Namely:

$$\langle f \rangle = \lim_{N \to \infty} \frac{f_1 + \cdots + f_N}{N} = \lim_{N \to \infty} \frac{1}{N} \sum_{k=1}^{N} f(x_k), \tag{4.37}$$

where $x_k \in \Omega$ are numbers randomly generated in Ω with uniform distribution by a random number generator. Therefore, the approximation for the integral of f is given by:

$$\int_{\Omega} f \; d\Omega \approx \mu(\Omega) \frac{1}{N} \sum_{k=1}^{N} f(x_k), \tag{4.38}$$

This approximation method for integrals is the so-called Monte-Carlo integration method. As N gets bigger, the precision of the method increases, as the error associated with the method is of order $\mathcal{O}(1/\sqrt{N})$ (by the law of large numbers) and does not depend on the number of dimensions. Meanwhile, methods such as the trapezoidal or Simpson's rule have explicit dependence on the number of dimensions d, with an error of order $\mathcal{O}(1/N^{k/d})$, where k is an integer which depends

on the order of the method. For the trapezoidal method $k = 3$, for Simpson's rule $k = 4$.

4.4 Numerical computation of the shear-induced hydrodynamic self-diffusivity

Now we present the procedure used for calculating the numerical values for the hydrodynamic self-diffusivity in a suspension of non-Brownian magnetic particles. The expression for the nondimensional self-diffusivity is given by:

$$\boldsymbol{f}^S(\alpha) \equiv \frac{\boldsymbol{D}^S}{\dot{\gamma} a^2 \phi} = \frac{3}{8\pi} \int_\Omega \Delta \boldsymbol{X} \Delta \boldsymbol{X} |y^{-\infty}| d\Omega. \tag{4.39}$$

For the case of magnetic particles with dipole moments, we have $d\Omega$ given by:

$$d\Omega = d\mathcal{P}_{\hat{\boldsymbol{p}}_1} d\mathcal{P}_{\hat{\boldsymbol{p}}_2} dA^{-\infty}, \tag{4.40}$$

where $\mathcal{P}_{\hat{\boldsymbol{p}}_k}$ is the probability for the particle to have its dipole moment orientation given by $\hat{\boldsymbol{p}}_k$. Therefore, we have the expression for $d\mathcal{P}_{\hat{\boldsymbol{p}}_k}$ in terms of the probability density $P_{\hat{\boldsymbol{p}}_k}$ as follows:

$$d\mathcal{P}_{\hat{\boldsymbol{p}}_k} = P_{\hat{\boldsymbol{p}}_k} d\hat{\boldsymbol{p}}_k = P_k(\theta_k, \varphi_k) \sin(\theta_k) d\theta_k d\varphi_k, \tag{4.41}$$

where we adopted a spherical coordinate parametrization for a sphere with unit radius. For large separations between the particles, we have a simple uniform probability density for the orientations, given by:

$$P_k(\theta_k, \varphi_k) = \frac{1}{4\pi} \tag{4.42}$$

The uniformity of the probability density is due to the isotropic shape of the particles and the absence of an external magnetic field. With these considerations in mind, equation (4.39) becomes

$$\boldsymbol{f}^S(\alpha) = \frac{3}{8\pi}\frac{1}{16\pi^2}\int_{A_{disp}} dA^{-\infty}\int_{S^2} d\hat{\boldsymbol{p}}_1\int_{S^2} d\hat{\boldsymbol{p}}_2 \Delta\boldsymbol{X}\Delta\boldsymbol{X}|y^{-\infty}|, \tag{4.43}$$

where S^2 is the surface of a unit sphere and A_{disp} is the area for which, given an initial pair of orientations, an initial configuration leads to a dispersive (*i.e.* non-aggregative) trajectory. In order to compute the numerical values of the integral in (4.43), we use the method of Monte-Carlo integration, in which (4.43) is approximated as follows:

$$\boldsymbol{f}^S(\alpha) \approx \frac{3}{8\pi}\frac{A^{-\infty}\pi^2}{4N}\sum_{k=1}^{N} \Delta\boldsymbol{X}_k\Delta\boldsymbol{X}_k|y_k^{-\infty}|\sin(\theta_1^k)\sin(\theta_2^k)\mathbb{I}_{A_{disp}}, \tag{4.44}$$

where $\mathbb{I}$ is the indicator function, defined as:

$$\mathbb{I}_A = \begin{cases} 1 & \text{if } x \in A \\ 0 & otherwise \end{cases} \tag{4.45}$$

The results for the self-diffusivities obtained by the Monte-Carlo integration are shown in Figure 4.5. For small values of the parameter α we were able to compare our numerical results with the theory of Cunha & Hinch [16]. In the present case, a perfect numerical fitting of our computational resuls is obtained as $\varepsilon = \alpha^{5/4}$. Under this condition, we observe a linear behavior of the self-diffusivity with $\delta^4 = \varepsilon^{0.4374}\left(\log(1/\varepsilon) + 1.347\right)^{-0.7012}$, as shown in the insert of Figure 4.5 and predicted by Cunha and Hinch[3].

It is important to note that the non-diagonal terms of the self-diffusivity tensor vanish due to inherent symmetries of the problem. Namely, we can perform a partition on the integral of the area on the four quadrants. For each pair of starting orientations in the first or fourth quadrants, there is a relative pair of orientations which results in a mirrored configuration in the second and third quadrants, respectively. This argument results in the nullity of the non-diagonal terms of the diffusivity.

[3]In the paper of Cunha and Hinch [16], δ is defined as being the net displacement of a test particle produced by small values of the irreversibility parameter ε. δ^4 is used by the fact that the self-diffusivity is related with a double integral of δ^2

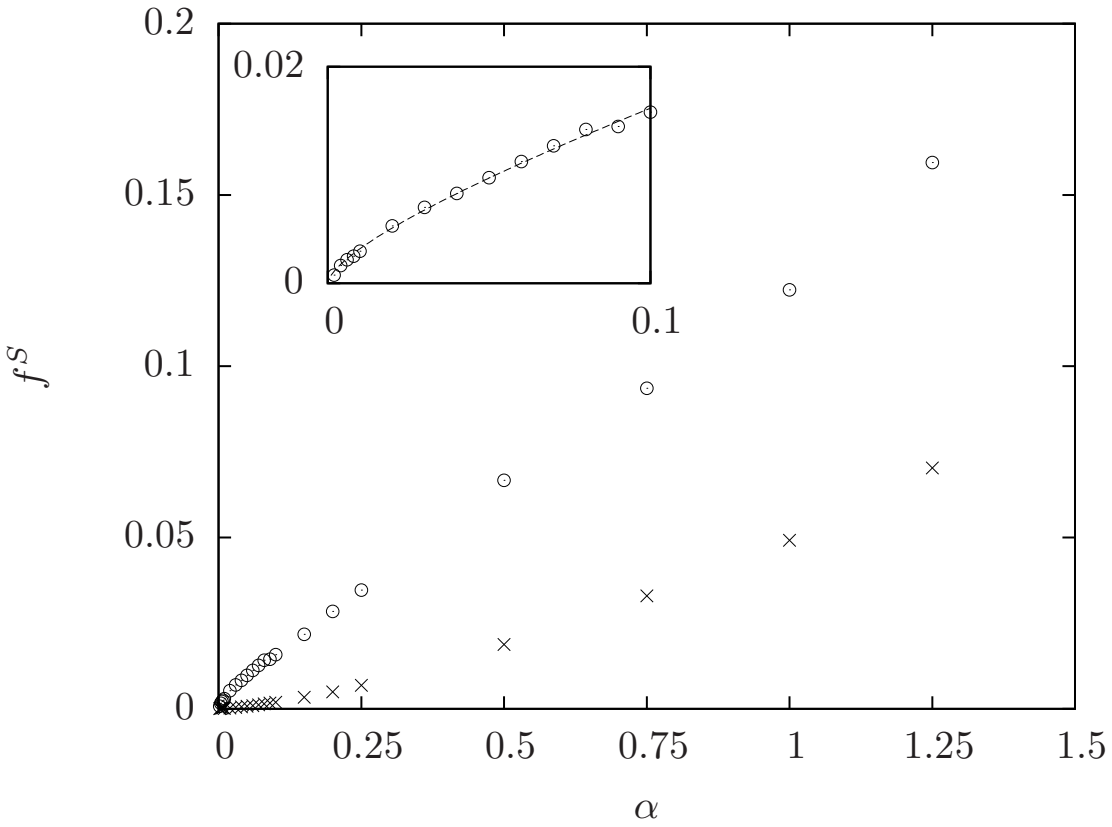

Figure 4.5: Nondimensional self-diffusivities as functions of the interaction parameter α. The $\odot$ points represent f^S_{yy} and $\times$ points are f^S_{zz}. The insert shows the comparison of the self diffusivities for small values of α with the theory of Cunha & Hinch. The dashed line is the function $0.1564\ \delta^4(\alpha)$.

In addition, the paper of Cunha & Hinch also shows that for small values of ε, the self-diffusivities in the $z-$direction are linear with ε. Using our equivalent intrinsic parameter $\varepsilon = \alpha^{5/4}$ for small values of α, the diffusivity in the $z-$direction f^S_{zz} is also quite linear with $\alpha^{5/4}$, as shown in Figure 4.6. While we can see an excellent agreement between our numerical simulation results and the theory of Cunha and Hinch [16] for small values of α, we have no experimental data to compare our results.

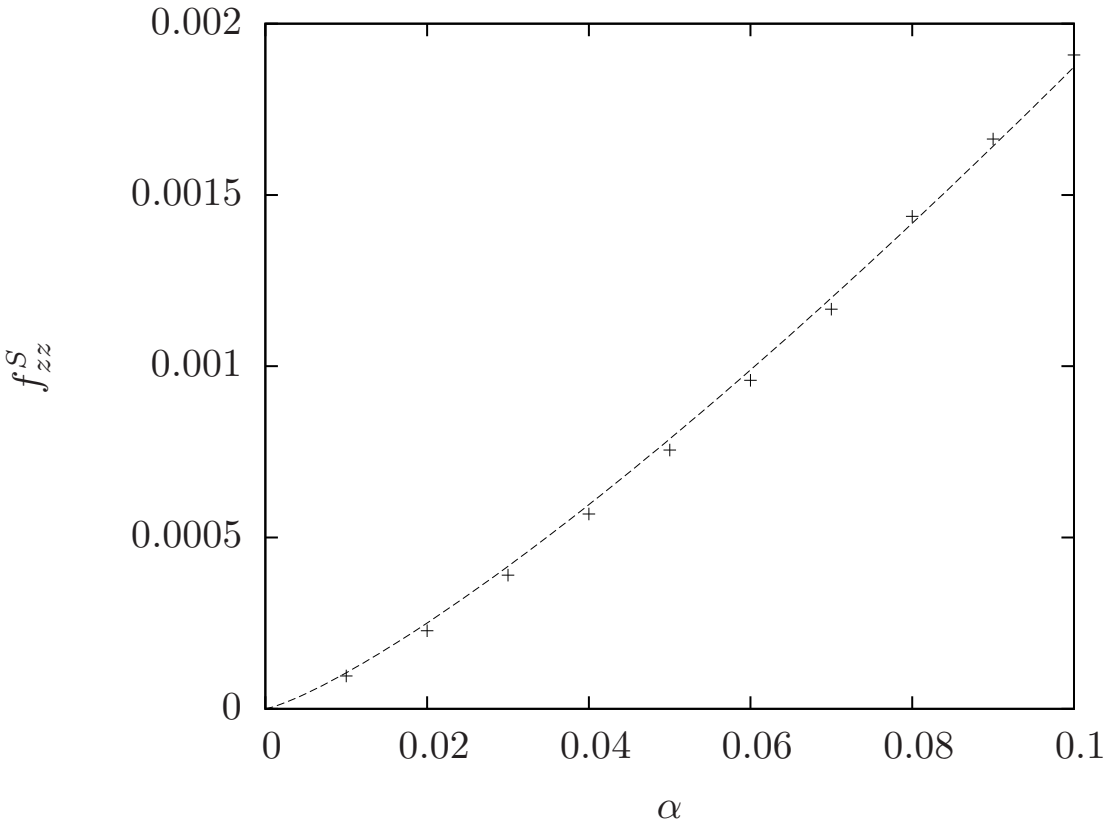

Figure 4.6: Numerical values for the self-diffusivity in the $z-$direction f_{zz}^S as a function of α. The dashed curve is the function $0.0333\ \alpha^{5/4}$.

4.5 Aggregative effects on the flux contribution of the down-gradient diffusivity

In our investigation of the diffusive phenomena in non-Brownian magnetic suspensions, the existence of attractive forces between the particles results in some problems in the computation of the gradient diffusivity. In the paper by [16], it was found that the gradient diffusivity for small concentration gradients was given by:

$$\boldsymbol{\mathcal{D}}^G = 2\boldsymbol{\mathcal{D}}^S + \boldsymbol{\mathcal{D}}^F, \tag{4.46}$$

where $\boldsymbol{\mathcal{D}}^S$ is the self diffusivity tensor and

$$\boldsymbol{\mathcal{D}}^F = n\dot{\gamma} \int_\Omega \Delta \boldsymbol{X}\boldsymbol{x}|y^{-\infty}|\, d\Omega \tag{4.47}$$

is a flux contribution. Writing this flux contribution in the form $\boldsymbol{\mathcal{D}}^F = \dot{\gamma}a^2\phi \boldsymbol{f}^F(\alpha)$, we have the explicit form of the integral for $\boldsymbol{f}^F(\alpha)$ given by:

$$\boldsymbol{f}^F(\alpha) = \frac{3}{8\pi}\frac{1}{16\pi^2}\int_{A_{disp}} dA^{-\infty} \int_{S^2} d\hat{\boldsymbol{p}}_1 \int_{S^2} d\hat{\boldsymbol{p}}_2\, \Delta \boldsymbol{X}\boldsymbol{x}|y^{-\infty}|. \tag{4.48}$$

It should be important to note that despite the asymmetry on the integrand tensor $\Delta \boldsymbol{X}\boldsymbol{x}$, which indicates the possibility of the tensor $\boldsymbol{\mathcal{D}}$ to be asymmetric, due to the symmetry of the problem, the diagonal terms cancel out by the same argument as the one for self-diffusivity. Results for the computation of $\boldsymbol{f}^G = 2\boldsymbol{f}^S + \boldsymbol{f}^F$ by the Monte-Carlo method are presented for some values of α in Table 4.1.

Table 4.1: Numerical values for the down gradient diffusivity computed by the Monte-Carlo method.

α	0.02	0.05	0.09
f^S_{yy}	$5,292 \times 10^{-3}$	$9,743 \times 10^{-3}$	$1,447 \times 10^{-2}$
f^G_{yy}	$1,543 \times 10^{-3}$	$1,067 \times 10^{-3}$	$-4,440 \times 10^{-2}$
f^S_{zz}	$2,276 \times 10^{-4}$	$7,556 \times 10^{-4}$	$1,663 \times 10^{-3}$
f^G_{zz}	$-8,025 \times 10^{-3}$	$-1,691 \times 10^{-2}$	$-0,808 \times 10^{0}$

The results shown in table 4.1 show the flux contributions are all negative for the cartesian components of the diffusivity tensor. This occurs due to the fact that trajectories with negative final displacements outnumber trajectories with positive ones, which is caused by the attractive nature of the dipole interaction.

Thus, the down-gradient diffusion coefficients in the z directions are negative, indicating a probable dominance of the aggregative effects over dispersive ones. On the other hand, the down-gradient diffusivity in the y direction is positive for small values of α. Even so, these values are smaller than the ones of $\boldsymbol{\mathcal{D}}^S$, indicating that the dispersive effect is drastically reduced due to the attractiveness of the magnetic

interactions, which are not taken into account by the self-diffusivity term. In fact, as the magnetic interaction parameter α increases, the magnetic dipolar attraction between the particles tends to grow, leading to higher values of the negative particle flux contribution. For future works, we propose the addition of a surfactant effect in our model, such as a short-range repulsive force [7], avoiding aggregative closed trajectories during particle collision. With these forces, we expect to obtain the correct values for the down-gradient diffusivities.

CHAPTER 5

AGGREGATION RATE

This chapter presents a basic discussion about particle aggregation and the rate of formation of particle aggregates. Then, we discuss the problem of aggregation in the context of a suspension of magnetic particles. In this case, the dipolar interaction between the particles influences the aggregation rate. By using our two-particle problem, we have computed the rate of particle doublet formation.

5.1 Particle aggregation mechanisms

Particle aggregation or coagulation is an intrinsic phenomenon in suspension dynamics. This phenomenon can be caused by several factors, such as Van der Waals colloidal attractive force, and magnetic dipole-dipole interactions [36]. In the latter, as the particles are brought close together, the magnetic forces between them may cause the particles to aggregate. Aggregation is usually an irreversible process and can make the suspension unstable.

Early mathematical description of the kinetics of aggregation was given by Smoluchowski [60], who provided an equation for the evolution of the number of

aggregates of different sizes. While some studies on coagulation focus on Brownian particles and diffusion limited aggregation, there are important studies on the coagulation of non-Brownian particles [35]. In particular, the work of Cunha & Couto [36] has investigated the aggregation of sedimenting non-Brownian magnetic particles in polydisperse dilute suspensions.

In this dissertation, we examine the aggregation phenomenon induced by shear flows in a dilute suspension of non-Brownian particles with dipole-dipole interactions. We shall perform a calculation of the aggregation rate for this dilute solution of magnetic particles interacting magnetically and hydrodynamically.

5.2 General remarks

In a particle suspension, as particles are brought close to each other, some short-range interaction effects may cause these particles to aggregate. Figure 5.1 illustrates the formation of a doublet due to short-range interactions.

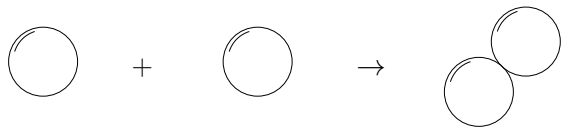

Figure 5.1: Schematic of a doublet structure formation by the aggregation of two particles.

As a real suspension evolves in time, different structures of larger agglomerates start to form due to interactions between other types of agglomerates. The formation of large clusters can increase the sedimentation velocity of larger agglomerates due to its dependence on the equivalent radius R of the agglomerate. Namely, as illustrated in Figure 5.2, the ratio between the sedimentation velocity U_A of an agglomerate and the sedimentation velocity U_S of a single particle is $\phi_a(R/a)^2$, where ϕ_a is the volume ratio of particles inside the agglomerate. Under this condition, the suspension becomes unstable.

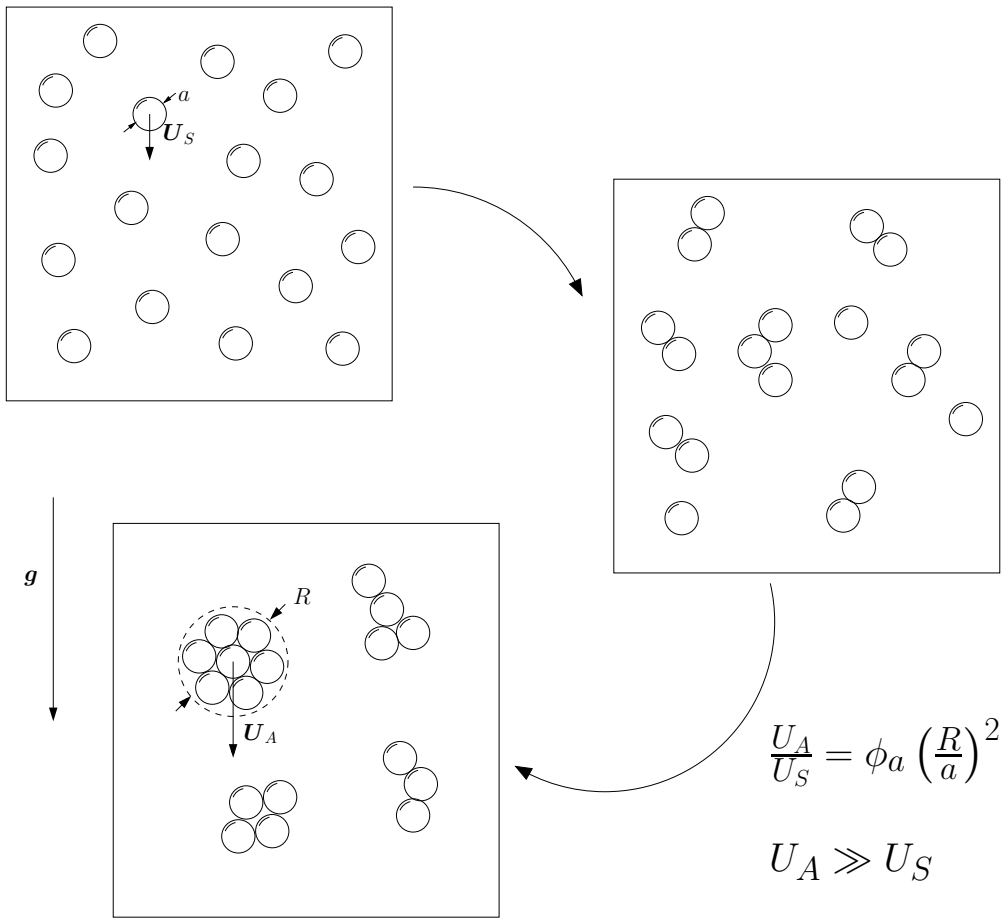

Figure 5.2: Schematic illustration of the formation of aggregates as the suspension evolves in time.

5.3 Rate of growth of an i^{th}-type agglomerate

The rate of aggregation for a i^{th}-type agglomerate is given by the rate at which particles of k and i^{th}-types aggregate to form a i^{th}-type subtracted from the rate at which $i-$type agglomerates aggregate with another particle forming another type of aggregate. Mathematically, the expression for dN_i/dt can be writen as:

$$\frac{dN_i}{dt} = A_{\rightarrow i} - A_{i\rightarrow} \tag{5.1}$$

The rate $A_{\rightarrow i}$ can be expressed as

$$A_{\rightarrow i} = \frac{N(N-1)}{2} \sum_{k=1}^{i-1} \mathcal{J}_{k,i-k} P_k P_{i-k} \approx \frac{1}{2} \sum_{k=1}^{i-1} \mathcal{J}_{k,i-k} N_k N_{i-k}, \tag{5.2}$$

where $\mathcal{J}_{ij}$ is the rate at which a i^{th}-type agglomerate aggregates with a j^{th}-type agglomerate. The expression for $A_{i\rightarrow}$ is given by

$$A_{i\rightarrow} = N(N-1) \sum_{k=1}^{\infty} \mathcal{J}_{ik} P_i P_k \approx \sum_{k=1}^{\infty} \mathcal{J}_{ik} N_i N_k. \tag{5.3}$$

Thus, the rate of change of $i-$type agglomerates is given by:

$$\frac{dN_i}{dt} = \frac{1}{2} \sum_{k=1}^{i-1} \mathcal{J}_{k,i-k} N_k N_{i-k} - \sum_{k=1}^{\infty} \mathcal{J}_{ik} N_i N_k. \tag{5.4}$$

Equation (5.4) is known as Smoluchowski coagulation equation [60] and represents the rate of increase of a k^{th}-type agglomerate as a function of the number of aggregates of other species and the rate of agglomerate formation between them.

5.4 Rate of formation of doublets due to the collision of two particles

An expression for the aggregation rate $\mathcal{J}_{11}$ can be found in a straightfoward way with some level of approximation. Let's consider the problem of two particles: a particle 1 initially at $\boldsymbol{Y}$ and a particle 2 initially at $\boldsymbol{X}$. Considering the fact that two particles aggregate as they collide in a certain region of aggregation, we can write

$$\mathcal{J}_{11} = \frac{\partial}{\partial t} \sum_{\Omega_{agg}} \sum_{\boldsymbol{Y}} \mathcal{P}_{col}(\boldsymbol{X}, \boldsymbol{Y}; t). \tag{5.5}$$

Now, we use the same expression for the collisional probability, given by $\mathcal{P}_{col}(\boldsymbol{X}; t|\boldsymbol{Y}) = P(\boldsymbol{X})|\boldsymbol{V}_2 - \boldsymbol{V}_1|\ t\ d\Omega$, where $d\Omega$ is an increment of the collisional area. Thus, the aggregation rate $\mathcal{J}_{11}$ is given by:

$$\mathcal{J}_{11} = P(\boldsymbol{X}) \int_{\Omega_{agg}} |\boldsymbol{V}_2 - \boldsymbol{V}_1| d\Omega, \tag{5.6}$$

where Ω_{agg} is the aggregative region of the collisional area.

5.5 Shear-induced aggregation in magnetic suspensions

Now we consider a homogeneous magnetic suspension of spherical non-Brownian particles undergoing an external simple shear flow. The relative velocity between the particles is given by $\dot{\gamma} y \hat{\boldsymbol{e}}_1$. In this case, for a suspension with a small number of agglomerates, the doublet formation rate is given by:

$$\frac{dN_2}{dt} = n_1 N_1 \dot{\gamma} \int_{\Omega_{agg}} |y^{-\infty}| d\Omega. \tag{5.7}$$

It should be important to note that equation (5.7) neglects agglomerate structures of order higher than two because these higher order structures have a very lower probability to occur compared to the doublets and isolated particles. As the suspension evolves and the number of higher order aggregates increases, this expression is no longer valid.

Expanding the integral in expression (5.7), the rate of doublet formation is given by:

$$\frac{dN_2}{dt} = \frac{n_1 N_1 \dot{\gamma}}{16\pi^2} \int_{A^{-\infty}} dA^{-\infty} \int_{S^2} d\hat{\boldsymbol{p}}_1 \int_{S^2} d\hat{\boldsymbol{p}}_2 |y^{-\infty}| \mathbb{I}_{\Omega_{agg}}, \tag{5.8}$$

where S^2 is the unity sphere and $\mathbb{I}$ is the indicator function given by:

$$\mathbb{I}_A(x) = \begin{cases} 1 & \text{if } x \in A \\ 0 & \text{otherwise} \end{cases} \tag{5.9}$$

Therefore, the integration performed on equation 5.8 is equivalent to integrating over each aggregative region for all possible initial orientations. The integral can be written in terms of nondimensional quantities as:

$$\frac{dN_2}{dt} = n_1 N_1 \dot{\gamma} a^3 \left[\frac{1}{16\pi^2} \int_{A^{-\infty}} dA^{-\infty} \int_{S^2} d\hat{\boldsymbol{p}}_1 \int_{S^2} d\hat{\boldsymbol{p}}_2 |y^{-\infty}| \mathbb{I}_{\Omega_{agg}} \right], \tag{5.10}$$

or:

$$\frac{dN_2}{dt} \equiv n_1 N_1 \dot{\gamma} a^3 J_{11}, \tag{5.11}$$

where J_{11} is given by the integral:

$$J_{11} = \frac{1}{16\pi^2} \int_{A^{-\infty}} dA^{-\infty} \int_{S^2} d\hat{\boldsymbol{p}}_1 \int_{S^2} d\hat{\boldsymbol{p}}_2 |y^{-\infty}| \mathbb{I}_{\Omega_{agg}}. \tag{5.12}$$

Writing the integral for J_{11} as an integral over the $6-$dimensional space considering a spherical coordinate parametrization for the initial orientations of the particles:

$$J_{11} = \frac{1}{16\pi^2} \int_{A^{-\infty}} dA^{-\infty} \int_0^{\pi} d\theta_1 \sin\theta_1 \int_0^{2\pi} d\varphi_1 \int_0^{\pi} d\theta_2 \sin\theta_2 \int_0^{2\pi} d\varphi_2 |y^{-\infty}| \mathbb{I}_{\Omega_{agg}}. \tag{5.13}$$

Now, we can use the Monte-Carlo method in order to approximate the integral for J_{11}. This approximation can be written as:

$$J_{11} \approx \frac{\pi^2 \tilde{A}^{-\infty}}{4\ N} \sum_k \sin(\theta_1^k) \sin(\theta_2^k) |y_k^{-\infty}| \mathbb{I}_{\Omega_{agg}}, \tag{5.14}$$

where the variables labeled with k are randomly generated with an uniform distribution. The function $\mathbb{I}_{\Omega_{agg}}$, which depends on the initial parameters of the particles, has the value 1 for aggregative trajectories and 0 for non-aggregative ones.

5.6 Scaling argument

We now use a simple scaling argument in order to predict the type of dependence of J_{11} with respect to α. By equation 5.13, it is straightfoward to see that

J_{11} is linear with the nondimensional area $\tilde{A}_{agg}$, which is a "standard" nondimensional aggregative area. This area depends on the characteristic length ℓ in a way that

$$A_{agg} \propto \ell^2. \tag{5.15}$$

The length scale ℓ is related to the strength of dipolar interactions between the particles. In this context, we define ℓ as being the scale on which the hydrodynamic forces balance the magnetic dipolar forces. When this balance occurs, we have $F_H \sim F_M$, where $F_H \sim 6\pi\mu aU$ and $F_M \sim \frac{3\mu_0 m_0^2}{4\pi\ell^4}$. Balancing both effects, we find ℓ to be given by:

$$\ell \sim a\alpha^{1/4}. \tag{5.16}$$

Therefore, we have:

$$J_{11} \propto \alpha^{1/2}. \tag{5.17}$$

Thus, this simple scaling argument suggests a square root dependence of J_{11} on α.

5.7 Numerical results

The numerical integration for J_{11} was performed numerically by using the Monte-Carlo method for the distinct values of α. The simulations for each point lasted for about 10 hours without parallelization and resulted in a relative numerical variance of approximately 10^{-2}.

We compare our numerical results with the predicted power law by fitting the numerical values for the aggregation rate with a curve obeying the power-law. The numerical results together with the power law curve are shown in Figure 5.3

By examining the graph in Figure 5.3, we can observe a good agreement between the numerical results and the scaling argument prediction. Comparing the

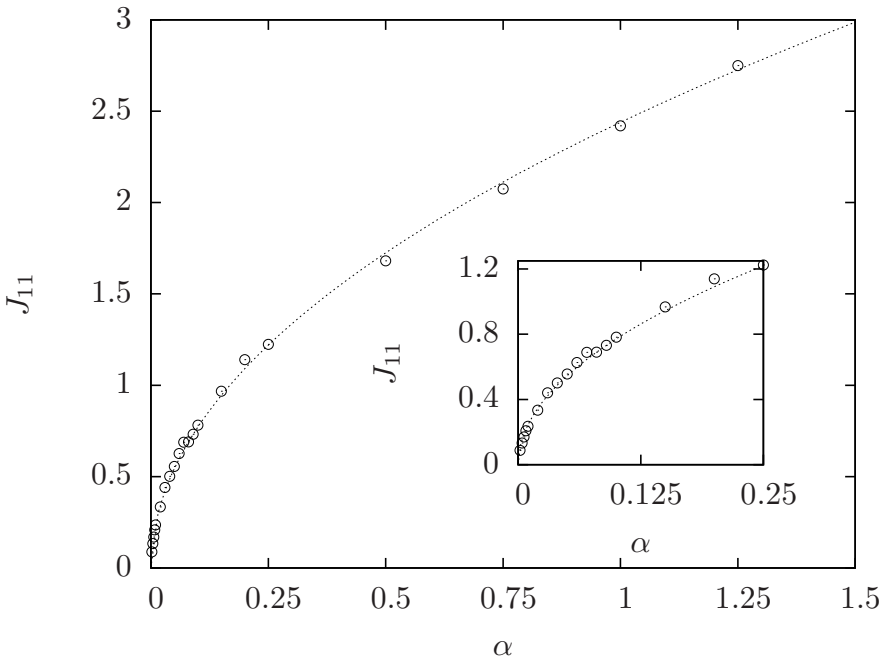

Figure 5.3: The doublet formation rate parameter J_{11} as a function of the dipolar interaction strength parameter α. The dots are the numerical results computed by the Monte-Carlo integration, while the dashed line is the fit function $A\alpha^{1/2}$, where the parameter $A = 2.43896$ was obtained by a numerical fit.

obtained result with the results found by Cunha & Couto [36], we can perceive substantial differences between the two results. Namely, the result found by Cunha & Couto does not appear to obey a simple power law, as predicted by the present work. This disagreement might be due to different factors, such as the presence of a short-range electrostatic repulsive force, avoiding particle aggregation, or the consideration of polydispersity.

CHAPTER 6

ROTATIONAL DYNAMICS AND MAGNETIZATION

In previous chapters, we have obtained numerical values for the shear-induced hydrodynamic diffusivity and aggregation rate of dilute magnetic suspensions. In this chapter, we investigate the magnetization of a sheared suspension of non-Brownian magnetic particles. First, we analyze the problem of a single isolated particle at low Reynolds number. With this problem, we are able to extract some information concerning non-equilibrium effects, due to the presence of the shear flow and an external magnetic field, on the magnetization of very dilute suspensions at high Péclet number, including properties such as the spinning behavior of the particles for high values of $\dot{\gamma}$. In the last part of this chapter, we perform a simple non-renormalized cluster expansion in order to obtain a second-order contribution for the magnetization using the dynamical simulation of two magnetic particles in creeping flow.

6.1 Single particle dynamics and the first order magnetization

In this chapter, we discuss the magnetization of a magnetic suspension of non-Brownian particles undergoing a simple shear flow with a uniform external magnetic field. Although simple, the problem of a single particle shall give some insight on the physical mechanisms of the problem for understanding the particle interaction with the flow and an external magnetic field.

Let's consider a very dilute suspension of spherical magnetic particles undergoing a simple shear flow and subjected to an applied external magnetic field $\boldsymbol{H}$ as sketched in figure 6.1. In the case on which the particles are separated far away from each other, the dynamics of each particle can be modeled as a single particle problem.

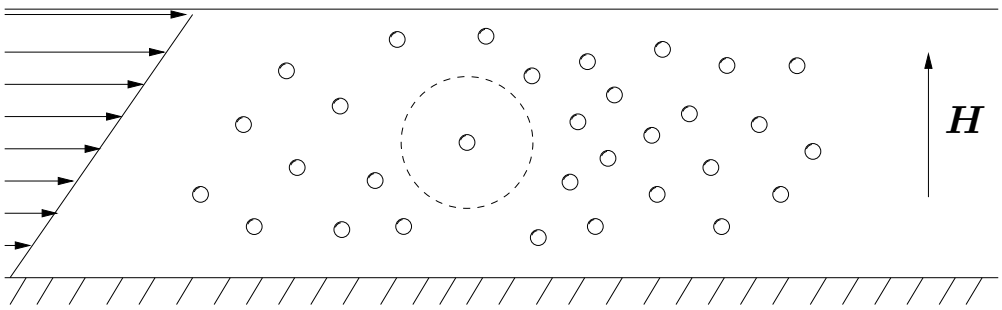

Figure 6.1: Sketch of the problem. A very dilute magnetic suspension undergoing an external simple shear flow with an external uniform magnetic field in the y direction.

The nondimensional equation for the rotational velocity of a single spherical magnetic particle moving in creeping flow free of inertia is given by (2.73). Namely,

$$\boldsymbol{\omega} = \boldsymbol{\Omega} + \boldsymbol{T}^M, \tag{6.1}$$

where $\boldsymbol{T}^M$ is the nondimensional magnetic torque exerted on the particle. The expression for this torque is given in a similar way as (2.97) by:

$$\boldsymbol{T}^M = \frac{\mu_0 m_0 H}{8\pi\mu\dot{\gamma}a^3}\hat{\boldsymbol{p}} \wedge \hat{\boldsymbol{h}}, \tag{6.2}$$

where $\hat{\boldsymbol{h}} = \boldsymbol{H}/H$ is the direction of the uniform magnetic field $\boldsymbol{H}$. In this context, we introduce the nondimensional parameter β defined as:

$$\beta \equiv \frac{\mu_0 m_0 H}{8\pi\mu\dot{\gamma}a^3}. \tag{6.3}$$

This parameter represents a ratio between the intensities of the external magnetic torque and the hydrodynamic torque. This parameter can also be interpreted as being a nondimensional magnetic field intensity. Thus, the equation for $\boldsymbol{\omega}$ takes the form

$$\boldsymbol{\omega} = \boldsymbol{\Omega} + \beta\ \hat{\boldsymbol{p}} \wedge \hat{\boldsymbol{h}}. \tag{6.4}$$

With the angular velocity in hands, we can write the equation for the evolution of the position unit vector $\hat{\boldsymbol{p}}$ as:

$$\frac{d\hat{\boldsymbol{p}}}{dt} = \boldsymbol{\omega} \wedge \hat{\boldsymbol{p}} = \boldsymbol{\Omega} \wedge \hat{\boldsymbol{p}} + \beta\ \hat{\boldsymbol{h}} - \beta\ (\hat{\boldsymbol{p}} \cdot \hat{\boldsymbol{h}})\hat{\boldsymbol{p}}, \tag{6.5}$$

or in component form:

$$\frac{dp_1}{dt} = \Omega_2 p_3 - \Omega_3 p_2 - \beta p_1(\hat{\boldsymbol{p}} \cdot \hat{\boldsymbol{h}}) + \beta\ h_1 \tag{6.6}$$

$$\frac{dp_2}{dt} = \Omega_3 p_1 - \Omega_1 p_3 - \beta p_2(\hat{\boldsymbol{p}} \cdot \hat{\boldsymbol{h}}) + \beta\ h_2 \tag{6.7}$$

$$\frac{dp_3}{dt} = \Omega_1 p_2 - \Omega_2 p_1 - \beta p_3(\hat{\boldsymbol{p}} \cdot \hat{\boldsymbol{h}}) + \beta\ h_3. \tag{6.8}$$

Thus, we have a system of equations which governs the rotational motion of a single magnetic rigid sphere in creeping flow in the presence of a uniform magnetic field. It is easy to verify that the system in question has the property of preserving the norm of the vector $|\hat{\boldsymbol{p}}|$ (which is equal to the unity in the context). Therefore, the manifold S^2 together with the family of solutions for (6.6) constitute a dynamical system on the surface S^2.

Now, we focus on the problem where the external flow is a simple shear flow in the plane xy. We also consider the magnetic field to be a uniform field pointing in the y direction. In this case, we have $\boldsymbol{\Omega} = -\frac{1}{2}\,\boldsymbol{e}_3$ and $\hat{\boldsymbol{h}} = \hat{\boldsymbol{e}}_2$, the set of equations take the form of:

$$\frac{dp_1}{dt} = \frac{1}{2}\,p_2 - \beta p_1 p_2 \tag{6.9}$$

$$\frac{dp_2}{dt} = -\frac{1}{2}\,p_1 - \beta (p_2)^2 + \beta \tag{6.10}$$

$$\frac{dp_3}{dt} = -\beta p_3 p_2. \tag{6.11}$$

This set of equations governs the evolution of the magnetic dipole orientation.

6.1.1 Stability analysis

We now investigate the fixed points of the dynamical system. In order to determine whether these fixed points are stable or unstable, we need to perform a stability analysis of the system.

The surface S^2 is an integral surface of the system of equations in (6.9). This set of differential equations, together with the restriction $|\hat{\boldsymbol{p}}| = 1$, describes a vector field $\boldsymbol{f} : S^2 \to TS^2$, where TS^2 is the tangent bundle of S^2.

In order to perform the stability analysis, we shall work in the coordinate charts. Thus, we parametrize the surface in spherical coordinates as follows:

$$p_1 = \cos\varphi \sin\theta \tag{6.12}$$

$$p_2 = \sin\varphi \sin\theta \tag{6.13}$$

$$p_3 = \cos\theta \tag{6.14}$$

with $\theta \in (0, \pi)$ and φ assuming different intervals with length 2π for the different patches. These parametrizations constitute a set of charts contained in an atlas for the surface S^2. It is important to note that these charts do not include the two

poles related to $\theta \in \{0, \pi\}$. Using the fact that $d\hat{\boldsymbol{p}}/dt = \dot{\theta}\boldsymbol{e}_\theta + \sin\theta\dot{\varphi}\boldsymbol{e}_\varphi$, we can write the set of differential equations in terms of the spherical coordinates as:

$$\begin{cases} \dot{\theta} = \beta\cos\theta\sin\varphi \\ \dot{\varphi} = -\dfrac{1}{2} + \beta\dfrac{\cos\varphi}{\sin\theta} \end{cases} \tag{6.15}$$

With this set of equations, we can perform the stability analysis of the system on the coordinate chart description. First, we have to identify the fixed points of the system. For the system in question, it is clear that for $\beta > 1/2$ we have two fixed points given by $\theta = \pi/2$ and $\varphi = \pm\arccos\frac{1}{2\beta}$. Similarly, for $\beta < 1/2$, we have two fixed points given by $\phi = 0$ and the two points where $\sin\theta = 2\beta$.

The Jacobian matrix of the system is given by:

$$J = \begin{bmatrix} -\beta\sin\theta\sin\varphi & \beta\cos\theta\cos\varphi \\ -\dfrac{\beta\cos\varphi\cos\theta}{\sin^2\theta} & -\beta\dfrac{\sin\varphi}{\sin\theta} \end{bmatrix} \tag{6.16}$$

Thus, for the case in which $\beta > 1/2$, we have all the eigenvalues given by the same value. Namely,

$$\lambda = -\beta\sin\varphi. \tag{6.17}$$

Thus, we have the folowing classification for the critical points for the different possible values of $\sin\varphi$:

$$\sin\varphi = +\sqrt{1 - \left(\frac{1}{2\beta}\right)^2} \quad \text{(stable)} \tag{6.18}$$

and

$$\sin\varphi = -\sqrt{1 - \left(\frac{1}{2\beta}\right)^2} \quad \text{(unstable)}. \tag{6.19}$$

This result is easily seen in the plot of the vector field over S^2, as shown in figure 6.2. A physical interpretation of the result is that any possible initial configuration

for the direction (except from the point of unstable equilibrium, which has measure zero) will eventually end at the stable orientation.

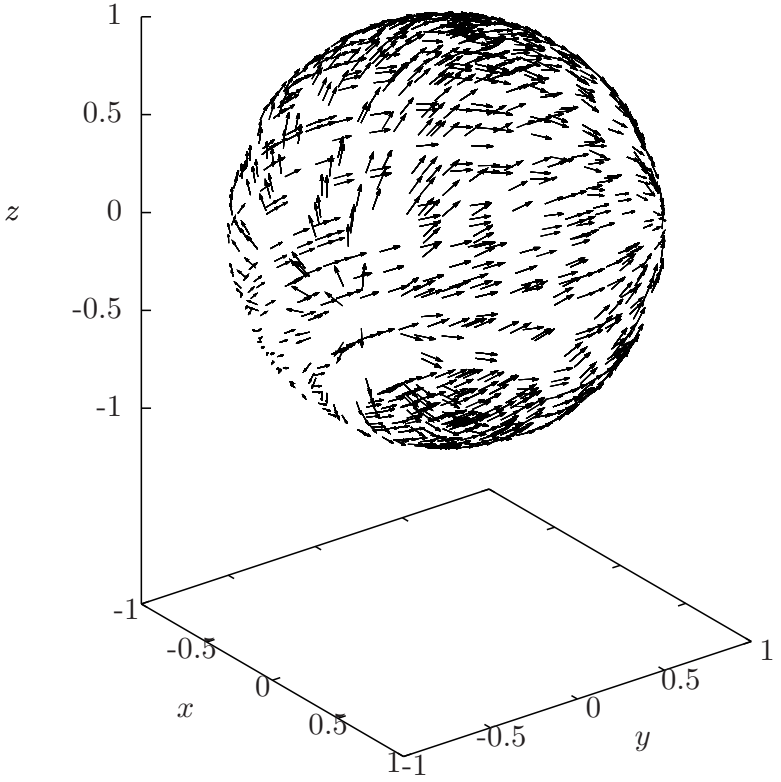

Figure 6.2: Representation of the vector field corresponding to the set of equations (6.9) on the imbedding of the unitary sphere S^2 in $\mathbb{R}^3$ for $\beta = 1.0$.

For values of $\beta < 1/2$, the equilibrium configuration of the system changes drastically. In this regime, the eigenvalues are given by:

$$\lambda = \pm i \frac{\beta}{|\tan\theta|} \quad \text{(neutral)} \tag{6.20}$$

For these values of β, the rotation induced by the fluid flow on the particle causes the particle to rotate around two possible axis.

Therefore, we can observe three main types of behavior for the system, illustrated by Figures 6.2, 6.3, and 6.4. These different behaviors are related to distinct values of the parameter β. In Figure 6.2, for $\beta > 1/2$, the system has a pair of

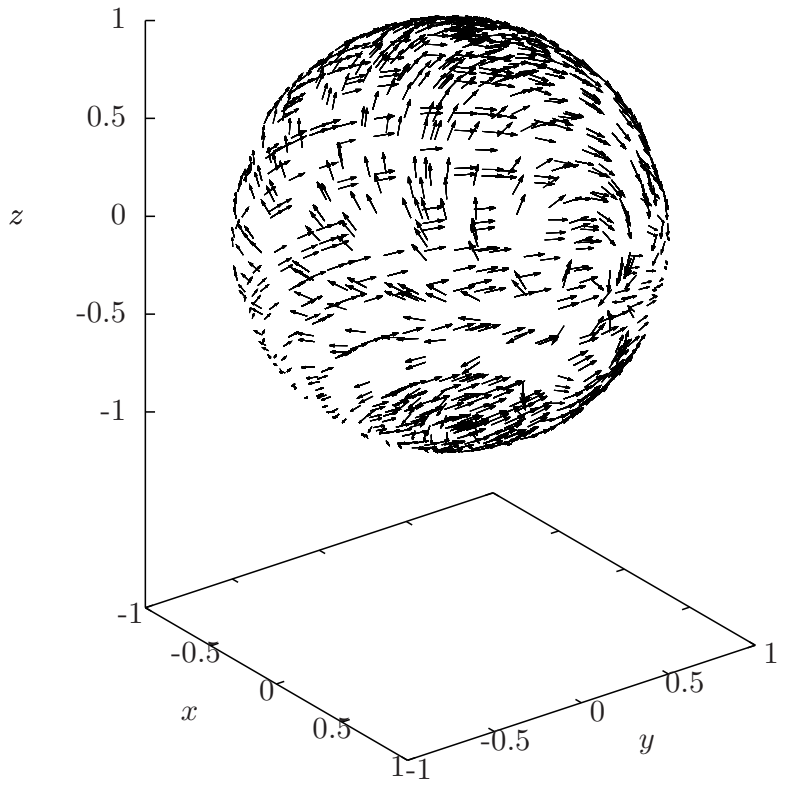

Figure 6.3: Representation of the vector field corresponding to the set of equations (6.9) on the imbedding of the unitary sphere S^2 in $\mathbb{R}^3$ for $\beta = 0.5$.

fixed points: a stable one and an unstable one. In this case, the effect of the external magnetic field surpasses the effect of the flow. As the value of β decreases, in the case of $\beta = 1/2$, as shown in Figure 6.3, we have a dipole behavior on the vector field, indicating the existence of a bifurcation on the system. At last, for values of $\beta < 1/2$, as shown in Figure 6.4, we have a vector field which indicates the existence of periodic orientational orbits. In fact, in the subsection 6.1.2, we prove this last statement by obtaining analytical expressions for the orbits of the system.

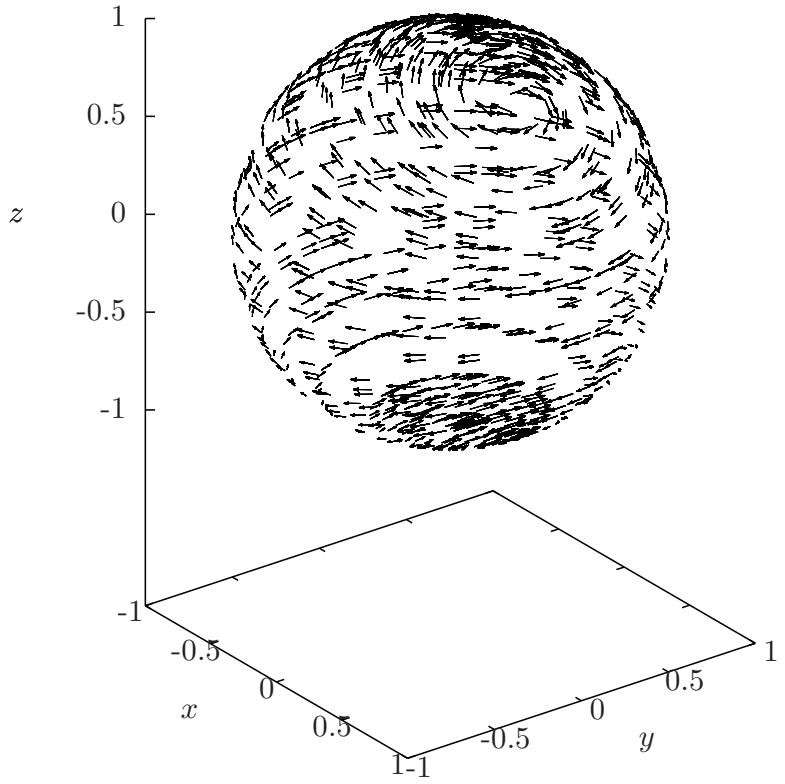

Figure 6.4: Representation of the vector field corresponding to the set of equations (6.9) on the imbedding of the unitary sphere S^2 in $\mathbb{R}^3$ for $\beta = 0.25$.

6.1.2 Analytical solution for the orbits

Although the set of differential equations governing the rotational dynamics of a magnetic particle in simple shear flow is non-linear, it is possible to find an analytic expression for the orbits of this system.

Combining both equations of the system in (6.15), we find a differential equation for φ as a function of θ. Namely,

$$\sin\varphi\frac{d\varphi}{d\theta} = -\frac{1}{2\beta\cos\theta} + \frac{\cos\varphi}{\sin\theta\cos\theta}. \tag{6.21}$$

Introducing the new variable $a = -\cos\varphi$, the differential equation for a in terms of θ is given by

$$\frac{da}{d\theta} + \frac{2a}{\sin 2\theta} = -\frac{1}{2\beta \cos\theta}, \tag{6.22}$$

which is a linear ordinary differential equation and can be solved by introducing an interating factor $\mu(\theta) = \csc 2\theta - \cot 2\theta$, which yields

$$a = -\frac{1}{\csc 2\theta - \cot 2\theta} \int \frac{d\theta}{2\beta} \frac{\sin\theta}{\cos^2\theta}. \tag{6.23}$$

Thus, by substituting the expression for $a = -\cos\varphi$ and making some simple algebraic manipulations, one finds that

$$\cos\varphi = \frac{1}{2\beta} \frac{1}{\sin\theta} + \frac{A}{\tan\theta}, \tag{6.24}$$

where A is an integration constant. Thus, we have found an exact analytical implicit expression for the orbits of the system.

Now, with this expression, we can plot the orbits of the system in order to capture and explore the dynamical behavior of the system for different values of the nondimensional magnetic field β. Figure 6.5 shows distinct configurations of the orbits of the system for different values of β. The results shown in Figure 6.5 are in close agreement with the behavior of the vector fields observed in Figures 6.2, 6.3, and 6.4, including the transition at $\beta = 0.5$. For values of $\beta < 1/2$, we can see that the orientational orbits are indeed closed and cyclic. As $\beta = 1.0$, in Figure 6.5 (a), the effects of the magnetic field dominate over the vorticity rotational effect, thus creating a stable fixed point in the system. As $\beta = 0.5$, in Figure 6.5 (b), both effects of shear vorticity and the external magnetic field balance each other. As $\beta < 0.25$, as shown in Figure 6.5 (c), the vorticity effect dominates the particle orientation. This dominance causes the arising of cyclic orbits.

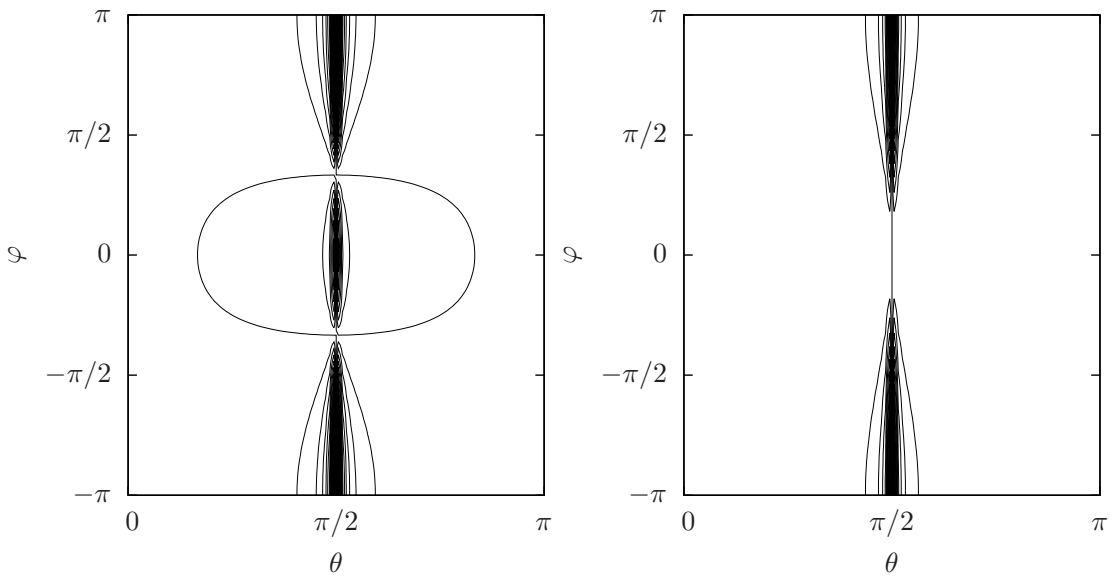

(a) $\beta = 1.00$ (b) $\beta = 0.50$

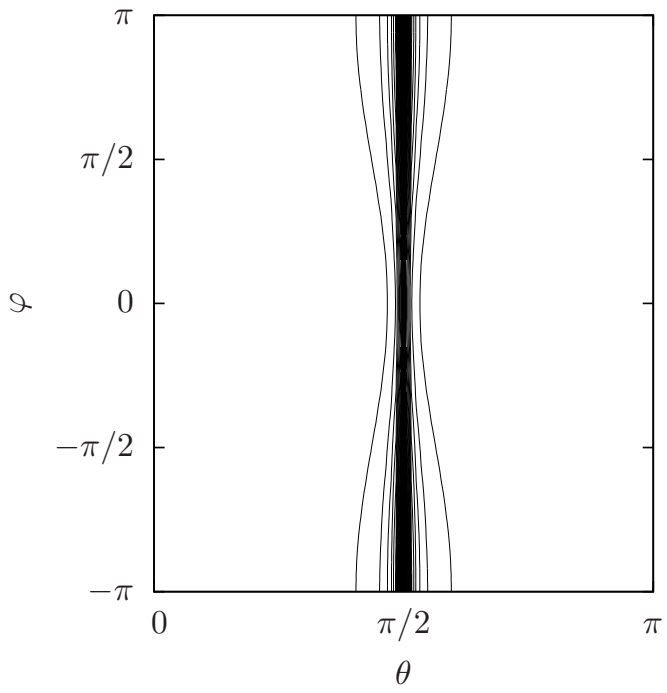

(c) $\beta = 0.25$

Figure 6.5: Orbits of the system in coordinate charts for different values of the nondimensional magnetic field β.

6.1.3 Magnetization

By examining the dynamical problem of a single particle, we can predict the magnetization of a very dilute non-Brownian suspension in the context with no interaction between the particles.

In chapter 2, the magnetization field was defined as being the spatial distribution of dipole moments. In the case of point dipoles, this distribution is a combination of Dirac's delta generalized functions. In our context, the property of interest is the averaged magnetization field.

For simplicity, we start by defining the average magnetization by a "volume average" approach. Using a similar argument to the one on chapter 2, which was used to introduce the notion of the continuum hypothesis, we define a small region $\delta V_{\boldsymbol{x}}$ at the neighborhood of the point $\boldsymbol{x}$ which contains a sufficiently large number of magnetic particles. Thus, we define the average magnetization at a point $\boldsymbol{x}$ as being:

$$\boldsymbol{M}(\boldsymbol{x}) = \frac{1}{V(\delta V_{\boldsymbol{x}})} \int_{\delta V_{\boldsymbol{x}}} \sum_{k=1}^{N} \boldsymbol{m}_k \delta(\boldsymbol{y} - \boldsymbol{x}_k) d\boldsymbol{y} = \frac{1}{V(\delta V_{\boldsymbol{x}})} \sum_{k=1}^{N_{\boldsymbol{x}}} \boldsymbol{m}_k, \tag{6.25}$$

where $N_{\boldsymbol{x}}$ is the number of particles contained in the region $\delta V_{\boldsymbol{x}}$. Alternativelly, we can write the equation for $\boldsymbol{M}$ as

$$\boldsymbol{M}(\boldsymbol{x}) = n(\boldsymbol{x}) \bar{\boldsymbol{m}}_{\boldsymbol{x}}, \tag{6.26}$$

where

$$\bar{\boldsymbol{m}}_{\boldsymbol{x}} = \frac{1}{N_{\boldsymbol{x}}} \sum_{k=1}^{N_{\boldsymbol{x}}} \boldsymbol{m}_k \tag{6.27}$$

is the mean value of the dipole moment of the particles in the region $\delta V_{\boldsymbol{x}}$.

Now we go back to our problem where particles in suspension do not interact with each other. In the case of very dilute suspensions, as illustrated in Figure 6.6,

the dynamics of each particle is independent of the others, due to the negligibility of their interactions. This independence enables us to treat each particle as an isolated particle suspended in a fluid undergoing a shear flow in the presence of an external magnetic field.

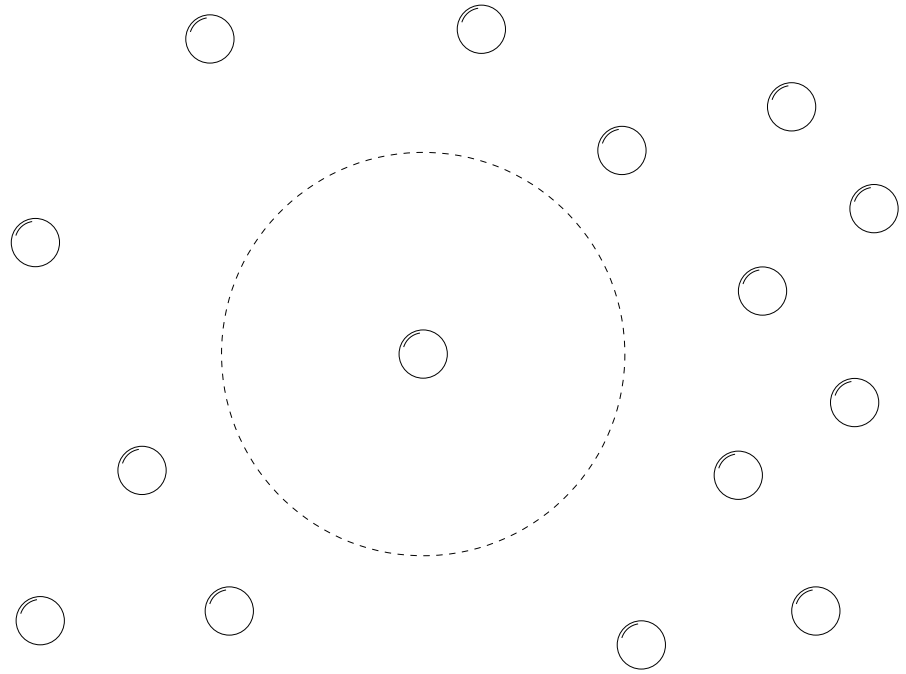

Figure 6.6: Illustration of a very dilute suspension (*i.e.* $\phi \ll 1$), where particle-particle interactions are neglected due to the fact that the particles are separated far apart from each other.

However, by the previous examination of the problem of a single particle, for $\beta > 1/2$, every trajectory starting from an initial orientation distinct from the unstable equilibrium point will end up at the stable equilibrium point. Thus, for the case of non-interacting particles, for values of β superior to $1/2$, the steady-state magnetization is known and is given by:

$$\boldsymbol{M} = nm_0 \left[\frac{1}{2\beta}\hat{\boldsymbol{e}}_1 + \sqrt{1 - \left(\frac{1}{2\beta}\right)^2}\hat{\boldsymbol{e}}_2 \right] + \mathcal{O}(\phi^2, \alpha) \tag{6.28}$$

This result shown in equation (6.28) is the leading order for the magnetization of the proposed problem of a very dilute suspension. As expected, at regimes of

strong fields ($\beta \gg 1$), the magnetization in the $y-$direction goes to $M_s = nm_0$, which indicates the alignment of all particles on the suspension with the magnetic field. This saturation of the magnetization in the $y-$direction is shown in Figure 6.7.

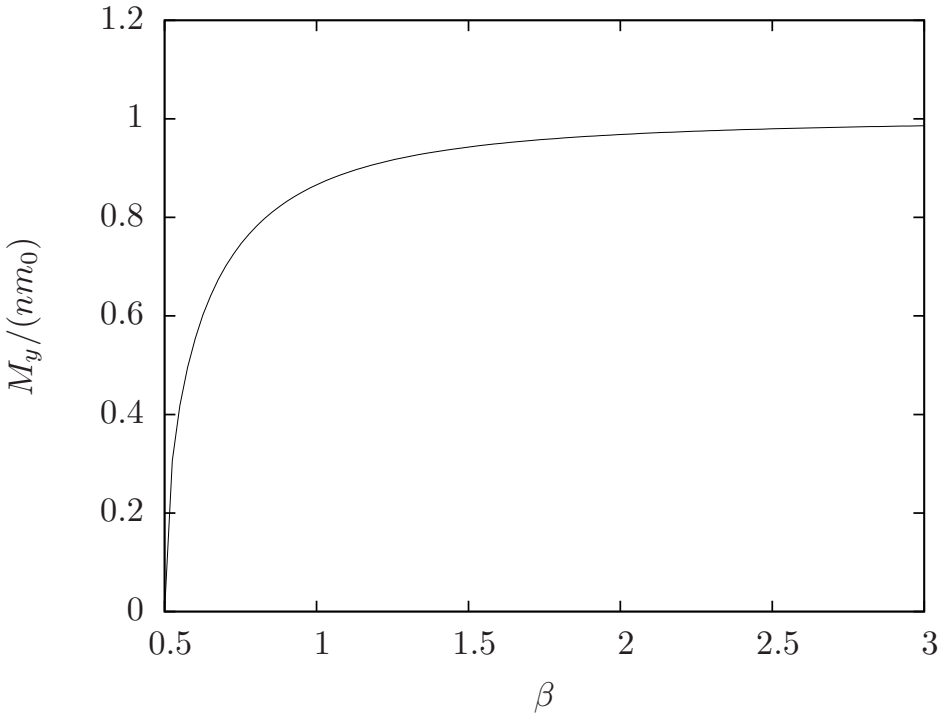

Figure 6.7: Saturation of the magnetization in the $y-$direction as a function of the field parameter β.

Thus, for values of β greater than $1/2$, we can see a behavior of the magnetization in the $y-$direction M_y in very dilute suspensions in the form of $M_y = M_s\mathscr{F}(\beta)$, with $\mathscr{F}(\beta) = \sqrt{1-(2\beta)^{-2}}$. There is a clear parallel between this form of the deterministic expression for the magnetization out of equilibrium for high Péclet numbers and classical equilibrium expressions such as Langevin's. Namely, Langevin's equation for a superparamagnetic material reads $M_y = M_s\mathscr{L}\left(\frac{\mu_0 m_0 H}{K_B T}\right)$, where $\mathscr{L}(x) = \coth(x) - \frac{1}{x}$ is the Langevin function.

It should be important to notice that the vorticity effect due to the external simple shear flow results in a non-zero magnetization in the $x-$direction. As we should discuss later, the component M_x of the magnetization is closely related to

the rotational viscosity effect.

6.1.4 Precession and Shliomis' equation

When studying the dynamics of a ferrofluid or another suspension of magnetic particles, the magnetization arrises naturally in the equations of motion [7, 11, 10]. Thus, a macroscopic equation for the evolution of this magnetization is needed in order to close the problem.

There are many equations describing the evolution of the magnetization field for ferrofluids. For the case of very diluted ferrofluids, Shliomis derived one of the first equations in [11].

$$\frac{\partial \boldsymbol{M}}{\partial t} + \boldsymbol{u} \cdot \nabla \boldsymbol{M} = \frac{1}{2}\boldsymbol{\xi} \times \boldsymbol{M} + \frac{1}{8\pi\mu a^3 n}\left(\boldsymbol{M} \times \boldsymbol{H}\right) \times \boldsymbol{M} - \frac{\boldsymbol{M} - \boldsymbol{M}_0}{\tau} \tag{6.29}$$

The derivation of this equation comes straight from differentiating and averaging the magnetization field, considering very dilute suspensions (without particle interactions), incompressible flow and making some considerations about the relaxation term, by using arguments from non-equilibrium thermodynamics.

Now, in order to write equation (6.29) in a nondimensional form, we have $||\boldsymbol{M}|| \sim M_s$, $||\boldsymbol{H}|| \sim H$, $||\boldsymbol{u}|| \sim \dot{\gamma} a$, $t \sim \dot{\gamma}^{-1}$ and $||\boldsymbol{x}|| \sim a$. Therefore, in terms of nondimensional variables, we have:

$$\frac{\partial \boldsymbol{M}}{\partial t} + \boldsymbol{u} \cdot \nabla \boldsymbol{M} = \frac{1}{2}\boldsymbol{\xi} \times \boldsymbol{M} + \beta\left(\boldsymbol{M} \times \boldsymbol{H}\right) \times \boldsymbol{M} - \frac{\boldsymbol{M} - \boldsymbol{M}_0}{Pe}, \tag{6.30}$$

where $Pe = \tau\dot{\gamma}$. For suspensions without magnetic relexation (*i.e.* $Pe \to \infty$) and considering spacial homogeneity, Shliomis' equation yields the same structure of equation (6.5). Namely:

$$\frac{\partial \boldsymbol{M}}{\partial t} = \frac{1}{2}\boldsymbol{\xi} \times \boldsymbol{M} + \beta\left(\boldsymbol{M} \times \boldsymbol{H}\right) \times \boldsymbol{M}. \tag{6.31}$$

For the case of a uniform external magnetic field, equation (6.31) is just the average of (6.5) for a very dilute suspension (neglecting dipole correlations). In fact, in this context we have $\boldsymbol{H} = \hat{\boldsymbol{h}}$ and $\boldsymbol{M} = \langle \hat{\boldsymbol{p}} \rangle$. Thus, the steady solutions and stability analysis for equation (6.5) also yield some information concerning Shliomis' equation for a uniform magnetic field without relaxation.

By our analysis, in the regime of $Pe \to \infty$, for $\beta < 1/2$, the problem of Shliomis' equation becames highly three-dimensional, as the orbits of the particles are mostly out of the xy plane. Therefore, we argue that there is an intrinsic three-dimensionality in the shliomis equation for high Péclet numbers, due to the asymmetry of the center of the periodic orientation orbits in the x direction.

6.2 Extracting the second order of the magnetization from two-particle numerical simulations

In the last section, we have obtained an analytical expression for the first order of the stationary non-equilibrium magnetization field in the context of high Péclet numbers through simple arguments over the problem of an isolated spherical rigid particle undergoing a simple shear flow in the presence of an external magnetic field. Now, we shall explore the effect of hydrodynamic and dipolar particle-particle interactions on the steady-state magnetization.

For this purpose, we shall expand our previous arguments developed in subsection 6.1.3 in order to propose a numerical method to calculate the order $\mathcal{O}(\lambda, \phi^2)$ of the magnetization by using the two-particle dynamics.

6.2.1 Cluster expansion for magnetization

In order to find an expression for the macroscopic magnetization field $\boldsymbol{M}$, we shall start from a microscopic point of view. As before, we consider the fixed magnetic dipole of a particle to be located at the center of the particle. It should

be important to note that although the dipole is a singularity, the particles have a finite radius. The microscopic magnetization field for a classical system of dipoles is given by:

$$\boldsymbol{M}(\boldsymbol{x}_0, \hat{\boldsymbol{p}}_0, \ldots \boldsymbol{x}_N, \hat{\boldsymbol{p}}_N; \boldsymbol{x}) = \sum_{k=0}^{N} m_0 \hat{\boldsymbol{p}}_k \delta(\boldsymbol{x} - \boldsymbol{x}_k). \tag{6.32}$$

In this problem, all the particles have the same size, same dipole moment intensity and are, in a classical sense, identical, so that the probability distribution is not affected by a change of the particle labels. Thus, the average magnetization is given by:

$$\langle \boldsymbol{M} \rangle (\boldsymbol{x}) = n(\boldsymbol{x}) \int m_0 \hat{\boldsymbol{p}}_0 P(\hat{\boldsymbol{p}}_0, \mathscr{C}_N | \boldsymbol{x}) d\hat{\boldsymbol{p}}_0 \, d\mathscr{C}_N, \tag{6.33}$$

where $P(\hat{\boldsymbol{p}}_0, \mathscr{C}_N | \boldsymbol{x})$ is the conditional probability distribution of the reference particle having orientation $\hat{\boldsymbol{p}}_0$ and the other dipoles having configuration $\mathscr{C}_N$ given that the reference particle is centered at $\boldsymbol{x}$. Now, we wish to break the complex problem of averaging over the configuration of many particles in multiple simpler problems involving fewer particles. Performing a cluster expansion on $\hat{\boldsymbol{p}}_0$, we find:

$$\hat{\boldsymbol{p}}_0 = \boldsymbol{d}^0 + \sum_{i}^{N} \boldsymbol{d}_i^1 + \sum_{i<j=1}^{N} \boldsymbol{d}_{ij}^2 + \ldots \tag{6.34}$$

where the term $\boldsymbol{d}^0$ represents the contribution of the dynamics of an isolated particle, the terms $\boldsymbol{d}^1$ represent the contribution due to the interactions between two particles, and so on. Therefore, the average magnetization takes the form of[1]:

$$\langle \boldsymbol{M} \rangle (\boldsymbol{x}) = n(\boldsymbol{x}) m_0 \left\langle \boldsymbol{d}^0 \right\rangle + n(\boldsymbol{x})^2 m_0 \int \boldsymbol{d}_1^1 g(\hat{\boldsymbol{p}}_0, \hat{\boldsymbol{p}}_1, \boldsymbol{r}) d\hat{\boldsymbol{p}}_0 \, d\hat{\boldsymbol{p}}_1 \, d\boldsymbol{r} + \ldots \tag{6.35}$$

where $g(\hat{\boldsymbol{p}}_0, \hat{\boldsymbol{p}}_1, \boldsymbol{r}) = P(\hat{\boldsymbol{p}}_0, \boldsymbol{x}_1, \hat{\boldsymbol{p}}_1 | \boldsymbol{x}) / P(\boldsymbol{x})$ is the normalized conditional probability distribution related to the two-particle problem. This function goes to 1 as

[1] At this point, it should be important to note that we had performed a slight change of notation in comparison to Chapter 3. Namely, we have re-labeled our reference particle 0 and the test particle (which collides with the reference particle) 1. Hence, the orientations $\hat{\boldsymbol{p}}_0$ and $\hat{\boldsymbol{p}}_1$ are related, respectively, to the reference and test particles

$\boldsymbol{r} = \boldsymbol{x}_1 - \boldsymbol{x}$ goes to infinity. Looking at equation (6.35), we see that the calculation of a order n^2 of the magnetization consists in the computation of the integral in equation (6.35), which is related to the two-particle trajectory problem. Truncating the cluster expansion in equation (6.34) at first and second orders, we find, respectively:

$$\boldsymbol{d}^0 = \hat{\boldsymbol{p}}_0^{(1)}, \tag{6.36}$$

$$\boldsymbol{d}_1^1 = \hat{\boldsymbol{p}}_0^{(2)} - \hat{\boldsymbol{p}}_0^{(1)}. \tag{6.37}$$

The general expression for a higher order of the expansion is well known and can be found with a high level of details in works such as [8]. In the present context, it is not necessary to present such generalization. It should be important to note that $\boldsymbol{d}_1^1$ vanishes as $\boldsymbol{r} \to \infty$. Nevertheless, one has to be careful when dealing with those integrals, as the magnetic torques are of order r^{-3}, which indicates long-range interactions, sometimes leading to non-converging integrals which require a renormalization procedure.

6.2.2 Probability distribution

The general probability distribution $P(\boldsymbol{X}, t)$ satisfies the equation of continuity already presented in Chapter 2. This equation can also be written in the form of:

$$\frac{\partial P}{\partial t} = \mathscr{L} P, \tag{6.38}$$

where $\mathscr{L} = -\frac{\partial}{\partial \boldsymbol{X}} \cdot (\boldsymbol{V}(*))$ is a linear time-independent operator and $\boldsymbol{V} = \frac{d\boldsymbol{X}}{dt}$ is the "velocity" of the random variable $\boldsymbol{X}$. In our problem, there is no random or stochastic contributions in this velocity term. The formal solution for this equation is, thus:

$$P(\boldsymbol{X}, t) = e^{t\mathscr{L}} P(\boldsymbol{X}, 0), \tag{6.39}$$

where $P(\boldsymbol{X}, 0)$ is a given initial probability distribution. An important property of this operator $\mathscr{L}$ is that it is the adjoint of the operator $\mathscr{L}^\dagger = \boldsymbol{V} \cdot \frac{\partial}{\partial \boldsymbol{X}}$. This operator appears in the evolution of a function of the variable $\boldsymbol{X}$:

$$f(\boldsymbol{X}, t) \equiv f(\boldsymbol{X}_t) = e^{t\mathscr{L}^\dagger} f(\boldsymbol{X}) \tag{6.40}$$

This expression means that we can compute the averages of a random variable $f(\boldsymbol{X})$ at a given time t by evolving the variable $\boldsymbol{X}$ using the dynamics of the system and taking the average over the initial probability distribution instead of finding an expression for the time-dependent probability distribution. Namely,

$$\langle f; t \rangle = \int f(\boldsymbol{X}) P(\boldsymbol{X}, t) d\boldsymbol{X} = \int f(\boldsymbol{X}_t) P(\boldsymbol{X}, 0) d\boldsymbol{X}. \tag{6.41}$$

This result can be found in classical textbooks such as [50] and it is very important to the numerical procedure, as it shows that once solved the dynamical problem, there is no need to solve the evolution of the probability distribution in order to perform the averages involving functions of the dynamical variables.

6.2.3 Numerical procedure

As it was seen in subsection 6.2.1, the second order of the magnetization would depend, theoretically, on the dynamical problem of two particles interacting in an infinite space. However, for our numerical computation, we make some changes to the problem in order to avoid dealing with infinite spaces and probably divergent integrals, which would force us to adopt a renormalization procedure, such as the one presented in [61].

The first modification to the problem is to change the infinite space to a space with bounded x length by imposing periodic conditions in the x direction. Then, we shall introduce cutoff distances in y and z in which the integrand is very small, meaning that beyond this region, the effects of interaction between the particles are negligible. Figure 6.8 illustrates the topology of the modified problem of two

particles[2].

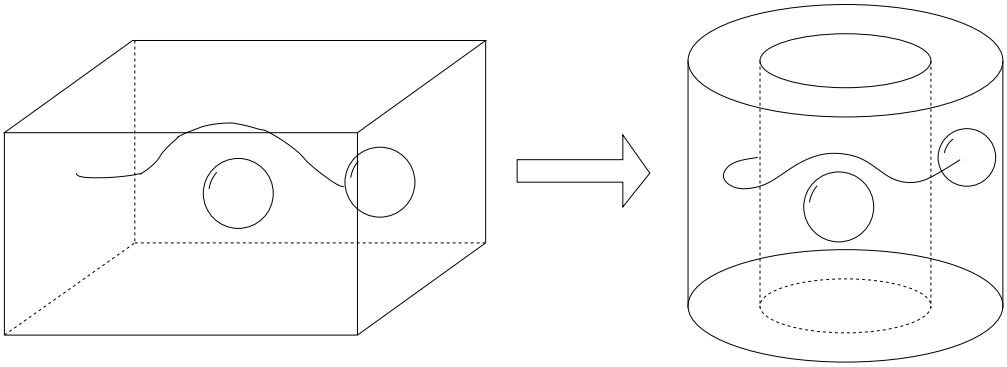

Figure 6.8: Modification on the topology of the problem of two particles

Now, we proceed to the explicit computation of the second order magnetization. Writing the expression for the magnetization on the following form:

$$\langle \boldsymbol{M} \rangle (\boldsymbol{x}) = n\boldsymbol{M}_1 + n^2 \boldsymbol{M}_2 + \mathcal{O}(n^3), \tag{6.42}$$

we can indentify the term $\boldsymbol{M}_2$ on equation (6.35) as being:

$$\boldsymbol{M}_2 = \lim_{t\to\infty} m_0 \int \left[\hat{\boldsymbol{p}}_0^{(2)} - \hat{\boldsymbol{p}}_0^{(1)}\right] g(\boldsymbol{r}, \hat{\boldsymbol{p}}_0^{(2)}, \hat{\boldsymbol{p}}_1^{(2)}; t) d\boldsymbol{r}\ d\hat{\boldsymbol{p}}_0^{(2)}\ d\hat{\boldsymbol{p}}_1^{(2)}, \tag{6.43}$$

where the term $\hat{\boldsymbol{p}}_0^{(1)}$ comes from the single particle problem and the limit $t \to \infty$ is taken because we are interested in the steady state of magnetization at high Péclet numbers. Given that the expression for the distribution function g is unknown, we make use of equation (6.41) to transfer the time-dependence from the probability distribution to the dynamical variables. Thus, one can choose an initial uniform distribution:

$$g(\boldsymbol{r}, \hat{\boldsymbol{p}}_0^{(2)}, \hat{\boldsymbol{p}}_1^{(2)}; 0) d\boldsymbol{r}\ d\hat{\boldsymbol{p}}_0^{(2)}\ d\hat{\boldsymbol{p}}_1^{(2)} = \frac{1}{(4\pi)^2} \mathbb{I}_{\Omega_{disp}} \sin(\theta_0)\sin(\theta_1) dV\ d\theta_0\ d\varphi_0\ d\theta_1\ d\varphi_1. \tag{6.44}$$

[2]We also define the distance between the particles to be the minimal distance, avoiding problems in the computation of forces and torques.

The choice for this uniform initial distribution is related to the fact that the integration domain is invariant to the transformations of the dynamical system. We expect that the chosen initial distribution converges to the steady-state solution at large times.

For the numerical evaluation of the integral, we use the Monte-Carlo integration method. Thus, the approximate expression for the integal is given by:

$$\boldsymbol{M}_2 \approx \frac{m_0 V_{sim} \pi^2}{4N} \sum_{k=1}^{N} \left[\hat{\boldsymbol{p}}_0^{(2)}(T) - \hat{\boldsymbol{p}}_0^{(1)}(T) \right] \sin(\theta_0^k(T)) \sin(\theta_1^k(T)) \mathbb{I}_{\Omega_{disp}}, \tag{6.45}$$

where V_{sim} is the volume of integration and T is a time large enough for the average to converge to the steady state. This expression shares a lot of similarities with the ones used to compute the diffusivities and doublet formation rate described in Chapters 4 and 5, respectively. Now, as we only deal with nondimensional quantities, we define a nondimensional magnetization:

$$\boldsymbol{M} \to \frac{m_0}{a^3} \boldsymbol{M}, \tag{6.46}$$

where a os the radius of a single particle in the monodisperse suspension. Thus, equation (6.42) transforms into:

$$\boldsymbol{M} = \phi \boldsymbol{M}_1(\beta) + \phi^2 \boldsymbol{M}_2(\alpha, \beta) + \mathcal{O}(\phi^3), \tag{6.47}$$

with

$$\boldsymbol{M}_2 \approx \frac{9}{64} \frac{\tilde{V}_{sim}}{N} \sum_{k=1}^{N} \left[\hat{\boldsymbol{p}}_0^{(2)}(T) - \hat{\boldsymbol{p}}_0^{(1)}(T) \right] \sin(\theta_0^k(T)) \sin(\theta_1^k(T)) \mathbb{I}_{\Omega_{disp}}, \tag{6.48}$$

With this expression, we are able to perform a numerical computation for the second order $\boldsymbol{M}_2$ of the magnetization.

6.2.4 Numerical results

The numerical computation for the second order magnetization has been performed for eight different values of α ranging from 0.05 to 0.4 and a fixed value for $\beta = 1$. This value for β was chosen simply due to the fact that it is greater than 1/2, as discussed before.

For the Monte-Carlo integration, we used 1×10^6 points, obtaining an estimate for the intrinscic error at order 1%. Figures 6.9 and 6.10 show the values obtained by the Monte-Carlo integration for different times and $\alpha = 0.15$, indicating the convergence to a steady state, considering the estimated error for the Monte-Carlo integration. In these figures, we can see a convergence of M_{2x} and M_{2y} for $t \sim 300\ t_{flow}$, with $t_{flow} = \dot{\gamma}^{-1}$.

The time range for simulation was set from $t = 0$ to $t = 500$. As we used $\beta = 1$, the time scale related to magnetic relaxation is at the same order of the characteristic time $\dot{\gamma}^{-1}$. For this reason, we consider $t = 500$ to be a time large enough in order to obtain a steady-state for the magnetization. Indeed, for values of α less than 0.35, we obtained a behavior good enough to be considered a steady state, such as the ones showed in Figures 6.9 and 6.10.

Considering that the magnetization has reached a steady state, we can plot the second order magnetization for different values of α by taking the average of the values that we considered to be inside the steady state, with an associated error given by the standard deviation. This result allows us to better understand how the hydrodynamic and magnetic interactions influence the magnetization for dilute non-Brownian magnetic suspensions. The results of the simulations for the x and y components of the second order magnetization are shown respectively by Figures 6.11 and 6.12 at $t = 300$ for different values of α.

For small values of α, we were able to fit a straight line on the data, indicating the existence of an expression for the magnetization of the form

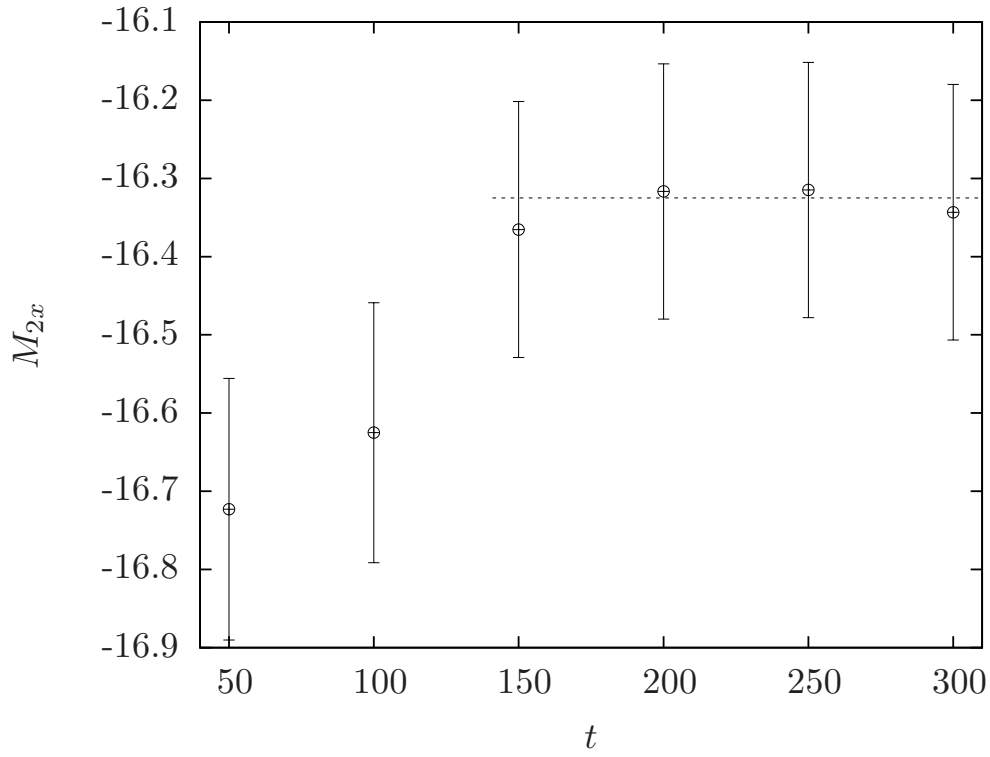

Figure 6.9: Nondimensional magnetization M_{2x} as a function of the nondimensional time for $t \in [0, 300]$, $\beta = 1.0$ and $\alpha = 0.15$. The errorbars indicate the intrinsic error estimated for the Monte-Carlo method. The dashed line indicates the average value which we consider to be the steady state.

$$M_x = M_{1x}\phi + M_{21x}\phi^2 + M_{22x}\alpha\ \phi^2 + \mathcal{O}(\alpha^2, \phi^3) \tag{6.49}$$

$$\text{and} \qquad M_y = M_{1y}\phi + M_{21y}\phi^2 + M_{22y}\alpha\ \phi^2 + \mathcal{O}(\alpha^2, \phi^3), \tag{6.50}$$

where M_{1x} and M_{1y} are determined by our first order analysis, from equation (6.28). In the case where $\beta = 1$, M_{21x}, M_{22x}, M_{21y}, and M_{22y} are found by the linear fitting of the results shown in Figures 6.11 and 6.12. Namely, for $\beta = 1$, we have:

$$M_x \approx 0.11936\phi - 17.0701\ \phi^2 + 5.12544\ \alpha\ \phi^2 + \mathcal{O}(\alpha^2, \phi^3) \tag{6.51}$$

$$\text{and} \qquad M_y \approx 0.20674\phi + 6.75379\ \phi^2 - 2.06662\ \alpha\ \phi^2 + \mathcal{O}(\alpha^2, \phi^3) \tag{6.52}$$

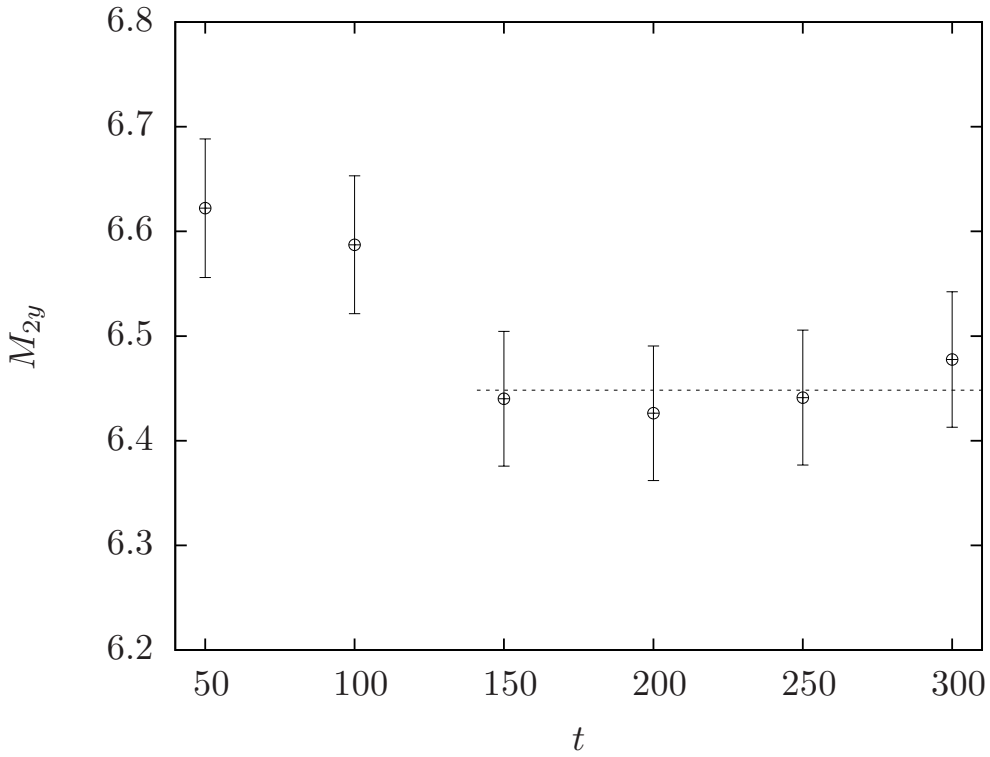

Figure 6.10: Nondimensional magnetization M_{2y} as a function of the nondimensional time for $t \in [0, 300]$, $\beta = 1.0$ and $\alpha = 0.15$. The errorbars indicate the intrinsic error estimated for the Monte-Carlo method. The dashed line indicates the average value which we consider to be the steady state.

By performing a simple asymptotic expansion, it is easy to see that for very small values of the volume fraction ϕ, the y component of the magnetization is much larger than the x component in the case of $\beta = 1$. Namely, we have $M_y/M_x \sim 1.7320 + 304.2930\ \phi$.

An interesting finding to emphasize is that the numerical results indicate the existence of a second-order contribution to the magnetization due to hydrodynamic interactions even in the absence of dipolar interactions between the particles. This contribution acts increasing the magnetization in the field direction. The fact that the hydrodynamic interactions help to increase the alignment of the particles with the field is probably due to hydrodynamic reflections of the magnetic torque induced by the field on a single particle. In fact, the hydrodynamic interactions between the particles produce a randomization effect on the suspension. In the

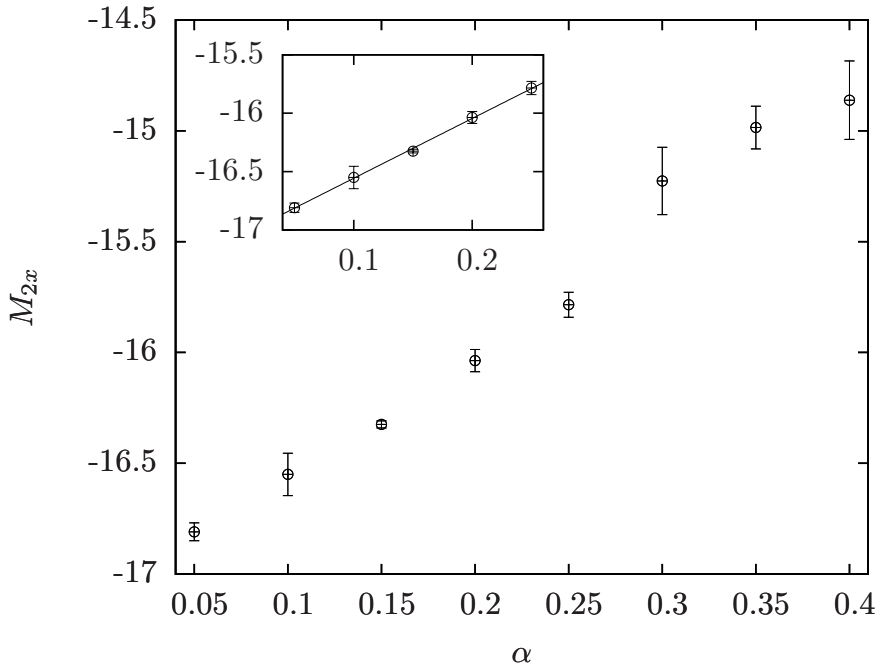

Figure 6.11: Simulation results of M_{2x} as a function of the dipolar interaction parameter α for $\beta = 1$. The insert shows a linear fit for small values of α.

absence of dipolar interactions between the particles, this effect tends to break the anisotropy due to shear vorticity, causing the particles to align with the field and, thus, increasing the magnetization component M_y. It should be interesting to note that this result contrasts with the first-order hydrodynamic contribution. Namely, while the shear viscosity effect tends to break the alignment of the particle with the magnetic field, hydrodynamic interactions increases this alignment.

In contrast, dipolar interactions increase the correlation between the orientation of the particles. The higher correlation of particle orientation decreases the randomization contribution of the hydrodynamic interactions. In real suspensions, the dipolar interactions produce an irreversible effect which can cause the formation of clusters of particles. For high Péclet numbers and $\beta \sim 1$, these particle clusters try to align with the flow direction, thus decreasing the y component of magnetization. This alignment may influence the rheology of the suspension, giving rise to effects such as normal stress differences.

Both of the discussed behaviors can be seen in Figure 6.13, which shows the

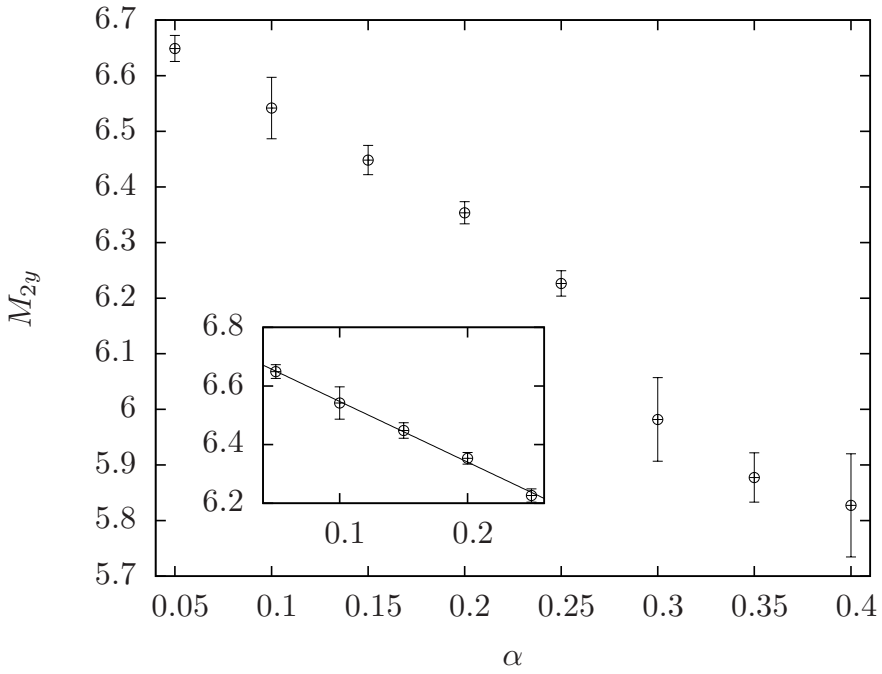

Figure 6.12: Simulation results of M_{2y} as a function of the dipolar interaction parameter α for $\beta = 1$. The insert shows a linear fit for small values of α.

y component of the nondimensional magnetization as a function of the volume fraction ϕ for different values of alpha. In fact, the increase of the parameter alpha results in a decrease the y component of the magnetization. For small values of the volume fraction ϕ, it is hard to distinguish between the values of magnetization for different values of α, as seen in the insert of Figure 6.13. In this context of small concentrations the particles are distanced far apart from each other, thus the effect of hydrodynamic interaction $\mathcal{O}(r^{-2})$ dominates over the dipole interaction effects $\mathcal{O}(r^{-3})$. For higher values of volume fraction, the effect of dipole interaction starts to appear more strongly.

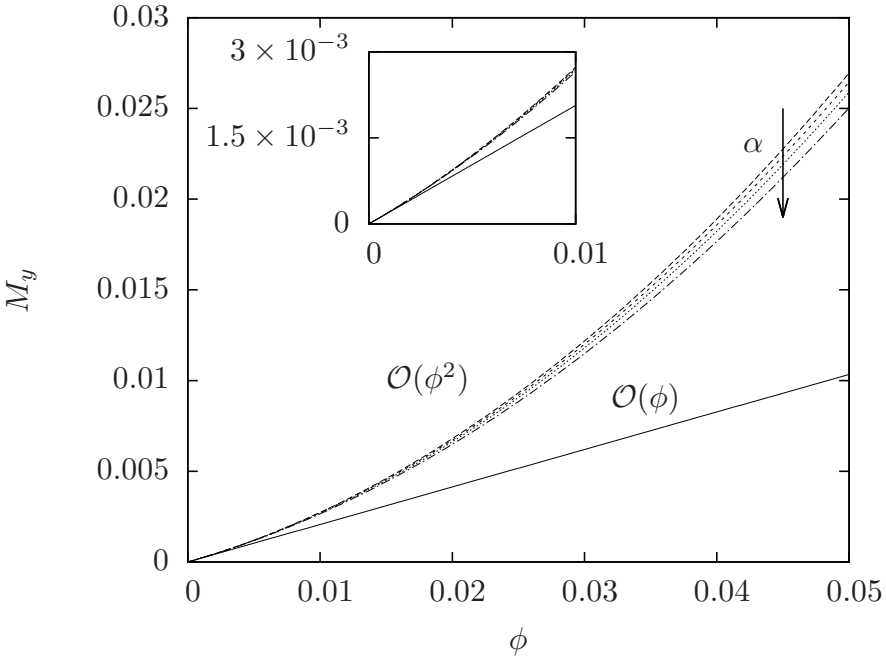

Figure 6.13: y component of the nondimensional magnetization as a function of the volume fraction ϕ for different values of α.

6.3 A brief discussion on the rotational viscosity

With the calculations presented in the present chapter, we can also obtain some results concerning the rotational viscosity of the suspension associated with the magnetic torque and consequently non-symmetric effects on the fluid (*i.e.* magnetoviscous effect) in the context of suspensions at high Péclet numbers. In simple shear, for a uniform external magnetic field in the y direction, we have by definition:

$$\eta_r = \mu_0 \frac{M_x H}{2\dot{\gamma}}. \tag{6.53}$$

Alternatively, in terms of the previously defined nondimensional quantities, we have:

$$\frac{\eta_r}{\mu} = 4\pi\beta M_x. \tag{6.54}$$

Therefore, by equation (6.28), we have the first order of rotational magnetization given by $\eta_r/\mu = 3\phi/2$. It should be important to note that the leading order of the rotational viscosity at a regime of high Péclet numbers in the presence of a uniform magnetic field does not depend on the intensity of the field itself. This result can be seen as an asymptotic limit of Shliomis' expression [11] at the limit of low temperatures. At second order, our numerical simulation results suggest that the isolated effect of hydrodynamic interactions between particles may result in a decrease on the rotational viscosity while the dipolar interactions between the particles may increase the magnetoviscous effect.

CHAPTER 7

CONCLUSION AND FUTURE WORK

> Begin at the beginning, the King said gravely, "and go on till you come to the end: then stop."
>
> Lewis Carroll, *Alice in Wonderland*

In this dissertation, we have explored the dynamics of a pair of magnetic particles undergoing a simple shear flow at low Reynolds numbers and high Péclet numbers. By the use of numerical simulations, we were able to analyze the dynamics of closed and open relative trajectories. We have also examined the interplay between these trajectories. In fact, by examining the plots of two-dimensional sections of the aggregative region, which is a subset of the 7−dimensional dynamical space, we were able to observe the complex behavior at the interface between the aggregative and dispersive regions.

By using the results of the dynamical simulation of two rigid magnetic spheres undergoing a simple shear flow, we were able to obtain values for transport properties of dilute magnetic suspensions, such as the shear-induced hydrodynamic

diffusivity and doublet formation rate. Also, we were able to obtain an exact expression for the first order magnetization for non-Brownian suspensions out of equilibrium undergoing a simple shear flow in the presence of a uniform external magnetic field. A numerical prediction for the second order of magnetization was also found by the use of the two-particle dynamical simulation developed in this work.

In the next sections of this chapter, we outline the main results of this work, highlighting the more interesting points.

7.1 Two-particle dynamics

In the investigation of the dynamics of two particles, we have found an unusual behavior on the relative trajectories of particles. Namely, some simulations yielded trajectories in which the test particle looped around the center a number of times. Some of these trajectories resulted in particles crossing the end plane with negative $y-$positions.

We analyzed the symmetry breaking of the problem through scatter sections, which represents the end positions of a uniform beam of particles after colliding with the reference particle at the origin. In addition, we also investigated the aggregative region of collisions in the starting plane for a given initial pair of orientations.

The results of the simulation indicate that the aggregative region (*i.e.* the starting points of closed trajectories) gets bigger with the increase of the attraction parameter α. The boundary region between the aggregative region and the region of open trajectories was found to be very irregular and appears to show some self-similar structures at the interface with the dispersive region.

7.2 Hydrodynamic diffusion and aggregation

Based on particle trajectory analysis we have computed self-diffusivities and the rate of particle aggregation for a dilute magnetic suspension with particles interacting hydrodynamically and magnetically. These macroscopic quantities are displayed as functions of the strength of the dipole-dipole magnetic interaction, which measures the relative importance between magnetic particle interaction in comparison with viscous effects in the suspension, including hydrodynamic interactions.

The self-diffusivities and the rate of particle aggregation were found to be increasing functions of the magnetic parameter α. By comparing the $\mathcal{O}(\phi)$ of the self-diffusivity of magnetic particles for small values of α with those of non-magnetic rough particles [16] for small values of roughness ε, we have seen that the values for the self-diffusivities are slightly greater for the case of rough particles. For instance, taking a value of roughness $\varepsilon = 4 \times 10^{-2}$, the dimensionless $\mathcal{O}(\phi)$ self-diffusivity is calculated as being approximately 0.015, while for the same value of α, the self-diffusivity is given approximately by 0.008. The value of α which gives the same value for the self-diffusivity as $\varepsilon = 4 \times 10^{-2}$ is $\alpha \approx 9 \times 10^{-2}$. In the asymptotic limit for small α we determined that: $\mathcal{D}^S_{yy} = \dot{\gamma} a^2 \phi f_{yy}(\alpha)$, with $f_{yy}(\alpha) \approx 0.1564\ \alpha^{0.5467} \left(\frac{5}{4}\log(1/\alpha) + 1.347\right)^{-0.7012}$, according to a theoretical prediction for a arbitrary small parameter breaking time-reversibility of particle trajectories [16]. In addition, the rate of doublet formation is predicted as being $dN_2/dt = n_1 N_1 \dot{\gamma} a^3 J_{11}$, with $J_{11} \approx 2.4389\ \alpha^{1/2}$.

In addition, some problems arose when trying to compute the down-gradient diffusivity numerically. The computation yielded negative values for the components of the diffusivity tensor, due to the magnetic attraction between the particles, even after excluding aggregative trajectories. Unlike the case investigated in the paper of [16], in which the flux contribution for the down-gradient diffusivity lead to an increase of the self-diffusivity, the flux terms numerically computed in our case were all negative and sometimes larger, in module, then the self-diffusion contribution. With the results from the numerical integration, we observed that the

order $\mathcal{O}(\phi)$ of shear-induced diffusion in the directions of higher aggregation can be dominated by the attraction between the particles even for small values of α.

7.3 Magnetization

In addition to the investigation of self-diffusivity and doublet formation rate, we also explored in this work the magnetization of non-Brownian solutions in a non-equilibrium regime. By investigating the problem of an isolated particle on shear flow, we were able to extract the first-order approximation for the magnetization of non-Brownian suspensions. In contrast with the problem for low or moderate Péclet numbers, the first order of the magnetization investigated here is completely deterministic, as the dynamics of the particles have a stable equilibrium point for values of $\beta > 1/2$. We were also able to determine analytic expressions for the orbits of the problem and to characterize the different behaviors for distinct values of the parameter β, which is related to the intensity of the field.

Moreover, we have used a non-renormalized cluster expansion, coupled with our numerical dynamical simulation of two particles, in order to find a numerical value for a second order of the magnetization. Our simulations have shown that the hydrodynamic interaction between the particles has significant contributions at second order. This result is intriguing, as it shows that even in the absence of dipolar interaction effects (*i.e.* $\alpha \to 0$), the hydrodynamic interaction between the particles alone can influence the second-order of magnetization.

7.4 Future work

The dynamical problem of two particles is a powerful tool for investigating physical properties of very dilute suspensions which depend on particle interaction. For future work, we suggest the implementation of polydispersity in the model, which is a significant parameter in real suspensions. With the implementation of polydispersity and the formulation presented in this work, one could obtain

the results for hydrodynamic diffusivity and doublet formation rate in the case of sedimentation considering the effects of particle rotation and averaging over all possible initial orientations. We should also explore the effect of a magnetic field over the doublet formation rate. We speculate that an increase in the magnetic field intensity should also increase the aggregation rate.

Other suggestions for future work include a different compactification for space of the dynamical system in order to compute the magnetization, comparing the results with the ones obtained in this work, and the implementation of the numerical computation of the second order of particle stress, in order to extract the effective viscosity of the suspension at order $\mathcal{O}(\phi^2)$. With this approach, we should be able to explore the rheology associated with the normal stress differences N_1 and N_2. With the present code, we can also obtain results for different kinds of external flow, such as oscillatory shear and step-strain, as well as implement a repulsion force (which physically would correspond to the introduction of a surfactant coating of the particle), in order to prevent the particles from aggregate. We speculate that this interaction should avoid (or at least, reduce) the negative values in the computation of the flux term of down-gradient diffusivity.

BIBLIOGRAPHY

[1] G. Batchelor, "Developments in microhydrodynamics," in *Theoretical and Applied Mechanics Congress*, pp. 33–55, 1977.

[2] W. B. Russel, D. A. Saville, and W. R. Schowalter, *Colloidal dispersions*. Cambridge university press, 1989.

[3] H. A. Barnes, J. F. Hutton, and K. Walters, *An introduction to rheology*, vol. 3. Elsevier, 1989.

[4] C. Rinaldi, A. Chaves, S. Elborai, X. T. He, and M. Zahn, "Magnetic fluid rheology and flows," *Current Opinion in Colloid & Interface Science*, vol. 10, no. 3-4, pp. 141–157, 2005.

[5] A. Einstein, *Investigations on the Theory of the Brownian Movement*. Courier Corporation, 1956.

[6] F. R. Cunha, "Fundamentos da hidrodinâmica de fluidos magnéticos," in *Turbulência* (B. S. Carmo, G. R. Assi, J. R. Meneghini, J. A. P. Aranha, and E. V. Volpe, eds.), vol. 8, ch. 7, pp. 257–339, Brazil: ABCM, 2012.

[7] R. E. Rosensweig, *Ferrohydrodynamics*. Courier Corporation, 2013.

[8] B. U. Felderhof, G. W. Ford, and E. G. D. Cohen, "Cluster expansion for the dielectric constant of a polarizable suspension," *Journal of Statistical Physics*, vol. 28, no. 1, pp. 135–164, 1982.

[9] B. Felderhof and R. Jones, "Orientational relaxation in a colloidal suspension of spheres," *Physical Review E*, vol. 48, no. 2, p. 1084, 1993.

[10] B. Felderhof, "Magnetoviscosity and relaxation in ferrofluids," *Physical Review E*, vol. 62, no. 3, p. 3848, 2000.

[11] M. I. Shliomis, "Effective viscosity of magnetic suspensions," *Zh. Eksp. Teor. Fiz*, vol. 61, no. 2411, p. s1971d, 1971.

[12] M. I. Shliomis, "Ferrohydrodynamics: Testing a third magnetization equation," *Physical Review E*, vol. 64, no. 6, p. 060501, 2001.

[13] S. Odenbach, *Colloidal magnetic fluids: basics, development and application of ferrofluids*, vol. 763. Springer, 2009.

[14] A. O. Ivanov and O. B. Kuznetsova, "Magnetic properties of dense ferrofluids: an influence of interparticle correlations," *Physical Review E*, vol. 64, no. 4, p. 041405, 2001.

[15] E. C. Eckstein, D. G. Bailey, and A. H. Shapiro, "Self-diffusion of particles in shear flow of a suspension," *Journal of Fluid Mechanics*, vol. 79, no. 01, pp. 191–208, 1977.

[16] F. R. Cunha and E. J. Hinch, "Shear-induced dispersion in a dilute suspension of rough spheres," *Journal of Fluid Mechanics*, vol. 309, pp. 211–223, 1996.

[17] C. Pozrikidis, "Interception of two spheroidal particles in shear flow," *Journal of non-newtonian fluid mechanics*, vol. 136, no. 1, pp. 50–63, 2006.

[18] M. Lopez and M. D. Graham, "Shear-induced diffusion in dilute suspensions of spherical or nonspherical particles: Effects of irreversibility and symmetry breaking," *Physics of Fluids*, vol. 19, no. 7, p. 073602, 2007.

[19] M. Loewenberg and E. J. Hinch, "Collision of two deformable drops in shear flow," *Journal of Fluid Mechanics*, vol. 338, pp. 299–315, 1997.

[20] F. R. Cunha and H. L. G. Couto, "Transverse gradient diffusion in a polydisperse dilute suspension of magnetic spheres during sedimentation," *Journal of Physics: Condensed Matter*, vol. 20, no. 20, p. 204129, 2008.

[21] F. R. Cunha, R. G. Gontijo, and Y. D. Sobral, "Symmetry breaking of particle trajectories due to magnetic interactions in a dilute suspension," *Journal of Magnetism and Magnetic Materials*, vol. 326, pp. 240–250, 2013.

[22] Y. Wang, R. Mauri, and A. Acrivos, "The transverse shear-induced liquid and particle tracer diffusivities of a dilute suspension of spheres undergoing a simple shear flow," *Journal of fluid mechanics*, vol. 327, pp. 255–272, 1996.

[23] R. H. Davis, "Hydrodynamic diffusion of suspended particles: a symposium," *Journal of Fluid Mechanics*, vol. 310, pp. 325–335, 1996.

[24] E. Guazzelli and L. Oger, *Mobile particulate systems*, vol. 287. Springer Science & Business Media, 2013.

[25] X. Grandchamp, G. Coupier, A. Srivastav, C. Minetti, and T. Podgorski, "Lift and down-gradient shear-induced diffusion in red blood cell suspensions," *Physical review letters*, vol. 110, no. 10, p. 108101, 2013.

[26] D. Leighton and A. Acrivos, "Measurement of shear-induced self-diffusion in concentrated suspensions of spheres," *Journal of Fluid Mechanics*, vol. 177, pp. 109–131, 1987.

[27] A. Acrivos, G. K. Batchelor, E. J. Hinch, D. L. Koch, and R. Mauri, "Longitudinal shear-induced diffusion of spheres in a dilute suspension," *Journal of fluid mechanics*, vol. 240, pp. 651–657, 1992.

[28] Y. Wang, R. Mauri, and A. Acrivos, "Transverse shear-induced gradient diffusion in a dilute suspension of spheres," *Journal of Fluid Mechanics*, vol. 357, pp. 279–287, 1998.

[29] V. Breedveld, D. van den Ende, A. Tripathi, and A. Acrivos, "The measurement of the shear-induced particle and fluid tracer diffusivities in concentrated suspensions by a novel method," *Journal of Fluid Mechanics*, vol. 375, pp. 297–318, 1998.

[30] M. Marchioro and A. Acrivos, "Shear-induced particle diffusivities from numerical simulations," *Journal of fluid mechanics*, vol. 443, pp. 101–128, 2001.

[31] A. Sierou and J. F. Brady, "Shear-induced self-diffusion in non-colloidal suspensions," *Journal of fluid mechanics*, vol. 506, p. 285, 2004.

[32] K. A. Kusters, J. G. Wijers, and D. Thoenes, "Aggregation kinetics of small particles in agitated vessels," *Chemical Engineering Science*, vol. 52, no. 1, pp. 107–121, 1997.

[33] S. Biggs, M. Habgood, G. J. Jameson, *et al.*, "Aggregate structures formed via a bridging flocculation mechanism," *Chemical Engineering Journal*, vol. 80, no. 1, pp. 13–22, 2000.

[34] J. H. Promislow, A. P. Gast, and M. Fermigier, "Aggregation kinetics of paramagnetic colloidal particles," *The Journal of chemical physics*, vol. 102, no. 13, pp. 5492–5498, 1995.

[35] R. H. Davis, "The rate of coagulation of a dilute polydisperse system of sedimenting spheres," *Journal of Fluid Mechanics*, vol. 145, pp. 179–199, 1984.

[36] F. R. Cunha and H. L. G. Couto, "On the influence of the hydrodynamic interactions on the aggregation rate of magnetic spheres in a dilute suspension," *Journal of Magnetism and Magnetic Materials*, vol. 323, no. 1, pp. 77–82, 2011.

[37] C. Hurd, "Varieties of magnetic order in solids," *Contemporary Physics*, vol. 23, no. 5, pp. 469–493, 1982.

[38] C. Kittel, P. McEuen, and P. McEuen, *Introduction to solid state physics*, vol. 8. Wiley New York, 1996.

[39] G. H. Wannier, *Statistical Physics*. Dover Publications, 2010.

[40] D. C. Mattis, *The theory of magnetism made simple: an introduction to physical concepts and to some useful mathematical methods*. World Scientific Publishing Company, 2006.

[41] W. F. Brown Jr, "Thermal fluctuations of a single-domain particle," *Physical Review*, vol. 130, no. 5, p. 1677, 1963.

[42] E. Ising, "Beitrag zur theorie des ferromagnetismus," *Zeitschrift für Physik*, vol. 31, no. 1, pp. 253–258, 1925.

[43] L. Onsager, "Crystal statistics. i. a two-dimensional model with an order-disorder transition," *Physical Review*, vol. 65, no. 3-4, p. 117, 1944.

[44] P. Langevin, "Sur la théorie du magnétisme," *J. Phys. Theor. Appl.*, vol. 4, no. 1, pp. 678–693, 1905.

[45] N. Bohr, *Studier over metallernes elektrontheori*. Thaning et Appel in Komm., 1911.

[46] R. Jones, "Adiabatic change in the smoluchowski equation: Orientational diffusion of polar particles," *The Journal of chemical physics*, vol. 119, no. 3, pp. 1517–1532, 2003.

[47] G. K. Batchelor, *An introduction to fluid dynamics*. Cambridge university press, 2000.

[48] S. Kim and S. J. Karrila, *Microhydrodynamics: principles and selected applications*. Courier Corporation, 2013.

[49] J. D. Jackson, "Classical electrodynamics," 1999.

[50] R. Zwanzig, *Nonequilibrium statistical mechanics*. Oxford University Press, USA, 2001.

[51] O. A. Ladyzhenskaya, *The mathematical theory of viscous incompressible flow*, vol. 2. Gordon & Breach New York, 1969.

[52] G. K. Batchelor and J. T. Green, "The determination of the bulk stress in a suspension of spherical particles to order c 2," *Journal of Fluid Mechanics*, vol. 56, no. 03, pp. 401–427, 1972.

[53] J. Happel and H. Brenner, *Low Reynolds number hydrodynamics: with special applications to particulate media*, vol. 1. Springer Science & Business Media, 2012.

[54] D. Jeffrey and Y. Onishi, "Calculation of the resistance and mobility functions for two unequal rigid spheres in low-reynolds-number flow," *Journal of Fluid Mechanics*, vol. 139, pp. 261–290, 1984.

[55] C. J. Lin, K. J. Lee, and N. F. Sather, "Slow motion of two spheres in a shear field," *Journal of Fluid Mechanics*, vol. 43, no. 01, pp. 35–47, 1970.

[56] G. Batchelor and J.-T. Green, "The hydrodynamic interaction of two small freely-moving spheres in a linear flow field," *Journal of Fluid Mechanics*, vol. 56, no. 2, pp. 375–400, 1972.

[57] M. v. Smoluchowski, "On the mutual action of spheres which move in a viscous liquid," *Bull. Acad. Sci. Cracovie A*, vol. 1, pp. 28–39, 1911.

[58] S. H. Strogatz, *Nonlinear dynamics and chaos: with applications to physics, biology, chemistry, and engineering*. CRC Press, 2018.

[59] C. P. Robert, *Monte carlo methods*. Wiley Online Library, 2004.

[60] M. V. Smoluchowski, "Drei Vortrage uber Diffusion, Brownsche Bewegung und Koagulation von Kolloidteilchen," *Zeitschrift fur Physik*, vol. 17, pp. 557–585, 1916.

[61] B. Cichocki and B. Felderhof, "Renormalized cluster expansion for multiple scattering in disordered systems," *Journal of statistical physics*, vol. 51, no. 1-2, pp. 57–76, 1988.

APPENDICES

I. LAW OF LARGE NUMBERS

In this appendix, we present a brief discussion on the law of large numbers. This law is the principle behind the Monte-Carlo integration, used extensevely in this work. For this purpose, first we present a derivation of the Chebychev's inequality and then use this inequality to derive the week law of large numbers.

I.1 Chebychev's inequality

Chebychev's inequality is an important relation which appears frequently in the context of functional analysis, measure theory and probability theory. In the context of probability theory, this inequality is closely related to the definition of statistical variance.

Considering a measureble set Ω and a function $\varphi : \Omega \to \mathbb{R}$ with $\varphi(x) \geq 0 \; \forall x \in \Omega$. For a given constant $\alpha \geq 0$, we define a set A with all the points $x \in \Omega$ in which $\varphi(x) > a$. Namely:

$$A = \{x \in \Omega \mid \varphi(x) > \alpha\}. \tag{I.1}$$

By integrating the function $\varphi(x)$ over the domain Ω, we find:

$$\int_{\Omega} \varphi d\mu = \int_{A} \varphi d\mu + \int_{\Omega \setminus A} \varphi d\mu \geq \int_{A} \varphi d\mu \geq \alpha \mu(A) \tag{I.2}$$

Therefore, we have the following inequality:

$$\mu(\{x \in \Omega \mid \varphi(x) > \alpha\}) \leq \frac{1}{\alpha} \int_{\Omega} \varphi d\mu. \tag{I.3}$$

This inequality is most known as Chebychev's inequality. The inequality was derived in a general form for a measure space $(\Omega, \mathcal{F}, \mu)$, with $\mathcal{F}$ being a $\sigma-$algebra

of the subsets of Ω and $\mu : \mathcal{F} \to [0, +\infty)$ is the measure. We now apply this concept to a probability space $(\Omega, \mathcal{F}, \mathcal{P})$, where Ω is the state space, $\mathcal{F}$ is the set of possible events and $\mathcal{P}$ is the probability measure, with the property $\mathcal{P}(\Omega) = 1$. In this context, we define the expectation, or average, of a random variable $\varphi : \Omega \to \mathbb{R}$ as being:

$$E[\varphi] = \langle \varphi \rangle = \int_{\Omega} \varphi \, d\mathcal{P}. \tag{I.4}$$

Now, we want to determine the probability of the "distance" between the value of a random variable φ exceeds a certain constant ε. It is clear that:

$$|\varphi - \langle \varphi \rangle| \geq \varepsilon \iff (\varphi - \langle \varphi \rangle)^2 \geq \varepsilon^2. \tag{I.5}$$

Thus, by applying Chebychev's inequality, we have:

$$\mathcal{P}(\{x \in \Omega \mid (\varphi(x) - \langle \varphi \rangle)^2 > \varepsilon^2\}) \leq \frac{1}{\varepsilon^2} \langle (\varphi(x) - \langle \varphi \rangle)^2 \rangle. \tag{I.6}$$

This probability goes to zero when the right handside of the equation goes to zero. The term $\langle (\varphi(x) - \langle \varphi \rangle)^2 \rangle$ is related to the deviation of the random variable from the average value. Hence, we can define the variance $D[\varphi]$ of a random variable φ as being:

$$D[\varphi] = \langle (\varphi(x) - \langle \varphi \rangle)^2 \rangle = \langle \varphi^2 \rangle - \langle \varphi \rangle^2 \tag{I.7}$$

I.2 Law of large numbers

Considering a random variable X given by:

$$X = \frac{X_1 + \cdots + X_N}{N}, \tag{I.8}$$

where $X_1, \ldots, X_N$ are also random variables with the same average and variance, so that

$$\langle X_1 \rangle = \langle X_2 \rangle = \cdots = \langle X_N \rangle \tag{I.9}$$

and

$$D[X_1] = D[X_2] = \cdots = D[X_N] = \sigma^2. \tag{I.10}$$

The average and variance of the random variable X are given respectively by:

$$\langle X \rangle = E \tag{I.11}$$

and

$$D[X] = \frac{\sigma^2}{N}. \tag{I.12}$$

By applying Chebychev's inequality, we have the probability of the distance between X and its average value being greater than a constant $\varepsilon > 0$ is

$$\mathcal{P}(\{(X - \langle X \rangle)^2 > \varepsilon^2\}) < \frac{\sigma^2}{\varepsilon^2 N}. \tag{I.13}$$

Therefore, we have:

$$\langle X \rangle - \varepsilon \leq X \leq \langle X \rangle + \varepsilon \tag{I.14}$$

with probability greater then $1 - \sigma^2/(\varepsilon^2 N)$ for every $\varepsilon > 0$. By choosing $N \gg \sigma^2/\varepsilon^2$ for ε arbitrarily small, we have

$$X \approx \langle X \rangle \tag{I.15}$$

with probability ≈ 1. This is known as the weak law of large numbers. This law is very important because it links the practical concept of avereging to the mathematical concept of expectation of a random variable.

II. ASYMPTOTIC EXPRESSIONS FOR MOBILITIES

In this appendix, we give details about the expressions for the mobility tensors for the problem of two particles in the far-field and near-field regions, which are used in the numerical simulations, as detailed in chapter 3. These results were extracted from the tables found in the book by Kim & Karrila [48], with results originally due to Jeffrey and Onishi [54], and were modified in order to fit this work. The components i and j of the mobility tensors given in equation (3.13) can be written in the most general form as follow:

$$a_{ij}^{(\alpha\beta)} = x_{\alpha\beta}^{a} \frac{r_i r_j}{r^2} + y_{\alpha\beta}^{a} \left(\delta_{ij} - \frac{r_i r_j}{r^2} \right) \tag{II.1}$$

$$b_{ij}^{(\alpha\beta)} = y_{\alpha\beta}^{b} \varepsilon_{ijk} \frac{r_k}{r} \tag{II.2}$$

$$c_{ij}^{(\alpha\beta)} = x_{\alpha\beta}^{c} \frac{r_i r_j}{r^2} + y_{\alpha\beta}^{c} \left(\delta_{ij} - \frac{r_i r_j}{r^2} \right) \tag{II.3}$$

$$g_{ijk}^{(\alpha\beta)} = x_{\alpha\beta}^{g} \left(\frac{r_i r_j}{r^2} - \frac{1}{3}\delta_{ij} \right) \frac{r_k}{r} + y_{\alpha\beta}^{g} \left(\frac{r_i \delta_{jk} + r_j \delta_{ik}}{r} + \frac{r_i r_j r_k}{r^3} \right) \tag{II.4}$$

$$h_{ijk}^{(\alpha\beta)} = y_{\alpha\beta}^{h} \left(\frac{\varepsilon_{ikl} r_l r_j + \varepsilon_{jkl} r_l r_i}{r^2} \right) \tag{II.5}$$

II.1 Far-field mobilities

a tensor:

$$x_{11}^{a} = \frac{1}{6\pi\mu a} \left[1 - 60 \left(\frac{a}{2r} \right)^4 + 352 \left(\frac{a}{2r} \right)^6 + 2688 \left(\frac{a}{2r} \right)^8 - 85504 \left(\frac{a}{2r} \right)^{10} \right] \tag{II.6}$$

$$x_{12}^{a} = -\frac{1}{6\pi\mu a}\left[-3\left(\frac{a}{2r}\right) + 8\left(\frac{a}{2r}\right)^{3} - 2400\left(\frac{a}{2r}\right)^{7} + 3840\left(\frac{a}{2r}\right)^{9} + 201216\left(\frac{a}{2r}\right)^{11}\right] \tag{II.7}$$

$$y_{11}^{a} = \frac{1}{6\pi\mu a}\left[1 - 68\left(\frac{a}{2r}\right)^{6} - 320\left(\frac{a}{2r}\right)^{8} - 4416\left(\frac{a}{2r}\right)^{10}\right] \tag{II.8}$$

$$y_{12}^{a} = \frac{1}{6\pi\mu a}\left[\frac{3}{2}\left(\frac{a}{2r}\right) + 4\left(\frac{a}{2r}\right)^{3} + 9072\left(\frac{a}{2r}\right)^{11}\right] \tag{II.9}$$

b tensor:

$$y_{11}^{b} = \frac{1}{4\pi\mu a^{2}}\left[208\left(\frac{a}{2r}\right)^{7} + 2432\left(\frac{a}{2r}\right)^{9} + 22272\left(\frac{a}{2r}\right)^{11}\right] \tag{II.10}$$

$$y_{12}^{b} = \frac{1}{4\pi\mu a^{2}}\left[-2\left(\frac{a}{2r}\right)^{2} - 7680\left(\frac{a}{2r}\right)^{10}\right] \tag{II.11}$$

c tensor:

$$x_{11}^{c} = \frac{1}{8\pi\mu a^{3}}\left[1 - 3\left(\frac{a}{r}\right)^{8} - 6\left(\frac{a}{r}\right)^{10}\right] \tag{II.12}$$

$$x_{12}^{c} = -\frac{1}{8\pi\mu a^{3}}\left(\frac{a}{r}\right)^{3} \tag{II.13}$$

$$y_{11}^{c} = \frac{1}{8\pi\mu a^{3}}\left[1 - 240\left(\frac{a}{2r}\right)^{6} - 2496\left(\frac{a}{2r}\right)^{8} - 18432\left(\frac{a}{2r}\right)^{10}\right] \tag{II.14}$$

$$y_{12}^{c} = \frac{1}{8\pi\mu a^{3}}\left[-4\left(\frac{a}{2r}\right)^{3} + 4800\left(\frac{a}{2r}\right)^{9} + 61440\left(\frac{a}{2r}\right)^{11}\right] \tag{II.15}$$

***g* tensor:**

$$x_{11}^g = 2a\left[200\left(\frac{a}{2r}\right)^5 - 1120\left(\frac{a}{2r}\right)^7 - 13056\left(\frac{a}{2r}\right)^9 + 220160\left(\frac{a}{2r}\right)^{11}\right] \tag{II.16}$$

$$x_{12}^g = -(2a)\left[5\left(\frac{a}{2r}\right)^2 - 32\left(\frac{a}{2r}\right)^4 + 8000\left(\frac{a}{2r}\right)^8 + 3200\left(\frac{a}{2r}\right)^{10}\right] \tag{II.17}$$

$$y_{11}^g = 2a\left[-\frac{160}{3}\left(\frac{a}{2r}\right)^7 - 768\left(\frac{a}{2r}\right)^9 - 3072\left(\frac{a}{2r}\right)^{11}\right] \tag{II.18}$$

$$y_{12}^g = -(2a)\left[\frac{32}{3}\left(\frac{a}{2r}\right)^4 - \frac{3200}{3}\left(\frac{a}{2r}\right)^{10}\right] \tag{II.19}$$

***h* tensor:**

$$y_{11}^h = -200\left(\frac{a}{2r}\right)^6 + 12800\left(\frac{a}{2r}\right)^{10} \tag{II.20}$$

$$y_{12}^h = 10\left(\frac{a}{2r}\right)^3 + 4000\left(\frac{a}{2r}\right)^9 + 64000\left(\frac{a}{2r}\right)^{11} \tag{II.21}$$

II.2 Near-field mobilities

For the expressions for the near-field mobilities, we introduce the variables ξ and L such that

$$\xi = \frac{r - 2a}{a} \tag{II.22}$$

$$L = -\log(\xi) \tag{II.23}$$

***a* tensor:**

$$x_{11}^a = \frac{1}{6\pi\mu a}\left[0.7750 + 0.930\xi - 0.9\xi^2 L - 2.685\xi^2\right] \tag{II.24}$$

$$x_{12}^a = -\frac{1}{6\pi\mu a}\left[0.7750 - 1.070\xi + 0.9\xi^2 L + 2.697\xi^2\right] \tag{II.25}$$

$$y_{11}^a = \frac{1}{6\pi\mu a}\frac{0.89056L^2 + 5.77196L + 7.06897}{L^2 + 6.04250L + 6.32549} \tag{II.26}$$

$$y_{12}^a = \frac{1}{6\pi\mu a}\frac{0.48951L^2 + 2.80545L + 1.98174}{L^2 + 6.04250L + 6.32549} \tag{II.27}$$

***b* tensor:**

$$y_{11}^b = \frac{1}{4\pi\mu a^2}\frac{0.13368L^2 + 0.19945L - 0.79238}{L^2 + 6.04250L + 6.32549} \tag{II.28}$$

$$y_{12}^b = -\frac{1}{4\pi\mu a^2}\frac{0.13368L^2 + 0.92720L + 0.18805}{L^2 + 6.04250L + 6.32549} \tag{II.29}$$

***c* tensor:**

$$x_{11}^c = \frac{1}{8\pi\mu a^3}\frac{2}{3}\frac{7\zeta(3) - \xi L}{\zeta(3)\left[4\zeta(3) - \xi L\right]} \tag{II.30}$$

$$x_{12}^c = -\frac{1}{8\pi\mu a^3}\frac{2}{3}\frac{\zeta(3) - \xi L}{\zeta(3)\left[4\zeta(3) - \xi L\right]} \tag{II.31}$$

$$y_{11}^c = \frac{1}{8\pi\mu a^3}\frac{0.26736L^2 + 0.60896L + 0.28111}{L^2 + 6.04250L + 6.32549} \tag{II.32}$$

$$y_{12}^c = \frac{1}{8\pi\mu a^3}\frac{0.26736L^2 + -1.05770L + 0.29981}{L^2 + 6.04250L + 6.32549} \tag{II.33}$$

Note: In these expressions, $\zeta(x)$ is the Riemann zeta function

***g* tensor:**

$$x_{11}^{g} = 2a\,(0.1792 - 0.8703\xi) \tag{II.34}$$

$$x_{12}^{g} = 2a\,(-0.3208 + 0.9184\xi) \tag{II.35}$$

$$y_{11}^{g} = 2a\frac{0.0145L^2 + 0.0786L - 0.3193}{L^2 + 6.04250L + 6.32549} \tag{II.36}$$

$$y_{12}^{g} = -2a\frac{0.0869L^2 + 0.2956L - 0.1584}{L^2 + 6.04250L + 6.32549} \tag{II.37}$$

***h* tensor:**

$$y_{11}^{h} = -\frac{0.1014L^2 - 0.0764L + 0.7905}{L^2 + 6.04250L + 6.32549} \tag{II.38}$$

$$y_{12}^{h} = \frac{0.3986L^2 + 1.0762L - 0.3510}{L^2 + 6.04250L + 6.32549} \tag{II.39}$$